

Symmetry and Topology in Superconductors - Odd-frequency pairing and edge states -

¹Yukio TANAKA ^{*}, ²Masatoshi SATO [†], and ^{3,4}Naoto NAGAOSA [‡]

¹*Department of Applied Physics, Nagoya University, Nagoya, 464-8603, Japan*

²*The Institute for Solid State Physics, The University of Tokyo, Kashiwanoha 5-1-5,
Kashiwa, Chiba, 277-8581, Japan*

³*Department of Applied Physics, The University of Tokyo, 7-3-1 Hongo, Bunkyo-ku,
Tokyo, 113-8656, Japan*

⁴*Cross-Correlated Materials Research Group (CMRG) and Correlated Electron
Research Group (CERG), RIKEN-ASI, Wako, Saitama 351-0198, Japan*

Superconductivity is a phenomenon where the macroscopic quantum coherence appears due to the pairing of electrons. This offers a fascinating arena to study the physics of symmetry breaking, *i.e.*, broken gauge symmetry. However, the important symmetries in superconductors are not only the gauge invariance. Especially, the symmetry properties of the pairing, *i.e.*, the parity and spin-singlet / spin-triplet, determine the physical properties of the superconducting state. Recently it has been recognized that there is the important third symmetry of the pair amplitude, *i.e.*, even or odd parity with respect to the frequency. The conventional uniform superconducting states correspond to the even-frequency pairing, but the recent finding is that the odd-frequency pair amplitude arises in the spatially non-uniform situation quite ubiquitously. Especially, this is the case in the Andreev bound state (ABS) appearing at the surface/interface of the sample. The other important recent development is on the nontrivial topological aspects of superconductors. As the band insulators are classified by topological indices into (i) conventional insulator, (ii) quantum Hall insulator, and (iii) topological insulator, also are the gapped superconductors. The influence of the nontrivial topology of the bulk states appears as the edge or surface of the sample, *i.e.*, bulk-edge correspondence. In the superconductors, this leads to the formation of zero energy ABS (ZEABS). Therefore, the ABSs at the surface/interface of the superconductors are the place where the symmetry and topology meet each other which offer the stage of rich physics. In this review, we discuss the physics of ABS from the viewpoint of the odd-frequency pairing, the topological bulk-edge correspondence, and the interplay of these two issues. It is described how the symmetry of the pairing and topological indices determine the absence/presence of the ZEABS, its energy dispersion, and properties as the Majorana fermions. Various related issues such as the Helium 3, transport of Majorana fermions, and tunneling spectroscopies are also briefly discussed.

KEYWORDS: Odd-frequency pairing, Andreev bound state, Bulk-edge correspondence, Majorana fermion, Topological index

1. Introduction

Two of the most important principles in physics are symmetry and topology, both of which are related to the quantum numbers and energy degeneracy of states.¹⁾ For

*E-mail address ytanaka@nuap.nagoya-u.ac.jp

†E-mail address msato@issp.u-tokyo.ac.jp

‡E-mail address nagaosa@ap.t.u-tokyo.ac.jp

the compact symmetry group such as the 2π rotation, the discrete quantum numbers result. However, even a slight breaking of the symmetry destroys these features, *i.e.*, the conservation law is violated and the degeneracy is lifted. In the many-body systems, it often happens that the symmetry is *spontaneously* broken as a collective phenomenon. Ferromagnetism and superconductivity are two representative examples of this spontaneous symmetry breaking characterized by the order parameters. The magnetization, which breaks the rotational symmetry in the spin space, and the pair amplitude, which breaks the gauge symmetry, are the corresponding order parameters, respectively. In sharp contrast to this, the topological quantum numbers are more robust against the perturbations. For example, the quantization of the magnetic flux captured by one vortex in a superconductor is quantized to be $\phi_0 = hc/(2e)$ even in the disordered case without the cylindrical symmetry. This is guaranteed by the single-valued property of the superconducting order parameter and the stability of its winding number. It is evident that the winding number around a singular point (the center of the vortex in the above example) does not change for the continuous deformation as long as the path does not cross the singular point. Therefore, the topological properties often lead to the robustness of the system against the weak and moderate perturbations protected by the topological quantum number.

It is not always clear how to separate the two origins of the quantum numbers, *i.e.*, symmetry and topology. Even more interesting is the interplay between these two principles. It often happens that they are entangled to give a rich variety of physical phenomena. In this review article, we describe how these two principles are merged into the novel properties of superconductors.

1.1 Symmetry classifications of bulk superconductors and relevant quantum phenomena

Symmetry of Cooper pair is a central topic in the physics of superconductivity. Here we discuss uniform bulk systems. It is established that Cooper pair is formed between two electrons. In accordance with the Fermi-Dirac statistics, pair amplitude, which is a wave function of Cooper pair, must have a sign change with the exchange of two electrons. Symmetry of Cooper pair is customary classified into spin-singlet even-parity and spin-triplet odd-parity where even (odd) refers to the orbital part of the pair amplitude. For example, *s*-wave and *d*-wave pairings belong to the former case while *p*-wave pairing belongs to the latter.²⁾ With broken inversion symmetry, spatial parity is no more a good quantum number. In that case, spin-singlet even-parity and spin-triplet

odd-parity pairings can mix with each other. The mixed parity pairing has become an important issue in non-centrosymmetric superconductors.^{3,4)} It is noted that both in spin-singlet even-parity and spin-triplet odd-parity pairings, the pair amplitude does not have a sign change with the exchange of two time variables for the two electrons forming the Cooper pair. However, there is a possibility that pair amplitude has a sign change by this operation.⁵⁾ The latter type of pairing is so called odd-frequency pairing originally proposed by Berezinskii.⁶⁾ There are two possibilities of odd-frequency pairing, *i.e.*, spin-singlet odd-parity and spin-triplet even-parity pairings. Thus, in the presence of both the inversion and spin-rotational symmetries, Cooper pairs are classified into (i)even-frequency spin-singlet even-parity (ESE), (ii)even-frequency spin-triplet odd-parity (ETO), (iii)odd-frequency spin-triplet even-parity (OTE), and (iv)odd-frequency spin-singlet odd-parity (OSO). In strongly correlated systems, due to the retardation effect of the electron interaction, there is a possibility for odd-frequency pairing in the bulk. After the prediction by Berezinskii,⁶⁾ there have been several theoretical proposals about odd-frequency pairing in the bulk.⁷⁻¹⁷⁾ However, up to now, odd-frequency bulk superconductor has not been established experimentally yet. Although it is not easy to realize odd-frequency gap function in uniform bulk systems, it is more promising to induce odd-frequency pair amplitude in the non-uniform system with lower symmetry.

Class	Time	Spin	Orbital	Total
ESE	+	-	+	-
ETO	+	+	-	-
OTE	-	+	+	-
OSO	-	-	-	-

Table I. The symmetry of pair amplitude with respect to the exchange of spins, spatial coordinates, and time variables for possible four classes. ESE, ETO, OTE and OSO denote even-frequency spin-singlet even-parity, even-frequency spin-triplet odd-parity, odd-frequency spin-triplet even-parity, and odd-frequency spin-singlet odd-parity.

Bergeret, Volkov and Efetov have clarified that in ferromagnet/superconductor heterostructures with inhomogeneous magnetization, odd-frequency pairing is generated in ferromagnet.¹⁸⁾ They have predicted the long range proximity effect by the odd-frequency pairing. Furthermore, one of the authors (Y.T.) has revealed that the odd-frequency pairing is possible in inhomogeneous superconducting systems even without

magnetic ordering.^{19–21)} We will show ubiquitous presence of odd-frequency pairing in §2.^{20,22)}

Symmetry of the Cooper pair influences tunneling phenomena in superconducting heterostructures. It is known that Andreev bound state (ABS) is generally generated at the surface of anisotropic superconductor where pair potential (energy gap function) has a sign change on the Fermi surface.^{23–31)} By properly taking into account of the Andreev reflection in anisotropic superconductors,^{32–34)} it has been proven that the ABS manifests itself as a zero bias conductance peak (ZBCP) of quasiparticle tunneling spectroscopy.^{25,28,35)} The presence of ZBCP has been observed in tunneling spectroscopy of high T_c cuprates.^{36–43)} It has been established that a dispersionless zero energy ABS (ZEABS)²⁵⁾ is generated at the surface for spin-singlet d_{xy} -wave superconductors. The existence of the ABS influences seriously on charge transport,^{44–46)} spin transport⁴⁷⁾ and magnetic responses.^{48–50)}

ABS is also expected for spin-triplet p -wave superconductors. It induces ZBCP in the tunneling spectroscopy.^{51,52)} However, proximity effect via ABS is completely different between spin-singlet superconductors and spin-triplet superconductors. The ABS cannot penetrate into a diffusive normal metal (DN) attached to the superconductor in the former case, while it is possible in the latter one. The underlying physics can be expressed by the symmetry of the induced odd-frequency pairing.¹⁹⁾ We will discuss these exotic phenomena in §2.

1.2 Topological orders and topological quantum numbers

Up to now, we have discussed the classifications of the superconductors by symmetry as an example of quantum states. Then, is there any other way to characterize the quantum phases of electronic systems? The answer is yes, and the topological orders and topological quantum numbers serve this purpose.⁵³⁾ Historically, the first topological ordered state in condensed matter physics is the quantum Hall system, *i.e.*, the two-dimensional electronic systems under strong magnetic field at low temperature, where the Hall conductance σ_H is quantized to be the integer times the unit e^2/h (integer quantum Hall effect (IQHE)) or its fractions (fractional quantum Hall effect (FQHE)) (e : unit charge, h : Planck constant). Here, the topological quantum number C_1 (integer, see eq.(48)) characterizing the topological order is related to the physical observable,

i.e., the Hall conductance σ_H as

$$\sigma_H = -\frac{e^2}{h}C_1, \quad (1)$$

which explains why σ_H is quantized as the integer multiple of e^2/h .⁵⁴⁾

Another important issue related to the IQHE is the one-dimensional channels along the edge of the sample.⁵⁵⁾ A classical picture for these edge channels is that the cyclotron motion of the electrons in the bulk is reflected at the boundary of the sample, forming the one-dimensional motion in one-direction. This property of "one-direction" is called "chiral". In the quantum mechanical picture, the two-dimensional electronic states under magnetic field form the Landau levels, whose energies are pushed up near the edges of the sample by the confining potential. As a consequence, some of the edge channels cross the Fermi energy, which carry current. A remarkable fact is that the direction of the propagating waves along these edge channels is one-way, *i.e.*, chiral, and those with the opposite direction are on the other side of the sample, *i.e.*, far away separated by the bulk. (Consider the cylindrical sample where the two edges are separated by the bulk.) Therefore, the backward scattering is strictly forbidden even if the impurity potential is there. This leads to the perfect one-dimensional conductance of each channel, and consequently the Hall conductance is given by

$$\sigma_H = \frac{e^2}{h}n \quad (2)$$

where n is the number of the edge channels including the sign representing the chirality. Comparing eqs.(1) and (2), one concludes that there is a relation between the bulk topological quantum number (C_1) and the edge channels (n).^{56,57)} This is called "bulk-edge correspondence" and will be explored more in details later. One can say that the one-dimensional electronic states are "split into halves" at the two edges of the sample according to the chiralities, and the fractionalized electrons become robust. This fractionalization of the electrons at the edge is realized/supported by the topological order in the bulk state.

FQHE is a more complex phenomenon where the electron-electron interaction plays the essential role. Therefore, one needs to study the many-body wave functions, and the topological quantum numbers characterizing the quantum states are much more intriguing. The readers are referred to the textbooks for the details.^{1,53)} However, conceptually the story is quite analogous and similar to the IQHE. The topological order in the bulk reflects itself as the edge channels at the boundary of the sample, *i.e.*, the

bulk-edge correspondence occurs.

A recent breakthrough is the discovery of the topological insulators which preserve the time-reversal symmetry T , *i.e.*, without the external magnetic field or the spontaneous magnetization.^{58,59)} With T -symmetry, the Hall response and hence the Chern number is zero. Therefore, it is required to define new topological quantum numbers to characterize the topological orders.

The concept of topologically nontrivial states of the single-particle Hamiltonian can be generalized to the superconducting state as long as one considers the BCS Hamiltonian in the Nambu representation;

$$H_{BCS} = \sum_{\mathbf{k}} \psi_{\mathbf{k}}^{\dagger} h(\mathbf{k}) \psi_{\mathbf{k}} \quad (3)$$

where $\psi_{\mathbf{k}} = (c_{n\mathbf{k}\uparrow}, c_{n\mathbf{k}\downarrow}, c_{n\mathbf{k}\uparrow}^{\dagger}, c_{n\mathbf{k}\downarrow}^{\dagger})^T$. A naive way is to consider the matrix elements of $h(\mathbf{k})$ as that of the Bloch states discussed above. However, the situation is not so trivial since the degrees of freedom are redundant in $\psi_{\mathbf{k}}$ and $\psi_{\mathbf{k}}^{\dagger}$. Consequently, the edge channels and surface states originating from the bulk-edge correspondence has the same redundancy, which sometimes leads to Majorana fermion. The present edge channels and surface states appear as the ABSs characterized by the symmetry of Cooper pair as discussed in the former subsection. Therefore, the physics is much richer in this topological superconductor than the non-interacting electron systems.

In this review, we discuss the recent developments on the topological superconductors as the merging point of the two principles, *i.e.*, symmetry and topology. The in-depth study of this issue will clarify the interplay between these two principles in physics. The plan of this review follows. In §2, the odd-frequency superconducting pairing induced by the extrinsic symmetry breaking such as spatial non-uniformity and/or the time-reversal symmetry breaking is studied to demonstrate how the superconductivity is influenced by the symmetries. In §3, we discuss the topology of the bulk states in superconductors and its relation to the surface/edge states (bulk-edge correspondence). Various related issues are described in §4. §4 is also devoted to the summary and future perspectives. Hereafter, we choose the unit $\hbar = k_B = 1$ unless explicitly written. Two key concepts in this review are odd-frequency pairing and edge states. In Fig.1, we show the relations between each subsection and above two key concepts explicitly. The readers who want to know the essence of the review urgently would be appreciated to look at Table IX in §4.

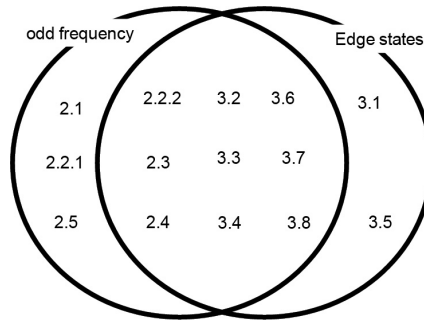


Fig. 1. The relations between each subsection and two key concepts, *i.e.*, odd-frequency pairing and edge states, in the present review.

2. Extrinsic symmetry breaking and odd-frequency pairing in superconductors

2.1 What is extrinsic symmetry breaking ?

In this section, we discuss what is an extrinsic symmetry breaking. Typical examples are breaking of the translational invariance or that of spin-rotational symmetry. In general, Cooper pair is formed between position \mathbf{r}_1 and \mathbf{r}_2 . Pair amplitude is a function of $\mathbf{r} = (\mathbf{r}_1 + \mathbf{r}_2)/2$ and $\bar{\mathbf{r}} = (\mathbf{r}_1 - \mathbf{r}_2)$. When we focus on the symmetry with respect to the exchange of two coordinates \mathbf{r}_1 and \mathbf{r}_2 , *i.e.*, $\bar{\mathbf{r}} \rightarrow -\bar{\mathbf{r}}$, we can define the parity of the Cooper pair. We employ the Fourier transformation from $\bar{\mathbf{r}}$ to \mathbf{k} . If we consider inhomogeneous superconducting systems, like vortex and junctions, translational symmetry is broken. In that system, parity of the Cooper pair is no more a good quantum number. Then, near the vortex core or the interface / surface of the superconductor, mixed parity state can be realized. To be more specific, let us consider normal metal / superconductor (N/S) junction where the symmetry of the superconductor belongs to ESE. Near the interface or in the normal metal, due to the breaking of translational symmetry, odd-parity state can be mixed. Since the spin rotational symmetry is not broken, pairing symmetry of spin should be singlet. To be consistent with Fermi Dirac statistics, the resulting Cooper pair should be odd in frequency. Then, we can expect OSO pairing is generated¹⁹⁾ near the interface and also inside normal metal. On the other hand, if symmetry in the bulk is ETO, then the induced pairing symmetry by breaking of the translational invariance or the spatial inversion symmetry is OTE.

Next, we discuss the breaking of the spin rotational symmetry only. By this symmetry breaking, spin-singlet and spin-triplet pairings are mixed with each other. Let us consider superconductor with ESE symmetry. In the presence of Zeeman magnetic field,

spin-triplet pairing state is generated. Since spatial parity is not broken, the induced pair amplitude should be OTE. On the other hand, if the pairing in the bulk is ETO, then the induced pair amplitude by breaking of spin rotational symmetry is OSO.

From this viewpoint, pairing symmetry in ferromagnet / superconductor (F/S) junction is very interesting. Here, we specify that the symmetry of the superconductor is spin-singlet s -wave one which belongs to ESE. In the light of above discussion, OSO pairing is induced in F by translational symmetry breaking. Also by the spin rotational symmetry breaking, OTE (ETO) pairing is generated from ESE (OSO) pairing. Thus, in F, all four kinds of pairings are basically possible.²²⁾ In the standard case accessible in experiments, F is in the diffusive regime. Then, basically only s -wave pairing is possible since it is robust against impurity scattering.⁶⁰⁾ The resulting pairing symmetries in F are only ESE s -wave and OTE s -wave. It has been shown that OTE pairing seriously influences on the density of states of quasiparticles. When OTE s -wave pairing dominates, quasiparticle density of state does not have a gap-like structure around zero energy.⁶¹⁾ In the extreme case, it has a zero energy peak (ZEP) structure.^{61,62)}

In §2.2 and §2.3, we restrict our discussion to ballistic transport regime. We will discuss relevant problems in diffusive regime in §2.4 and §2.5.

2.2 N/S junction with ballistic system

In this subsection, we consider superconducting proximity effect and resulting ubiquitous presence of odd-frequency pairing in N / S junctions.⁶³⁾ In general, physical quantities have spatial dependence near the interface. There are two characteristic length scales: i) The inverse of the Fermi wave length and ii) coherence length ξ given by $\xi = v_F/\Delta$, where v_F is the Fermi velocity and Δ is the energy gap (pair potential) in the superconductor. Here, we are interested in physical quantities varying slowly over the coherence length. In the present situation, it is appropriate to use quasiclassical Green's function method where high energy degrees of freedom are integrated out.⁶⁴⁻⁶⁷⁾ The quasiclassical Green's function is obtained from Gor'kov Green's function by integrating the energy and is concentrating on the low energy scale measured from the Fermi energy level. In this approximation, quasiparticles feel the pair potential depending on their direction of their motions on the Fermi surface.

In the following, we consider two-dimensional N ($x < 0$) / S ($x > 0$) junctions in the ballistic limit (Fig. 2). For the bulk superconductor, we choose even-frequency ESE or ETO pairings. As regards the spin-triplet ETO pairing, we choose $S_z = 0$ for simplicity.

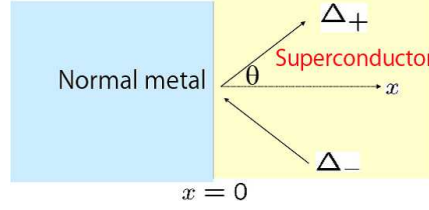


Fig. 2. (Color online) Schematic illustration of normal metal (semi-infinite) / superconductor (semi-infinite) junction. Δ_+, Δ_- denote pair potentials felt by right going (toward positive x) and left going (toward negative x) quasiparticles, respectively.

There is no essential difference even if we consider spin-triplet pairing with $S_z = 1$. We assume a thin insulating barrier located at the N/S interface ($x = 0$) modeled by a delta functional potential $H\delta(x)$. The reflection coefficient and transmission coefficient of the junction for the quasiparticle with the injection angle θ is given by $R = Z^2 / (Z^2 + 4 \cos^2 \theta)$ and $T_m = 1 - R$, respectively, with $Z = 2H/v_F$, where θ ($-\pi/2 < \theta < \pi/2$) is measured from the normal to the interface.

Here, we introduce quasiclassical retarded (advanced) Green's functions $g_{\pm}^{\text{R(A)}}(\varepsilon, \theta, \mathbf{r})$, and $f_{\pm}^{\text{R(A)}}(\varepsilon, \theta, \mathbf{r})$ where θ is given by $\mathbf{k} = k_F(\cos \theta, \sin \theta)$. $g_{+}^{\text{R(A)}}(\varepsilon, \theta, \mathbf{r})$ ($g_{-}^{\text{R(A)}}(\varepsilon, \theta, \mathbf{r})$) is the Green's function of quasiparticle at position \mathbf{r} , energy ε with injection angle θ ($\pi - \theta$). $f_{\pm}^{\text{R(A)}}(\varepsilon, \theta, \mathbf{r})$ denotes anomalous Green's function which becomes zero in the normal state. $f_{\pm}^{\text{R(A)}}(\varepsilon, \theta, \mathbf{r})$ can be decomposed into $f_{1\pm}^{\text{R(A)}}(\varepsilon, \theta, \mathbf{r})$ and $f_{2\pm}^{\text{R(A)}}(\varepsilon, \theta, \mathbf{r})$,

$$f_{\pm}^{\text{R(A)}}(\varepsilon, \theta, \mathbf{r}) = f_{1\pm}^{\text{R(A)}}(\varepsilon, \theta, \mathbf{r}) - i f_{2\pm}^{\text{R(A)}}(\varepsilon, \theta, \mathbf{r})$$

with

$$f_{1\pm}^{\text{R}}(\varepsilon, \theta, \mathbf{r}) = -f_{1\pm}^{\text{A}}(-\varepsilon, \theta, \mathbf{r}),$$

$$f_{2\pm}^{\text{R}}(\varepsilon, \theta, \mathbf{r}) = f_{2\pm}^{\text{A}}(-\varepsilon, \theta, \mathbf{r}). \quad (4)$$

From this definition, it is clear that $f_{1\pm}^{\text{R(A)}}(\varepsilon, \theta, \mathbf{r})$ ($f_{2\pm}^{\text{R(A)}}(\varepsilon, \theta, \mathbf{r})$) corresponds to the odd (even)-frequency pairing. Due to the translational invariance in the direction parallel to the interface $x = 0$, we can simply replace \mathbf{r} by x . $g_{\pm}^{\text{R(A)}}(\varepsilon, \theta, x) = g_{\pm}^{\text{R(A)}}$, $f_{1\pm}^{\text{R(A)}}(\varepsilon, \theta, x) = f_{1\pm}^{\text{R(A)}}$, and $f_{2\pm}^{\text{R(A)}}(\varepsilon, \theta, x) = f_{2\pm}^{\text{R(A)}}$ satisfy following so called the Eilenberger equation⁶⁸⁾

$$\mp i | v_F x | \frac{\partial}{\partial x} \hat{g}_{\pm}^{\text{R(A)}} = [\hat{H}, \hat{g}_{\pm}^{\text{R(A)}}] \quad (5)$$

with

$$\hat{H} = \varepsilon \hat{\tau}_3 + i \hat{\tau}_2 \bar{\Delta}_{\pm}(x)$$

and

$$\hat{g}_{\pm}^{\text{R(A)}} = g_{\pm}^{\text{R(A)}} \hat{\tau}_3 + f_{1\pm}^{\text{R(A)}} \hat{\tau}_1 + f_{2\pm}^{\text{R(A)}} \hat{\tau}_2.$$

Here, τ_i ($i = 1-3$) is the Pauli matrix in the electron-hole space. If we write it explicitly decomposing each τ_i component, following three equations are derived

$$\mp i |v_{Fx}| \partial_x f_{1\pm} = -2i\varepsilon f_{2\pm} - 2\bar{\Delta}_{\pm}(x)g_{\pm}, \quad (6)$$

$$\mp i |v_{Fx}| \partial_x f_{2\pm} = 2i\varepsilon f_{1\pm}, \quad (7)$$

$$\mp i |v_{Fx}| \partial_x g_{\pm} = 2\bar{\Delta}_{\pm}(x)f_{1\pm}. \quad (8)$$

Here, we omit the superscripts R and A. All the Green's functions in eqs. (6)-(8) have the same analytical properties, *i.e.*, R and A are not mixed. In the above, $v_{Fx} = v_F \cos \theta$ is the x -component of the Fermi velocity and $\bar{\Delta}_{\pm}(x)$ is the pair potential felt by \pm direction in Fig. 2. In general, quasiparticle is scattered from electron(hole)-like quasiparticle to hole(electron)-like one by the pair potential. As seen from the Eilenberger equations, the scattering of quasiparticle by the pair potential is a driving force to produce pair amplitudes $f_{1\pm}$ and $f_{2\pm}$. It should be remarked that $\bar{\Delta}_{\pm}$ and $f_{2(1)\pm}$ are different physical quantities. Even if $\bar{\Delta}_{\pm}$ is absent in a certain place x , $f_{2(1)\pm}$ may take a nonzero value by the proximity effect. $\bar{\Delta}_{\pm}(x)$ can be expressed by $\bar{\Delta}_{\pm}(x) = \Delta(x)\Phi_{\pm}(\theta)\Theta(x)$.⁶⁶⁾ For s , $d_{x^2-y^2}$, d_{xy} , p_x and p_y -wave superconductors, $\Phi_{+(-)}(\theta)$ is given by 1 (1), $\cos 2\theta$ ($\cos 2\theta$), $\sin 2\theta$ ($-\sin 2\theta$), $\cos \theta$ ($-\cos \theta$), and $\sin \theta$ ($\sin \theta$), respectively. For sufficiently large magnitude of $|x|$ with $x > 0$, $\Delta(x)$ converges to Δ_0 , which is the bulk value of the pair potential. g_{\pm} , $f_{1\pm}$ and $f_{2\pm}$ satisfy the normalization condition

$$g_{\pm}^2 + f_{1\pm}^2 + f_{2\pm}^2 = 1. \quad (9)$$

We first note the general features of the pair amplitudes $f_{1\pm}$ and $f_{2\pm}$. In normal state without $\bar{\Delta}_{\pm}$, $f_{1\pm} = 0$, $f_{2\pm} = 0$, and $g_{\pm} = 1$. This describes the quasiparticle without pair amplitudes. In bulk superconductors with $\bar{\Delta}_{\pm} = \Delta_0$ for $\Delta_0 > 0$, we obtain $f_{1\pm} = 0$ since there is no spatial dependence of $\bar{\Delta}_{\pm}$. For spin-singlet s -wave superconductor, $g_{\pm} = \varepsilon/\sqrt{\varepsilon^2 - \Delta_0^2}$, $f_{2\pm} = \Delta_0/\sqrt{\Delta_0^2 - \varepsilon^2}$. At $\varepsilon = 0$, $g_{\pm} = 0$ and $f_{2\pm} = 1$. This means the absence of quasiparticle and only the presence of Cooper pair at $\varepsilon = 0$.

In order to discuss the parity with respect to the frequency much more clearly,

it is useful to use the Matsubara frequency representation: The real energy ε is replaced by $i\omega_n$ where the Matsubara frequency ω_n is given by $\omega_n = 2\pi T(n + 1/2)$ with temperature T and integer n . Here, we pay attention to the $i\omega_n$ and θ dependences of $f_{1\pm} = f_{1\pm}(i\omega_n, \theta, x)$, $f_{2\pm} = f_{2\pm}(i\omega_n, \theta, x)$. For $x = \infty$, eqs. (6)-(8) lead to $f_{2\pm}(i\omega_n, \theta, \infty) = \Delta_0 \Phi_{\pm} / \sqrt{\Delta_0^2 \Phi_{\pm}^2 + \omega_n^2}$, $f_{2\pm}(i\omega_n, \theta, x) = f_{2\pm}(-i\omega_n, \theta, x)$ and $f_{1\pm}(i\omega_n, \theta, x) = 0$. This means that only even-frequency pairing is possible in the bulk. Although $f_{1\pm}(i\omega_n, \theta, x)$ is absent in the bulk, it has a nonzero value due to the spatial change of the pair potential $\bar{\Delta}_{\pm}$. As seen from eqs. (6)-(8), $f_{1\pm}(i\omega_n, \theta, x) = -f_{1\pm}(-i\omega_n, \theta, x)$ and $f_{2\pm}(i\omega_n, \theta, x) = f_{2\pm}(-i\omega_n, \theta, x)$ are always satisfied. This means that the symmetry of $f_{1\pm}(x, i\omega_n, \theta)$ belongs to odd-frequency pairing.²⁰⁾ Furthermore, as seen from eqs. (6)-(8),

$$v_{fx}^2 \partial_x^2 f_{1\pm} - 4(\omega_n^2 + \bar{\Delta}_{\pm}^2(x)) f_{1\pm} \pm 2i |v_{Fx}| [\partial_x \bar{\Delta}_{\pm}(x)] g_{\pm} = 0 \quad (10)$$

is satisfied in the Matsubara representation. It is clear that the spatial dependence of the pair potential $\bar{\Delta}_{\pm}(x)$ is a source of the generation of odd frequency pair amplitude $f_{1\pm}$.

We discuss the parity of $f_{1\pm}(i\omega_n, \theta, x)$ and $f_{2\pm}(i\omega_n, \theta, x)$. $\Phi_{\pm}(-\theta) = \Phi_{\mp}(\theta)$ is satisfied for an even-parity superconductor, while $\Phi_{\pm}(-\theta) = -\Phi_{\mp}(\theta)$ is satisfied for an odd-parity one. It follows from eqs. (6)-(8) that $f_{1\pm}(i\omega_n, \theta, x) = -f_{1\mp}(i\omega_n, -\theta, x)$ and $f_{2\pm}(i\omega_n, \theta, x) = f_{2\mp}(i\omega_n, -\theta, x)$ for an even-parity superconductor and $f_{1\pm}(i\omega_n, \theta, x) = f_{1\mp}(i\omega_n, -\theta, x)$ and $f_{2\pm}(i\omega_n, \theta, x) = -f_{2\mp}(i\omega_n, -\theta, x)$ for an odd-parity superconductor. Note that the parity of the odd-frequency pair amplitude $f_{1\pm}(i\omega_n, \theta, x)$ is different from that of the bulk superconductor.

Next, we discuss the values of the pair amplitudes at the interface $x = 0$. For this purpose, it is convenient to express the above anomalous Green's function as⁶⁹⁾

$$f_{1\pm} = \frac{\pm i(F_{\pm} + D_{\pm})}{1 - D_{\pm} F_{\pm}}, \quad f_{2\pm} = \frac{D_{\pm} - F_{\pm}}{1 - D_{\pm} F_{\pm}}, \quad (11)$$

where D_{\pm} and F_{\pm} satisfy the Eilenberger equations in the Riccati parameterization⁶⁹⁾

$$v_{Fx} \partial_x D_{\pm} = -\bar{\Delta}_{\pm}(x)(1 - D_{\pm}^2) + 2\omega_n D_{\pm} \quad (12)$$

$$v_{Fx} \partial_x F_{\pm} = -\bar{\Delta}_{\pm}(x)(1 - F_{\pm}^2) - 2\omega_n F_{\pm}. \quad (13)$$

Since the interface is flat, $F_{\pm} = -RD_{\mp}$ for $\omega_n > 0$ and $F_{\pm} = -R^{-1}D_{\mp}$ for $\omega_n < 0$ hold at $x = 0$ ⁶⁹⁾ with reflection coefficient R . If we denote ω_n dependences of D_{\pm} and F_{\pm} explicitly, $D_{\pm}(\omega_n) = 1/D_{\pm}(-\omega_n)$ and $F_{\pm}(\omega_n) = 1/F_{\pm}(-\omega_n)$ are satisfied.

We concentrate on two extreme cases with (A) $\Phi_+(\theta) = \Phi_-(\theta)$ and (B) $\Phi_+(\theta) = -\Phi_-(\theta)$. In the first case, there is no sign change of the pair potential felt by the quasiparticle reflected at the interface. Then, ABS is absent. On the other hand, in the second case, due to the sign change of the pair potential,²⁸⁾ ABS is generated near the interface. By using Riccati parameters defined above, it is easy to express that

$$\begin{aligned} f_{1\pm} &= \pm i(1-R)D_+/(1+RD_+^2), & f_{2\pm} &= (1+R)D_+/(1+RD_+^2), & \omega_n &> 0 \\ f_{1\pm} &= \pm i(R-1)D_+/(R+D_+^2), & f_{2\pm} &= (1+R)D_+/(R+D_+^2), & \omega_n &< 0 \end{aligned} \quad (14)$$

for the case (A) and

$$\begin{aligned} f_{1\pm} &= i(1+R)D_+/(1-RD_+^2), & f_{2\pm} &= \pm(1-R)D_+/(1-RD_+^2), & \omega_n &> 0 \\ f_{1\pm} &= i(1+R)D_+/(R-D_+^2), & f_{2\pm} &= \mp(1-R)D_+/(R-D_+^2), & \omega_n &< 0 \end{aligned} \quad (15)$$

for the case (B), respectively. In the low transparent limit with $T_m \rightarrow 0$ ($R \rightarrow 1$), only $f_{2\pm}$ is nonzero for the case (A) and $f_{1\pm}$ is nonzero for the case (B) where T_m is a transmission coefficient. However, even in the case (A), the mixture of odd and even-frequency pairings occur at the interface for general R . The underlying physics behind these results can be qualitatively explained as follows. Due to the breakdown of the translational invariance, even- and odd-parity pairings are coupled near the interface. To be consistent with the Fermi-Dirac statistics, the interface-induced pair amplitude $f_{1\pm}$ should be odd in frequency with odd(even)-parity, when the pair potential has an even(odd)-parity.²⁰⁻²²⁾ Note that $f_{1\pm}$ is pure imaginary and $f_{2\pm}$ is a real number, and there is a $\pm\pi/2$ phase between them. This twist of the phase is forced by the coexistence of the even- and odd-frequency components near the interface so as to be compatible with the time-reversal symmetry in the bulk superconductor.²⁰⁾ We summarize above results in Table II.

Finally, we comment that analytical solution of Eilenberger equation is possible in a special case for fixed θ . If we choose spatial dependence of $\bar{\Delta}_+(x)$ as

$$\Delta_+(x) = -\Delta_-(x) = \Delta_0 \tanh(x/\xi_0) \quad (16)$$

with a certain constant ξ_0 , we obtain following results,

$$g_+ = g_- = \frac{1}{\omega_n^2 + \Delta_0^2} \left[\omega_n + \frac{\Delta_0^2}{2\omega_n} \operatorname{sech}^2\left(\frac{x}{\xi_0}\right) \right],$$

$$f_{1+} = f_{1-} = \frac{i}{\omega_n^2 + \Delta_0^2} \frac{\Delta_0^2}{2\omega_n} \operatorname{sech}^2\left(\frac{x}{\xi_0}\right),$$

	Symmetry in bulk	Sign change	Interface
(1-1)	ESE (s , $d_{x^2-y^2}$ wave)	No	ESE +(OSO)
(1-2)	ESE (d_{xy} wave)	Yes	OSO +(ESE)
(2-1)	ETO (p_y wave)	No	ETO +(OTE)
(2-2)	ETO (p_x wave)	Yes	OTE +(ETO)

Table II. Paring symmetry in the bulk and that at the N/S interface. The pair amplitude in the bracket is suppressed in the low transparency limit.

$$f_{2+} = -f_{2-} = \frac{\Delta_0}{\omega_n^2 + \Delta_0^2} \tanh\left(\frac{x}{\xi_0}\right). \quad (17)$$

It is evident that odd-frequency pair amplitude $f_{1\pm}$ is localized near $x = 0$ similar to zero energy quasiparticle state as seen from g_{\pm} . Similar spatial dependence is realized in spin-singlet d_{xy} -wave and spin-triplet p_x -wave superconductor for low transparent limit.

In §2.2.1 and §2.2.2, we illustrate these results by numerical calculations. In order to understand the angular momentum dependence of pair amplitudes, we define \hat{f}_1, \hat{f}_2 as

$$\hat{f}_{1(2)} = \begin{cases} f_{1(2)+}(i\omega_n, \theta, x), & \text{for } -\pi/2 < \theta < \pi/2, \\ f_{1(2)-}(i\omega_n, \pi - \theta, x), & \text{for } \pi/2 < \theta < 3\pi/2. \end{cases} \quad (18)$$

We decompose $\hat{f}_{1(2)}$ into various angular momentum components.

2.2.1 Proximity effect in spin-singlet s -wave superconductors

We choose conventional spin-singlet s -wave superconductor as a typical example of ESE pairing. As seen from Table II(1-1), both ESE and OSO pairing exist at the N/S interface. We plot in Fig. 3 the s -wave component of $\hat{f}_2 E_s(x)$ and the p_x -wave component of $\hat{f}_1 O_{p_x}(x)$.

As seen from Fig. 3(a), the pair potential $\Delta(x)$ is suppressed for fully transparent case (a) ($T_m = 1, R = 0$) due to the penetration of Cooper pair into normal metal. At the same time, odd-frequency pair amplitude $O_{p_x}(x)$ is enhanced at the interface. On the other hand, for low transparent case (b) ($T_m < 1$), $O_{p_x}(x)$ is almost zero and $\Delta(x)$ remains constant up to the interface.

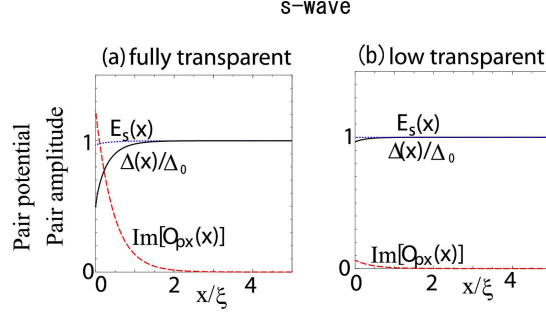


Fig. 3. (Color online) Spatial dependence of the pair potential for spin-singlet s -wave superconductor. Distance x is normalized by $\xi = v_F/\Delta_0$. Pair potential normalized by its value in the bulk (solid line). Even frequency pair amplitude $E_s(x)$ (dotted line), and odd frequency pair amplitude $O_{p_x}(x)$ (dashed line). (a) Fully transparent case with $Z = 0$ and (b) Low transparent case with $Z = 5$. $\omega_n = \pi T$ and $T = 0.05T_C$. T_C is the transition temperature of bulk superconductor. $R = Z^2/(Z^2 + 4 \cos^2 \theta)$.

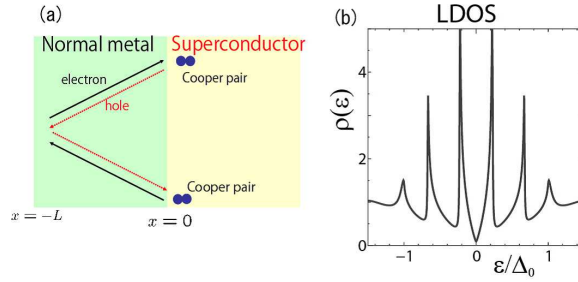


Fig. 4. (Color online) (a) Formation of standing wave by the closed loop of electron and hole. (b) Local density of state of quasiparticle $\rho(\varepsilon)$,

In order to highlight the effect of the induced odd-frequency pairing more clearly, here we consider N/S junction with finite length of N⁽²¹⁾ [see Fig.4 (a)]. We assume that the transparency at the interface is unity. In the present system, it is known that ABS with nonzero energy is formed⁷⁰⁾ as a standing wave which is generated by the interference between electron and hole in N. As seen in Fig.4 (b), there are many peaks in local density of state (LDOS), which have been observed as Rowell-McMillan oscillation in tunneling spectroscopy.^{70,71)} Here, we focus on this well-known phenomena in the light of odd-frequency pairing. Let us consider the pair amplitudes in the normal metal which are decomposed into components with different injection angle θ . We will define the following spatially averaged odd-frequency pair amplitude $F_{1+}^{(N)}(\varepsilon, \theta)$ and even-frequency pair amplitude $F_{2+}^{(N)}(\varepsilon, \theta)$

$$F_{1(2)+}^{(N)}(\varepsilon, \theta) = \frac{1}{L} \int_{-L}^0 f_{1(2)+}^R(\varepsilon, \theta, x) dx. \quad (19)$$

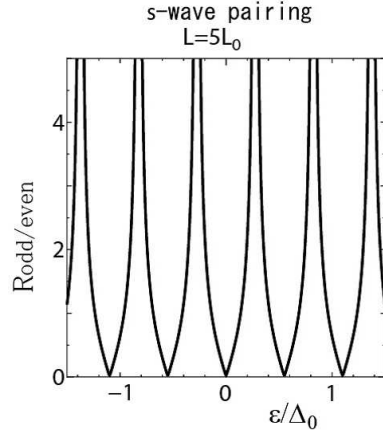


Fig. 5. Ratio of the spatially averaged odd-frequency pair amplitude to that of even-frequency one $R_{\text{odd/even}}$ is plotted as a function of ε for $\theta = 0$, $Z = 0$, $L = 5L_0$, and $L_0 = v_F/(\pi T_C)$.

Then we introduce the ratio of $F_{1+}^{(N)}(\varepsilon, \theta)$ to $F_{2+}^{(N)}(\varepsilon, \theta)$ as

$$R_{\text{odd/even}} = \frac{|F_{1+}^{(N)}(\varepsilon, \theta)|}{|F_{2+}^{(N)}(\varepsilon, \theta)|} = \left| \tan \left(\frac{2\varepsilon L}{v_{Fx}} \right) \right|. \quad (20)$$

As seen in Fig. 5, in a certain energy regime, the magnitude of the odd-frequency pair amplitude exceeds over that of even-frequency one. It is remarkable that odd-frequency pairing can become dominant even in simple normal metal / spin-singlet s -wave superconductor junctions for high transparency at the interface. In the extreme case with $L \gg L_0$ for fully transparent N/S interface, ABS levels with nonzero energy are given by^{70,71}

$$\varepsilon_n = \frac{\pi v_{Fx}}{2L}(n + 1/2), \quad n = 0, 1, 2, \dots \quad (21)$$

It should be noted that just at $\varepsilon = \varepsilon_n$, $F_{2+}^{(N)}(\varepsilon, \theta)$ vanishes and $R_{\text{odd/even}}$ diverges. Thus, the well-known quasiparticle bound states in N/S junction with conventional spin-singlet s -wave superconductor can be expressed by the generation of odd-frequency pairing.

For low transparency limit, *i.e.*, $T_m \rightarrow 0$, the present ABS disappears since the coupling between N and S is weakened. Thus, the present OSO state is sensitive to the transparency at the interface. (We represent such a state in the bracket in Table II.)

In the next subsection, we will focus on spin-triplet p_x -wave superconductor, where odd-frequency pairing exceeds over even-frequency one at the interface independent of the transparency.

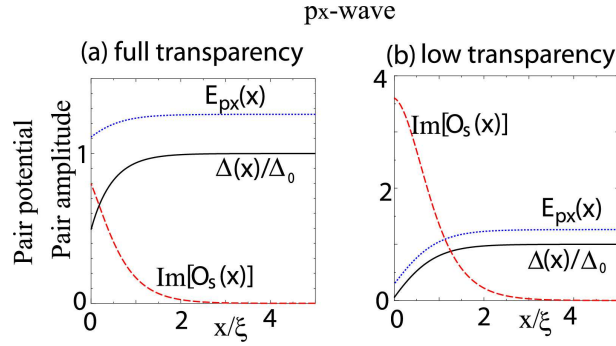


Fig. 6. (Color online) Spatial dependence of the pair potential for spin-triplet p_x -wave superconductor similar to Fig. 3. Distance x is normalized by $\xi = v_F/\Delta_0$. Pair potential normalized by its value in the bulk (solid line), Even frequency pair amplitude $E_{p_x}(x)$ (dotted line), and odd frequency pair amplitude $O_s(x)$ (dashed line). (a) Fully transparent case with $Z = 0$, @ (b) Low transparent case with $Z = 5$. $\omega_n = \pi T$ and $T = 0.05T_C$.

2.2.2 Andreev bound state in unconventional superconductor

In this subsection, we show that the mid gap ZEABS specific to unconventional (anisotropic) superconductor is expressed by odd-frequency pairing.⁶³⁾ We focus on the case with $\Phi_+\Phi_- < 0$ where mid gap ABS is generated. In this case, as discussed in §2.2, eq.(15) is satisfied by using Riccati parameters. In the low transparency limit with $T_m \rightarrow 0$ ($R \rightarrow 1$), only the $f_{1\pm}$ is nonzero. Namely, only the odd-frequency pair amplitude exists at the interface for $T_m \rightarrow 0$. First, we focus on the spatial dependence of the pair potential and pair amplitudes for spin-triplet p_x -wave superconductor. We plot in Fig. 6 the p_x -wave component of ETO pairing $E_{p_x}(x)$ and the s -wave component of OTE pairing $O_s(x)$.

For fully transparent junctions, similar to spin-singlet s -wave junction case (Fig. 3(a)), odd-frequency component of the pair amplitude $O_s(x)$ becomes of the same order of even-frequency one $E_{p_x}(x)$ as shown in Fig. 6(a). For low transparent junction, $O_s(x)$ largely exceeds over $E_{p_x}(x)$ near the interface while $\Delta(x)$ is suppressed [Fig. 6(b)]. The corresponding LDOS $\rho(\varepsilon)$ at $x = 0$ has a ZEP for spin-triplet p_x -wave superconductor junction (curve (a) in Fig. 7), while $\rho(\varepsilon)$ has a gapped line shape for spin-singlet s -wave superconductor junction. Similar ZEP also appears for spin-singlet d_{xy} -wave superconductor. ZEP of $\rho(\varepsilon)$ ubiquitously appears for unconventional superconductor junctions, where the pair potential changes sign on the Fermi surface.^{25, 27, 28)} Experimentally, ZBCP by this ZEP has been observed in many unconventional superconductors including cuprate.^{28, 36, 38–43, 72–78)} It is noted that in the presence of the ZEP

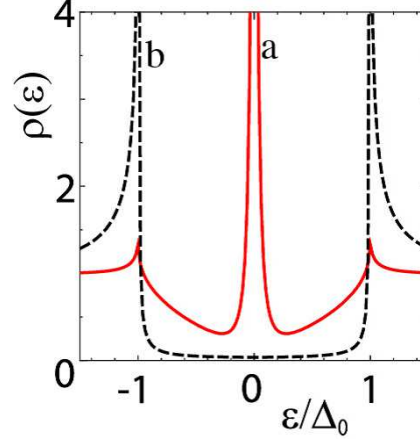


Fig. 7. (Color online) Quasiparticle density of state $\rho(\varepsilon)$ normalized by its value in the normal state at the N/S interface for $Z = 5$. (a) Spin-triplet p_x -wave superconductor junction. (b) Spin-singlet s -wave superconductor junction.

originating from ABS, the magnitude of the odd-frequency pairing is enhanced.

Hereafter, we discuss more details about the odd-frequency pairing in the low transparency limit. As shown in the last paragraph, only $f_{1\pm}$ exists for $R \rightarrow 1$ with $\Phi_+ \Phi_- < 0$. In this limit, $f_{2\pm}$ becomes zero and $f_{1\pm}$ is given by $f_{1\pm} = 2iD_+/(1 - D_+^2)$. Furthermore, ABS is expressed only by the induced odd-frequency pairing. Then, \hat{f}_1 in eq.(18) is given by

$$\hat{f}_1 = \begin{cases} \frac{2iD_+(\theta)}{1-D_+^2(\theta)}, & -\pi/2 < \theta < \pi/2 \\ \frac{-2iD_-(\pi-\theta)}{1-D_-^2(\pi-\theta)}, & \pi/2 < \theta < 3\pi/2 \end{cases}. \quad (22)$$

with $D_+(\theta) = -D_-(\theta)$ and $D_-(\pi - \theta) = D_+(\theta)$. Here, we explicitly write the θ dependence of D_+ . When the parity of bulk superconductor is even [odd], $D_+(\theta) = D_+(\pi + \theta) = D_-(\theta)$ [$D_+(\theta) = -D_+(\pi + \theta) = -D_-(\theta)$] is satisfied. Thus, \hat{f}_1 has an odd-parity (even-parity), when the bulk pairing symmetry is even-parity(odd-parity). The difference in the parity of the induced odd-frequency pairing results in a serious difference when we consider proximity effects into DN attached to superconductor.^{20, 79)} In DN, only s -wave even parity pairing is possible. Thus, pair amplitudes with angular momentum larger than 0 cannot penetrate into DN. This implies that odd-frequency pairing generated from d_{xy} -wave superconductor cannot enter into DN^{80, 81)} since it is expressed by OSO pairing. On the other hand, for p_x -wave superconductor, ABS can enter into DN⁸²⁻⁸⁴⁾ since it is expressed by OTE including s -wave channel.^{21, 79, 85)}

If we neglect the spatial change of the pair potential near the interface, it is possible

to obtain D_+ and \hat{f} analytically. Since D_+ is given by $\Delta_+ / (\omega_n + \sqrt{\omega_n^2 + \Delta_+^2})$, \hat{f}_1 is given by

$$\hat{f}_1 = \begin{cases} \frac{i\Delta_+(\theta)}{\omega_n}, & -\pi/2 < \theta < \pi/2 \\ \frac{-i\Delta_-(\pi-\theta)}{\omega_n}, & \pi/2 < \theta < 3\pi/2 \end{cases} \quad (23)$$

For spin-triplet p_x -wave bulk superconductor, the resulting \hat{f}_1 is

$$\hat{f}_1 = \frac{i\Delta_0}{\omega_n} |\cos \theta|,$$

while for spin-singlet d_{xy} -wave bulk superconductor, the resulting \hat{f}_1 is

$$\hat{f}_1 = \frac{i\Delta_0}{\omega_n} |\sin 2\theta| \operatorname{sgn}(\sin \theta).$$

Reflecting on the ZEABS, \hat{f}_1 is proportional to the inverse of ω_n for both cases. The difference of the parity of \hat{f}_1 between two cases appears in the topological features of wave function of two ABSs as will be discussed in §3.3.

2.3 Odd-frequency pairing in vortex core

In this subsection, we discuss the pairing symmetry in vortex core.⁸⁶⁾ The study of the mixed state in type-II superconductors, where magnetic flux enters a sample in the form of quantized vortices, has a long history.^{87,88)} It is known that the ABS is generated in the Abrikosov vortex core due to the spatial structure of the pair potential.^{89–96)} One of the manifestations of the bound states is the enhancement of LDOS in the core, observable as a ZBCP by scanning tunneling spectroscopy (STM).^{90,97)} Since an Abrikosov vortex breaks translational symmetry in a superconductor, we can expect the emergence of an odd-frequency pairing state around the vortex even in a conventional spin-singlet s -wave superconductor.

Here, based on the quasiclassical theory, we clarify a pairing symmetry in the vortex core. The electronic structure at the core of a single Abrikosov vortex in a ballistic superconductor is described by the quasiclassical Eilenberger equations.^{68,98,99)} We assume that the pairing symmetry of bulk superconductor is ESE or ETO. Along a trajectory $\mathbf{r}(x') = \mathbf{r}_0 + x' \hat{\mathbf{v}}_F$ with unit vector $\hat{\mathbf{v}}_F$ parallel to the Fermi velocity \mathbf{v}_F , the Eilenberger equations are generally represented in a 4×4 matrix.⁶⁹⁾ For a singlet (triplet) superconductor with $S_z = 0$, these equations are reduced to the set of two decoupled differential equations of the Riccati type for the functions $a(x')$ and $b(x')$ ^{98,99)}

$$v_F \partial_{x'} a(x') + [2\omega_n + \bar{\Delta}^* a(x')] a(x') - \bar{\Delta} = 0,$$

$$v_F \partial_{x'} b(x') - [2\omega_n + \bar{\Delta} b(x')] b(x') + \bar{\Delta}^* = 0 \quad (24)$$

where ω_n is the Matsubara frequency. Quasiparticle Green's function g and anomalous Green's function f are expressed by a and b as $g = (1-ab)/(1+ab)$ and $f = 2a/(1+ab)$, respectively. For simple case of a cylindrical Fermi surface, the Fermi velocity can be written as $\mathbf{v}_F = v_F(\cos \theta, \sin \theta)$. We choose the following form of the pair potential:

$$\bar{\Delta} = \bar{\Delta}(\mathbf{r}, \theta) = \Delta_0 \Phi(\theta) F(r) \exp(im\varphi)$$

with $r = \sqrt{x^2 + y^2}$, $\exp(i\varphi) = (x + iy)/r$ and integer m . The center of a vortex is situated at $x = y = 0$ and $\exp(im\varphi)$ is the phase factor which originates from the vortex. We consider axially symmetric cores. For the calculation of the normalized local DOS by its value in the normal state, the quasiclassical propagator has to be integrated over the angle θ which defines the direction of the Fermi velocity. The normalized LDOS in terms of functions a and b is given by

$$\rho(\mathbf{r}_0, \varepsilon) = \int_0^{2\pi} \frac{d\theta}{2\pi} \text{Re} \left[\frac{1-ab}{1+ab} \right]_{i\omega_n \rightarrow \varepsilon + i\delta}, \quad (25)$$

where ε denotes the quasiparticle energy with respect to the Fermi level and δ is an effective broadening parameter of quasiparticle energy level. In the actual numerical calculations, we will fix this value as $\delta = 0.1\Delta_0$.

First, we show the general property of the symmetry at the vortex center independent of the detailed spatial dependence of $\bar{\Delta}$. Let us consider a trajectory passing through the center of the vortex. By setting $x' = 0$ at the center of the vortex, we obtain $b(x', i\omega_n) = -1/a(-x', -i\omega_n)$ from the Eilenberger equations with odd integer m . Similarly, we obtain $b(x', i\omega_n) = 1/a(-x', -i\omega_n)$ for even integer m . Thus, at the vortex center $x' = 0$, we get $f(i\omega_n) = -f(-i\omega_n)$ in the former case, while $f(i\omega_n) = f(-i\omega_n)$ in the latter. Since we do not consider the Zeeman effect, spin flip does not occur in the present system. Thus, we can summarize pairing symmetry at the vortex center in Table III based on the broken inversion symmetry and Fermi-Dirac statistics.⁸⁶⁾

For conventional ESE s -wave case, there have been several studies of multi-flux state with $m \geq 1$ ^{100,101)} in the context of superconducting quantum dot where normal nano-scale region is surrounded by superconductor. It has been shown that ZEP in the DOS only appears for odd number m at the vortex center.^{100,101)} This statement is consistent with our present results for the conventional spin-singlet s -wave case, where odd-frequency pairing is generated only for odd integer m .

In general, the most stable vorticity is $|m| = 1$ realized in Abrikosov vortex. As

	bulk state	vorticity m	parity of the bulk states	symmetry at the center
(1)	ESE	odd	even	OSO
(2)	ESE	even	even	ESE
(3)	ETO	odd	odd	OTE
(4)	ETO	even	odd	ETO

Table III. Pairing symmetry in the vortex state.

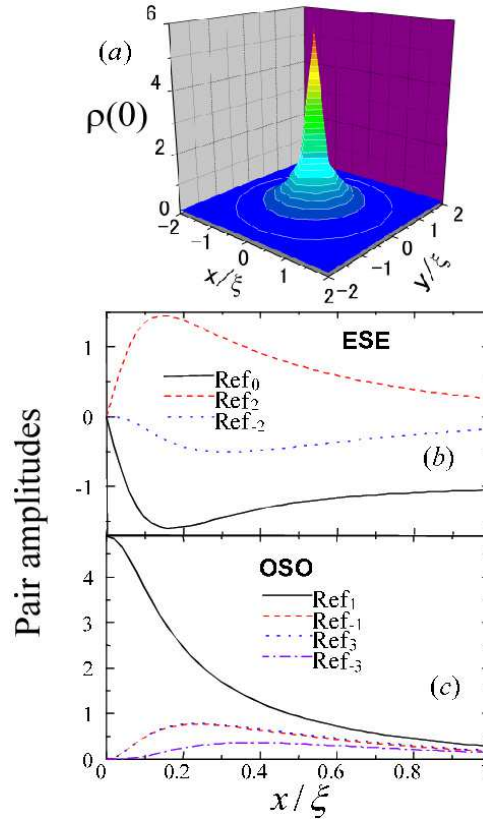


Fig. 8. (Color online) (a) Normalized LDOS around the vortex at $\varepsilon = 0$. The center of the vortex is situated at $x = y = 0$. (b) Spatial dependencies of various pairing components at $\varepsilon = 0$. Spatial dependencies of (b) ESE component and (c) OSO component. [Reproduced from Fig. 1 of Phys. Rev. B 78 012508 (2008) by T. Yokoyama, *et. al.*]

a symmetry of the bulk superconductor, we choose ESE s -wave pairing. Also, spatial dependence of the gap is chosen as $F(r) = \tanh(r/\xi)$, where $\xi = v_F/\Delta_0$ is the coherence length. Due to the broken translational symmetry of the system, various pairing symmetries are mixed near the vortex within the spin-singlet pairings. We decompose anomalous Green's function $f^R(\varepsilon, \theta)$ into various angular momentum components at

the center of the core, and $f^R(\varepsilon, \theta)$ can be given by

$$f^R(\varepsilon, \theta) = \sum_{l_z=0, \pm 1, \pm 2, \dots} f_{l_z} \exp(il_z \theta). \quad (26)$$

All the above pairing components f_{l_z} are spin singlet. Spatial dependence of the LDOS around the vortex at $\varepsilon = 0$ is shown in Fig. 8 (a). It has a peak just at the core center. The spatial dependencies of decomposed anomalous Green's function f_{l_z} at $\varepsilon = 0$ are shown in Figs. 8 (b) and (c). Interestingly, only OSO pairing component $\text{Re}(f_1)$ is nonzero at the center of the vortex core. Thus, we see that anomalous Green's function at the core center has chiral p -wave symmetry.

It is interesting to consider the bulk chiral superconductor with the angular momentum l . The corresponding pair potential is given by $\bar{\Delta} = \Delta_0 \Phi(\theta) F(r) \exp(il_z \theta) \exp(im\varphi)$. At the center of the core, it is shown analytically that the angular momentum of the pair amplitude is $l_z + m$. Here, we choose Abrikosov vortex in bulk chiral p -wave superconductor with $l_z = 1$. As seen from Table III(3), symmetry at the center of core is OTE. The angular momentum of the pair amplitude depends on whether chirality and vorticity is antiparallel or parallel. For the antiparallel case ($m = -1$), the OTE s -wave pairing is generated at the vortex core,¹⁰²⁾ while for the parallel case ($m = 1$), the OTE d -wave symmetry is realized at the core. Since s -wave pair amplitude is robust against impurity scattering,⁶⁰⁾ it is useful to consider impurity scattering effect on the vortex core state (odd-frequency pairing) to distinguish two states. We introduce this effect within the Born approximation, where we denote the impurity scattering rate in the normal state Γ with $\Gamma = 1/(2\tau)$ with mean free path $v_F \tau$. The resulting LDOS of anti-parallel and parallel vortex case is shown in Fig. 9. The ZEP is robust with the increase of Γ for anti-parallel vortex case while it is fragile against Γ for parallel vortex case.¹⁰³⁻¹⁰⁶⁾

The robustness of the ZEP at the vortex center against nonmagnetic impurities for antiparallel case originates from the odd-frequency s -wave pair amplitude. In the actual sample of spin-triplet chiral p -wave superconductor, degenerated chiral state, *i.e.*, $l_z = 1$ and $l_z = -1$, form a domain structure. Near the antiparallel vortex core, strong ZEP of LDOS is expected, while near the parallel vortex core, weak ZEP appears. Accordingly, measurements of the ZEP of LDOS in the presence of impurities reflects the detection of the symmetry of odd-frequency pair amplitude at the center of the core as shown in Fig. 10.

Extension of the calculation in the Abrikosov vortex lattice has been done by

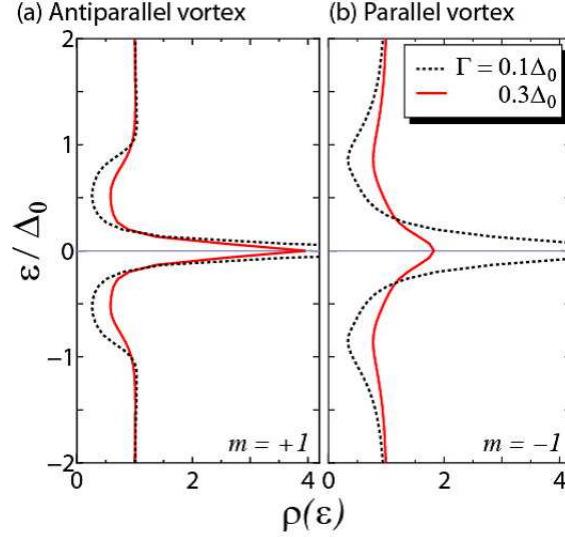


Fig. 9. (Color online) The LDOS at the vortex center for the antiparallel (a) and (b) the parallel vortex. The dashed and solid lines are plots for $\Gamma = 0.1\Delta_0$ and $0.3\Delta_0$, respectively. [Reproduced from Fig. 3 of Phys. Rev. Lett. 102 117003(2009) by Y. Tanuma *et. al.*]

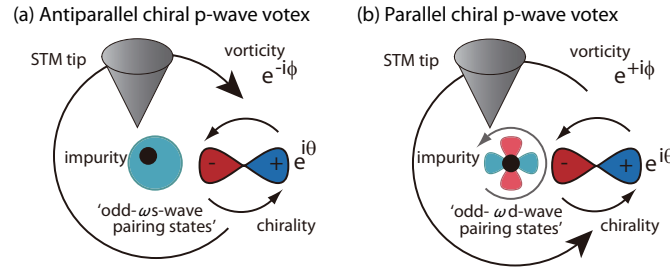


Fig. 10. (Color online) Schematic illustration of odd- ω pair amplitude for (a) the antiparallel and (b) the parallel vortex in chiral p -wave SCs. The arrows represent the phase rotation. [Reproduced from Fig. 4 of Phys. Rev. Lett. 102 117003(2009) by Y. Tanuma *et. al.*]

Yokoyama *et. al.*¹⁰⁷⁾ They have found that only odd-frequency pairing exists at core centers.

2.4 Anomalous proximity effect in spin-triplet superconductor junctions

In this subsection, we discuss the anomalous proximity effect specific to spin-triplet superconductor junctions. We consider diffusive normal metal(DN) ($0 < x < L$) / superconductor (S) ($x > L$) junction where the length of DN is L as shown in Fig. 11. We assume that the DN is attached to the normal electrode at $x = 0$. The interface between the DN and the superconductor (S) at $x = L$ has a resistance R_b and the N/DN interface at $x = 0$ has a resistance R_b . We also denote resistance in DN as R_d .

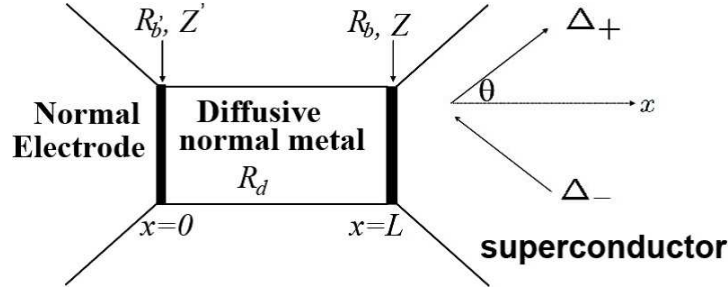


Fig. 11. Schematic illustration of the model of normal electrode attached to diffusive normal metal (DN) / superconductor (semi-infinite junction). [Revised from Fig.1 of Phys. Rev. B 72 140503(R) (2005) by Y. Tanaka *et. al.*]

For $R_b = \infty$, the present model is reduced to the DN/S bilayer with vacuum at the DN free surface.

We assume that pairing symmetry in S is ESE or ETO in the ballistic regime. We choose $S_z = 0$ for ETO case. In the DN region, only the s -wave pairing which is robust against impurity can survive in the limit of strong disorder. Since there is no spin-flip in the present junctions, spin structure of pair amplitude in DN is the same as that in bulk. Then, the pairing symmetry in the DN can be derived in accordance with Fermi-Dirac statistics. If the pairing symmetry in the bulk is ESE, the resulting symmetry in DN is ESE s -wave. On the other hand, if the pairing symmetry in the bulk is ETO, the resulting symmetry in DN is OTE s -wave. In DN, it is convenient to use Usadel equation which is derived from Eilenberger equation in the diffusive limit after angular average of the direction of motion. The Green's functions in Usadel equation do not have a θ dependence anymore due to the isotropization by impurity scattering. Here, in order to calculate LDOS in the DN region, we use retarded Green's function. Due to the fermion's commutation relation and complex conjugation of Green's function, anomalous Green's function should satisfy $f_{1(2)}^R(\varepsilon, x) = [f_{1(2)}^A(\varepsilon, x)]^*$ where the suffix 1 and 2 denote odd and even-frequency component. $f_1^R(\varepsilon, x) = -[f_1^R(-\varepsilon, x)]^*$ is satisfied by the relation $f_1^R(\varepsilon, x) = -f_1^A(-\varepsilon, x)$. On the other hand, $f_2^R(\varepsilon, x) = [f_2^R(-\varepsilon, x)]^*$ is satisfied by the relation $f_1^R(\varepsilon, x) = f_2^A(-\varepsilon, x)$. Usadel equation¹⁰⁸⁾ in DN is given by

$$D \frac{\partial^2 \zeta}{\partial x^2} + 2i\varepsilon \sin \zeta = 0, \quad (27)$$

with diffusion constant D . $g^R(\varepsilon, x)$ and $f_2^R(\varepsilon, x)$ are parameterized by $g^R(\varepsilon, x) = \cos \zeta$, $f_2^R(\varepsilon, x) = \sin \zeta$, and $f_1^R(\varepsilon, x) = 0$, when the bulk superconductor has an ESE symmetry. On the other hand, $g^R(\varepsilon, x) = \cos \zeta$, $f_1^R(\varepsilon, x) = \sin \zeta$, and $f_2^R(\varepsilon, x) = 0$ are satisfied

when the bulk superconductor has an ETO symmetry. The boundary condition of ζ is given by⁸⁰⁻⁸³⁾

$$\frac{L}{R_d} \left(\frac{\partial \zeta}{\partial x} \right) \Big|_{x=L} = \frac{\langle F_1 \rangle}{R_b}, \quad (28)$$

$$F_1 = \frac{2T_1(f_S \cos \zeta_L - g_S \sin \zeta_L)}{2 - T_1 + T_1(\cos \zeta_L g_S + \sin \zeta_L f_S)} \quad (29)$$

at DN/S interface ($x = L$) and

$$\frac{L}{R_d} \left(\frac{\partial \zeta}{\partial x} \right) \Big|_{x=0} = \frac{\langle F_2 \rangle}{R_{b'}}, \quad F_2 = \frac{2T_2 \sin \zeta_0}{2 - T_2 + T_2 \cos \zeta_0}, \quad (30)$$

at normal electrode /DN interface ($x = 0$). Here, $\zeta_L = \zeta |_{x=L}$, and $\zeta_0 = \zeta |_{x=0}$. $\langle \dots \rangle$ denotes the angular average of the injection angle θ of quasiparticles,

$$\langle F_{1(2)}(\theta) \rangle = \frac{\int_{-\pi/2}^{\pi/2} d\theta \cos \theta F_{1(2)}(\theta)}{\int_{-\pi/2}^{\pi/2} d\theta T_{1(2)} \cos \theta}, \quad (31)$$

$$T_1 = \frac{4 \cos^2 \theta}{Z^2 + 4 \cos^2 \theta}, \quad T_2 = \frac{4 \cos^2 \theta}{Z'^2 + 4 \cos^2 \theta}, \quad (32)$$

$T_{1,2}$ denotes the transmission coefficient at the interface with barrier parameters Z and Z' . g_S and f_S are determined by the pair potential in bulk superconductor with $g_S = (g_+ + g_-)/(1 + g_+g_- + f_+f_-)$, $g_{\pm} = \varepsilon/\sqrt{\varepsilon^2 - \Delta_{\pm}^2}$, $f_{\pm} = \Delta_{\pm}/\sqrt{\Delta_{\pm}^2 - \varepsilon^2}$, and $\Delta_{\pm} = \Delta_0 \Phi_{\pm}$. For even-parity bulk superconductor, $f_S = (f_+ + f_-)/(1 + g_+g_- + f_+f_-)$ and for odd-parity superconductor $f_S = i(f_+g_- - f_-g_+)/(1 + g_+g_- + f_+f_-)$.^{82,83)} Here, we neglect the spatial dependence of Δ_{\pm} . By solving, above Usadel equation with proper boundary condition we can determine the pair amplitude in DN and the resulting density of state.

	Bulk	interface	DN
(1-1)	ESE (s , $d_{x^2-y^2}$ -wave)	ESE (OSO)	ESE(s -wave)
(1-2)	ESE (d_{xy} -wave)	OSO (ESE)	No
(2-1)	ETO (p_y -wave)	ETO (OTE)	No
(2-2)	ETO (p_x -wave)	OTE (ETO)	OTE(s -wave)

Table IV. Paring symmetry in the bulk, at the interface, and in DN.

The obtained results are summarized in Table IV. LDOS $\rho(\varepsilon)$ normalized by its value in the normal state is plotted in Fig. 12. The pair amplitude \hat{f}_1 and \hat{f}_2 at the interface of S side discussed in §2.2 can not enter into DN if their angular momentum l is not zero. When the symmetry of the bulk superconductor is ESE s -wave (1-1), $f_1^R(\varepsilon, \theta) = 0$ and $f_2^R(\varepsilon, \theta) \neq 0$ are satisfied. This means that ESE s -wave pair is induced in DN. The OSO pair amplitude induced at the interface can not enter into DN due to the odd-parity. The LDOS has a gap like structure as shown in Fig. 12(a). This is a standard proximity effect known for the mesoscopic superconducting systems.^{109–112)} The order of the magnitude of the energy gap is Thouless energy $E_{Th} = D/L^2$ in DN. When the symmetry of the bulk superconductor is ESE d_{xy} -wave (1-2), the resulting ζ is zero and $f_1^R(\varepsilon, \theta) = f_2^R(\varepsilon, x) = 0$ inside DN. Then the resulting $\rho(\varepsilon)$ is unity as shown in Fig. 12(b). The OSO pair amplitude at the interface can not enter into DN. Also, the subdominant ESE state can not enter since its angular momentum l is $l \geq 2$. This is the reason for the absence of the proximity effect into DN. In other words, mid gap ABS generated at the interface can not penetrate into DN for bulk spin-singlet d_{xy} -wave superconductor. For ETO state with p_y -wave pairing (2-1), ζ is zero and $f_1^R(\varepsilon, \theta) = f_2^R(\varepsilon, \theta) = 0$ inside DN. Then the resulting $\rho(\varepsilon)$ is unity as shown in Fig. 12(c). In this case, pair amplitudes at the S side of the interface have angular momenta with $l > 0$. Proximity effect specific to spin-triplet superconductor appears for ETO p_x -wave bulk superconductor case (2-2). The resulting ζ and $f_1^R(\varepsilon, x)$ are nonzero in DN with $f_2^R(\varepsilon, x) = 0$. It is remarkable that $\rho(\varepsilon)$ has a sharp ZEP. This is a new type of proximity effect. The present anomalous proximity effect is generated by odd-frequency pairing.⁷⁹⁾ The mid gap ABS at the interface can penetrate into DN.^{82,83)} In this case, mid gap ABS can be interpreted as an OTE pairing which has an s -wave component.⁷⁹⁾ Then, the proximity effect into DN becomes possible.

Although we have shown anomalous proximity effect for ETO p_x -wave superconductor, it appears for generic ETO superconductor as far as the the interface induced OTE pair amplitude has an s -wave component.^{82,83)} ETO p_y -wave case is exceptional since OTE s -wave component is canceled by the angular integral of θ in the boundary condition. One of the strong candidate material of ETO p -wave superconductor is realized in chiral p -wave superconductor Sr_2RuO_4 where ZBCP originating from ABS^{51,113)} has been observed.^{73–75)} In this case, ZEP of $\rho(\varepsilon)$ in DN by the anomalous proximity effect appears. In the actual calculation, we must extend boundary condition at DN/S interface.⁵⁰⁾ In Fig. 13, we plot LDOS $\rho(\varepsilon)$ for various parameters. The height of the ZEP

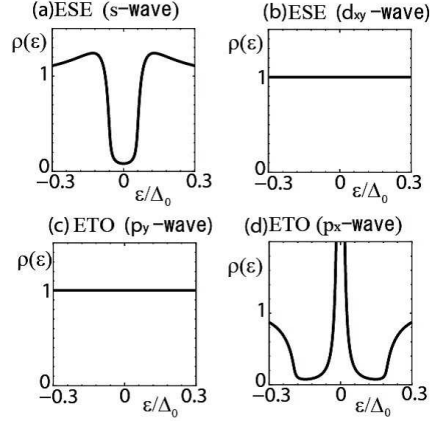


Fig. 12. LDOS $\rho(\varepsilon)$ of quasiparticle inside the diffusive normal metal at $x = L/2$. Symmetry in the bulk superconductor is (a)ESE s -wave, (b)ESE d_{xy} -wave, (c)ETO p_y -wave, and (d)ETO p_x -wave.

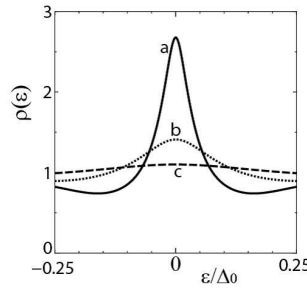


Fig. 13. Similar plot to Fig. 12 of $\rho(\varepsilon)$ inside the diffusive normal metal at $x = L/2$ for ETO chiral p -wave superconductor. $Z = Z' = 1$, $R_d/R_b = 1$ and $E_{Th} = 0.25\Delta_0$. (a) $R_d/R_{b'}$ = 0.01, (b) $R_d/R_{b'}$ = 1, and (c) $R_d/R_{b'}$ = 100. [Revised from Fig.2(a) of Phys. Rev. B 72 140503(R) (2005) by Y. Tanaka *et al.*]

of LDOS increases with the decrease of $R_d/R_{b'}$ since the odd pair amplitude $f_1^R(\varepsilon, x)$ is more strongly confined within DN for large magnitude of $R_{b'}$.

In order to detect anomalous proximity effect by odd-frequency pairing, we propose an experimental setup using scanning tunneling spectroscopy (STS) as shown in Fig. 14. The ZEP of LDOS can be detected by scanning tunneling spectroscopy (STS) and we can distinguish anomalous proximity effect by OTE pairing from conventional proximity effect by ESE pairing. However, to fabricate well-controlled surface of junctions available for STS is not so easy at present. In order to detect anomalous proximity effect, Asano *et al.* proposed a T -shaped junction⁸⁵⁾ which is more accessible for the fabrication as shown in Fig. 15. In this system, the proximity effect from the superconductor modifies the conductance between two electrodes depending remarkably on the pairing symmetry:

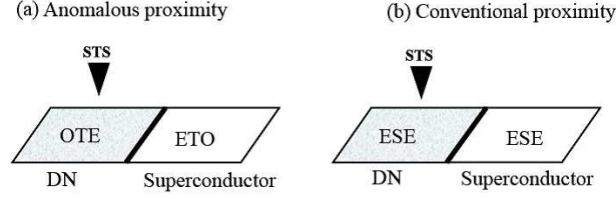


Fig. 14. Schematic illustration of an experimental setup by scanning tunneling microscope (STM) in diffusive normal metal (DN) attached to a superconductor. (a) Anomalous proximity effect in DN/ETO superconductor junction. (b) Conventional proximity effect in DN/ETO superconductor junction. The pair amplitude has an OTE and ESE symmetry for anomalous case (a) and conventional case (b), respectively. Only for anomalous proximity case (a), the LDOS has a zero energy peak.

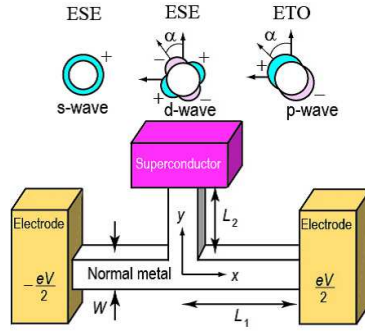


Fig. 15. (Color online) Schematic illustration of an experimental setup by T -shaped proximity structure. We consider spin-singlet s -wave, d -wave and spin-triplet p -wave pair superconductors. [Reproduced from Fig.1 of Phys. Rev. Lett. 99 067005 (2007) by Y. Asano *et. al.*]

spin-singlet or spin-triplet. Only for spin-triplet pairing, OTE state can be generated and conductance has a zero bias peak.

The anomalous proximity effect induces an peculiar response of DN to external magnetic field. When a magnetic field is applied parallel to the interface, the magnetic field in the DN behaves as $H(x) \sim \exp(-x/\lambda(x))$ with the local penetration depth $\lambda(x)$, which is given by

$$\frac{1}{\lambda^2(x)} = \frac{T \sum_{\omega_n} f_1^2(i\omega_n, x)}{\lambda_0^2}, \quad (33)$$

using Matsubara representation as shown in eq. (18) of ref.¹¹⁴⁾ or eq. (2.5) of ref.¹¹⁵⁾ with $\lambda_0^{-2} = 32\pi^2 e^2 N(0)D$. In Fig. 16, the averaged value of λ^2 , ($\bar{\lambda}_{av}^2 = L / \int_0^L \frac{dx}{\lambda^2(x)}$) is plotted as a function of temperatures (T), where T_C is the transition temperature of bulk superconductor. As is shown in Fig. 16 by curves c and d, $\bar{\lambda}_{av}^2 > 0$ for corresponding ESE superconductor junctions. Thus $\bar{\lambda}_{av}$ is a real number and a magnetic field is screened by

the usual Meissner effect in the DN irrespective of the fact whether bulk superconductor keeps T symmetry or not. On the other hand, in ETO superconductor junctions, we find $\bar{\lambda}_{av}^2 < 0$ as shown by curves a and b. Therefore, the $\bar{\lambda}_{av}$ becomes a purely imaginary number in the anomalous proximity case. This is the consequence of the fact that the pair amplitude $f_1(i\omega_n, x)$ is purely imaginary. The negative value of $\bar{\lambda}_{av}^2$ means the generation of negative superfluid density locally. It is a novel feature of the anomalous proximity effect that the applied magnetic field is not screened in the DN region and is screened only by the S region. The magnetic field can spatially oscillate in DN and paramagnetic state becomes possible. The paramagnetic Meissner effect in the surface of high Tc cuprate has been studied¹¹⁶⁾ and anomalous temperature dependence of the penetration depth has been reported.^{117,118)} Recently, Asano *et. al* have calculated dynamical response of OTE pairing to the electromagnetic field.¹¹⁹⁾ It has been found that the surface impedance ($Z = R - iX$) of a DN has anomalous features where R and Z are resistance and reactance, respectively. In contrast to the standard relation ($R \ll X$), an anomalous relation $R > X$ is satisfied at low temperatures.

Before closing this subsection, it is noted that purely odd-frequency pairing is realized in DN for DN/ETO superconductor junctions. The present odd-frequency pairing in DN arouses plenty of anomalous quantum phenomena including enhanced Josephson current in S/DN/S junctions.⁸⁴⁾ Since there are many new quantum phenomena relevant to anomalous proximity effect via odd-frequency pairing, we hope it will be verified by experiments in Sr_2RuO_4 junctions.^{50,85,119)}

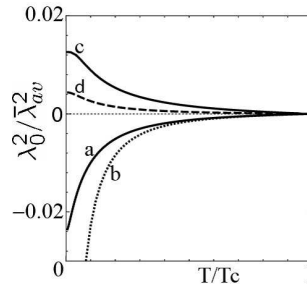


Fig. 16. Averaged value of the Meissner screening length $\bar{\lambda}_{av}^2$ is plotted for various superconductor with $Z = 1$, $R_d/R_b = 1$, $Z' = 1$, $R_d/R_b' = 1$ and $E_{Th} = 0.25\Delta_0$, respectively. (a)ETO chiral p -wave, (b)ETO p_x -wave, (c)ESE s -wave and (d)ESE chiral d -wave superconductors. [Revised from Fig.3 of Phys. Rev. B 72 140503(R) (2005) by Y. Tanaka *et. al.*]

2.5 odd-frequency pairing in ferromagnet / superconductor junctions

In this subsection, we discuss proximity effect in diffusive ferromagnet (DF)/ superconductor (S) junctions. The presence of odd-frequency pairing in DF/S junction has been originally proposed by Bergeret Volkov and Efetov.^{18,120} In their work, since inhomogeneous ferromagnet is assumed, equal-spin-triplet odd-frequency pairing is generated by the spin flip of an electron.^{18,120,121} Then, so called long range proximity effect appears,^{18,120–123} where the characteristic length of proximity effect is not $\sqrt{D/\hbar}$ but $\sqrt{D/T}$ similar to the conventional proximity effect without exchange energy h , where DF becomes diffusive non-magnetic metal denoted as DN in previous subsections. It is noted that there have been several relevant theoretical^{124–128} and experimental^{129–133} works in DF/S junctions up to now. Although original idea by Bergeret *et. al* has assumed inhomogeneous magnetization, it is possible to generate odd-frequency pairing even if we assume uniform ferromagnet with constant h in DF. Here, we discuss the symmetry of pair amplitudes and resulting LDOS.⁶¹ We assume ESE superconductor and ETO one with $S_z = 0$. In this case, straightforward extension of the previous subsection becomes possible.

Before calculation of LDOS by Usadel equation, we discuss general properties. In DF, only even parity s -wave pairing symmetry is possible due to the impurity scattering. When the symmetry of bulk superconductor is ESE, original pairing symmetry in DF without h is ESE as discussed in previous subsection. By the nonzero h , OTE pairing is induced by the explicit spin rotational symmetry breaking. On the other hand, when the bulk symmetry is ETO, only OTE pairing is possible in DF without h . Then, ESE pairing is induced by h . Thus for generic case, both ESE and OTE pair amplitudes exist in DF. Hereafter, we assume that the magnitude of h is much smaller than Fermi energy in S and DF. In this case, it is possible to apply Usadel equation. The boundary condition of the Green's function discussed in previous section is also available now. In the present case, we must pay attention to the direction of S_z in the Green's function which we have not explicitly written in the previous sections. As in the case of §2.4, we neglect the spatial dependence of pair potential in the bulk. Then the bulk Green's function g_{\pm} and f_{\pm} are given as follows

$$\begin{aligned}
 g_+ &\equiv g_{\uparrow,\uparrow}^R(\varepsilon, \theta) = g_{\downarrow,\downarrow}^R(\varepsilon, \theta) \\
 g_- &\equiv g_{\uparrow,\uparrow}^R(\varepsilon, \pi - \theta) = g_{\downarrow,\downarrow}^R(\varepsilon, \pi - \theta)
 \end{aligned}
 \tag{34}$$

$$f_+ \equiv f_{\uparrow,\downarrow}^R(\varepsilon, \theta) \quad f_- \equiv f_{\uparrow,\downarrow}^R(\varepsilon, \pi - \theta). \quad (35)$$

For ESE superconductor, $f_{\uparrow,\downarrow}^R(\varepsilon, \theta) = -f_{\downarrow,\uparrow}^R(\varepsilon, \theta)$ is satisfied while $f_{\uparrow,\downarrow}^R(\varepsilon, \theta) = f_{\downarrow,\uparrow}^R(\varepsilon, \theta)$ is satisfied for ETO one. g_{\pm} and f_{\pm} are given by $g_{\pm} = \varepsilon/\sqrt{\varepsilon^2 - \Delta_{\pm}^2}$ and $f_{\pm} = \Delta_{\pm}/\sqrt{\Delta_{\pm}^2 - \varepsilon^2}$, respectively, with $\Delta_{\pm} = \Delta_0\Phi_{\pm}$ as in the last subsection. In DF, ζ in eq. (27) follows

$$D\frac{\partial^2\zeta}{\partial x^2} + 2i(\varepsilon + h)\sin\zeta = 0. \quad (36)$$

with $\sin\zeta = f_{\uparrow,\downarrow}^R(\varepsilon, x)$. On the other hand, $\sin\bar{\zeta}$ with $\sin\bar{\zeta} = f_{\downarrow,\uparrow}^R(\varepsilon, x)$ satisfies

$$D\frac{\partial^2\bar{\zeta}}{\partial x^2} + 2i(\varepsilon - h)\sin\bar{\zeta} = 0 \quad (37)$$

The boundary condition of ζ is given by eqs. (29) (30).^{80,82)} On the other hand, the boundary condition of $\bar{\zeta}$ is given by

$$\frac{L}{R_d} \left(\frac{\partial\bar{\zeta}}{\partial x} \right) \Big|_{x=L} = \frac{\langle \bar{F}_1 \rangle}{R_b}, \quad (38)$$

at the DF/S interface. \bar{F}_1 is given by

$$\bar{F}_1 = \frac{2T_1(f_S \cos\bar{\zeta}_L - g_S \sin\bar{\zeta}_L)}{2 - T_1 + T_1(\cos\bar{\zeta}_L g_S + \sin\bar{\zeta}_L f_S)} \quad (39)$$

for ETO superconductor and

$$\bar{F}_1 = \frac{2T_1(-f_S \cos\bar{\zeta}_L - g_S \sin\bar{\zeta}_L)}{2 - T_1 + T_1(\cos\bar{\zeta}_L g_S - \sin\bar{\zeta}_L f_S)} \quad (40)$$

for ESE superconductor. At the interface between normal electrode and DF,

$$\frac{L}{R_d} \left(\frac{\partial\bar{\zeta}}{\partial x} \right) \Big|_{x=0} = \frac{\langle \bar{F}_2 \rangle}{R'_b}, \quad \bar{F}_2 = \frac{2T_2 \sin\bar{\zeta}_0}{2 - T_2 + T_2 \cos\bar{\zeta}_0}. \quad (41)$$

Here, $\bar{\zeta}_L = \bar{\zeta}|_{x=L}$, $\bar{\zeta}_0 = \bar{\zeta}|_{x=0}$. Even-frequency and odd-frequency pair amplitudes are given by

$$f_2^R(\varepsilon, x) = (\sin\zeta - \sin\bar{\zeta})/2 \quad (42)$$

and

$$f_1^R(\varepsilon, x) = (\sin\zeta + \sin\bar{\zeta})/2, \quad (43)$$

respectively. After solving Usadel equation, we can determine the symmetry of pair amplitudes in DF as shown in Table V. Proximity effect is absent for cases (1-2) and (2-

	Bulk	DN ($h = 0$)	DF
(1-1)	ESE (s , $d_{x^2-y^2}$ -wave)	ESE	ESE + OTE
(1-2)	ESE (d_{xy} - wave)	No	No
(2-1)	@ETO (p_y - wave)	No	No
(2-2)	ETO (p_x - wave)	OTE	OTE + ESE

Table V. Symmetries of Cooper pair in Ferromagnet (diffusive) / superconductor junctions. The bold letter expresses the symmetry induced by the exchange field h in DF.

1). For (1-1) and (2-2) cases, pairing symmetries in DF are ESE and OTE, respectively.

In the following, we calculate $f_2^R(\varepsilon, x)$, $f_1^R(\varepsilon, x)$, and LDOS $\rho(\varepsilon)$. $\rho(\varepsilon)$ in DF is given by

$$\rho(\varepsilon) = \frac{1}{2}(\text{Re} \cos \zeta + \text{Re} \cos \bar{\zeta}) \quad (44)$$

We consider a model similar to Fig. 11, where DN is replaced by DF. We assume ESE s -wave superconductor as a bulk state and choose $Z = 3$, $Z' = 3$, $E_{Th} \equiv D/L^2 = 0.1\Delta$, $R_d/R'_b = 0.1$. Pair amplitudes at $x = 0$, *i.e.*, the interface between normal electrode and DF, are plotted in Fig. 17.

From the definition of Green's function, imaginary part of $f_2^R(\varepsilon, x)$ and real part of $f_1^R(\varepsilon, x)$ become zero at $\varepsilon = 0$ for any h . For $h = 0$, $f_1^R(\varepsilon, x)$ is zero and only $f_2^R(\varepsilon, x)$ has a nonzero value.^{109,112)} With the increase of h , the magnitude of $f_2 = f_2^R(\varepsilon, x)$ around $\varepsilon = 0$ is suppressed. On the other hand, the magnitude of the imaginary part of $f_1 = f_1^R(\varepsilon, x)$ is enhanced by h . The corresponding $\rho(\varepsilon)$ is shown in Fig. 18. For $h = 0$, $\rho(\varepsilon)$ has a mini gap in consistent with previous theory.¹⁰⁹⁾ $\rho(\varepsilon)$ is sensitive to h . For $h/\Delta = 0.05$, $\rho(\varepsilon)$ has a ZEP. The presence of ZEP of $\rho(\varepsilon)$ in F/S junction has been discussed in previous works.^{124,134-137)} It has been clarified that for $E_{Th} \sim 2hR_b/R_d$, $\rho(\varepsilon)$ has a ZEP.^{138,139)} This condition is consistent with the present choice of the parameters. As seen from Figs. 17 and 18, $\rho(\varepsilon = 0)$ is enhanced when the imaginary part of $f_1^R(\varepsilon, x)$ has a large value (Fig. 17(d)). It is noted that odd-frequency pair amplitude plays a pivotal role for the generation of ZEP.^{138,139)}

In Fig. 19, we study the crossover between ESE and OTE pairings. We plot $\text{Re}f_2$ and $\text{Im}f_1$ as a function of h for $\varepsilon = 0$ at (a) $x = 0$, (b) $x = L/2$ and (c) $x = L$ in Fig. 19. $\text{Re}f_1$ increases from zero with h and it has a maximum at a certain value of h .

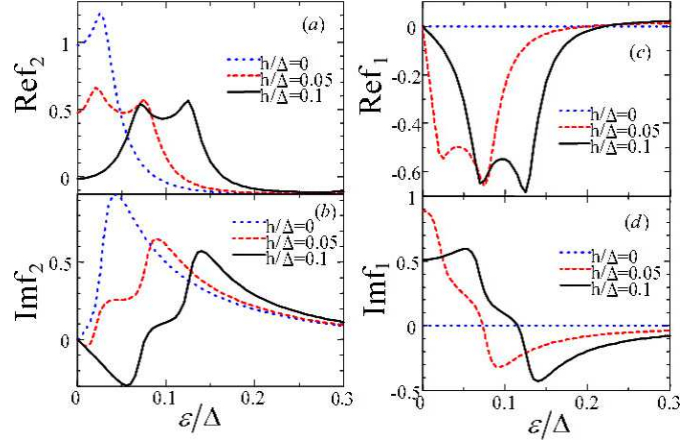


Fig. 17. (Color online) Real and Imaginary parts of pair amplitudes $f_2 = f_2^R(\varepsilon, x)$ and $f_1 = f_1^R(\varepsilon, x)$ at $x = 0$ are plotted for DF/S junctions with $R_d/R_b = 1$ for various exchange energy h . The pairing symmetry of f_2 and f_1 are ESE and OTE, respectively. [Reproduced from Fig. 2 of Phys. Rev. B, **75**,134510,(2007) by Yokoyama *et al.*]

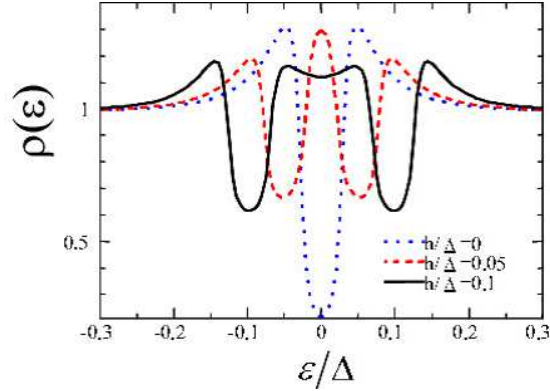


Fig. 18. (Color online) Normalized quasiparticle density of state $\rho(\varepsilon)$ at $x = 0$ for DF/S junctions is plotted as a function of ε for $R_d/R_b = 1$. [Reproduced from Fig. 3 of Phys. Rev. B, **75**,134510,(2007) by Yokoyama *et al.*]

As shown in Fig. 19(a) and Fig. 19(b), if the value of h is larger than this value, OTE pairing becomes dominant. If we use $\sin \bar{\zeta}(\varepsilon) = -\sin \zeta^*(-\varepsilon)$ and $\cos \bar{\zeta}(\varepsilon) = \cos \zeta^*(-\varepsilon)$ with $\zeta = \zeta(\varepsilon)$ and $\bar{\zeta} = \bar{\zeta}(\varepsilon)$, following relations are satisfied in pair amplitudes in DF,

$$f_1 = f_1^R(\varepsilon, x) = [\sin \zeta(\varepsilon) + \sin \zeta^*(-\varepsilon)]/2, \quad (45)$$

$$f_2 = f_2^R(\varepsilon, x) = [\sin \zeta(\varepsilon) - \sin \zeta^*(-\varepsilon)]/2. \quad (46)$$

The ratio of f_2 to f_1 at $\varepsilon = 0$ is given by

$$\frac{f_2}{f_1} = \frac{\tan \operatorname{Re}\zeta(0)}{i \tanh \operatorname{Im}\zeta(0)}. \quad (47)$$

If $|\operatorname{Re}\zeta(0)| < |\operatorname{Im}\zeta(0)|$ is satisfied, the crossover occurs and the OTE pair amplitude becomes dominant. The threshold h , where the present crossover occurs, is given by $h \sim (R_d/R_b)(E_{Th}/2)$.⁶¹⁾

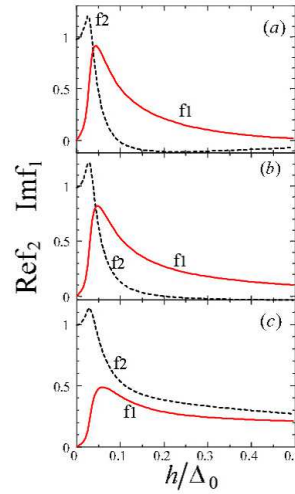


Fig. 19. (Color online) Pair amplitudes with ESE symmetry $f_2 = f_2^R(\varepsilon, x)$ and that with OTE symmetry $f_1 = f_1^R(\varepsilon, x)$ at $\varepsilon = 0$ are plotted as a function of h . (a) $x = 0$ (normal electrode /DF interface). (b) $x = L/2$ (middle of DF). (c) $x = L$ (DF/S interface). [Reproduced from Fig. 5 of Phys. Rev. B, **75**,134510,(2007) by Yokoyama *et. al.*.]

The generation of OTE state is possible without using DF region.^{140–142)} Linder *et al.* has clarified that even in DN/S junctions, if the interface is spin active, OTE pairing can be induced in DN where the bulk symmetry is ESE *s*-wave.^{140,141)} In this case, also ZEP of LDOS can be expected. Recently, Yokoyama *et. al.* has predicted the presence of anomalous Meissner effect is generated by the spin active interface. The magnetic susceptibility has a nonmonotonic temperature dependence accompanied by its sign change. Correspondingly, magnetic field and current density can spatially oscillate in DN.¹⁴³⁾ We hope these features will be observed by experiments with μ SR or microwave resonance.

Proximity effect in fully polarized ferromagnet, *i.e.*, half metal(HM), has become a hot topic now. Keizer *et. al.* reported the existence of Josephson coupling in superconductor/half metal/superconductor (S/HM/S) junctions,¹²⁹⁾ where symmetry of super-

conductor is conventional ESE s -wave. One of the possible pairing carrying a Josephson current in HM is a ETO p -wave pairing generated by the spin flip scattering at the interface.¹⁴⁴⁾ In real S/HM/S junctions, however, half metals are close to the dirty limit in the diffusive transport regime. Then more promising symmetry which can carry Josephson current is OTE s -wave pairing. Stimulated by the experiment by Keizer *et. al*, there have been several theoretical proposals^{145–149)} and an experimental report.¹⁵⁰⁾ Since the magnitude of the exchange energy is large, theoretical treatment is not so straightforward. Asano *et. al* have used a recursive Green’s function in the lattice model (see Fig. 20) and calculated pair amplitudes, LDOS and Josephson current. In the actual calculation, by changing the exchange potential V_{ex} , they have studied Josephson current in S/DN/S, S/DF/S and S/HM/S junctions. At the interface, spin flip scattering is introduced. On-site site scattering potentials are given randomly. The spin-flip scattering

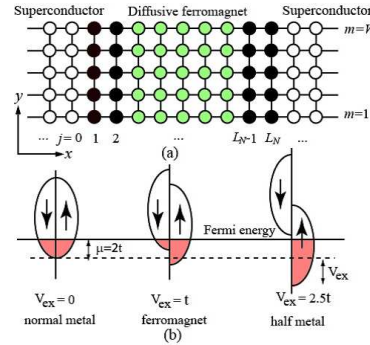


Fig. 20. (Color online) (a) A schematic figure of a SFS junction on the tight-binding lattice. (b) The density of states for each spin direction. The Josephson junction is of the S/DN/S, S/DF/S, and S/HM/S type for $V_{ex}/t = 0, 1$ and 2.5 , respectively. V_{ex} is the exchange potential in DF and HM. [Reproduced from Fig. 1 of Phys. Rev. Lett, **98**,107002,(2007) by Asano *et. al.*]

at the junction interfaces opens the Josephson coupling via odd-frequency spin-triplet Cooper pairs. In the middle of HM, the pairing symmetry is purely OTE state with equal-spin-triplet pairing. In Fig. 21(a), the pair amplitudes in the middle of the DF and DN are plotted for S/HM/S and S/DN/S junctions, respectively. For S/HM/S junction, the pair amplitude is an odd-function of ω_n and has an OTE symmetry. On the other hand, it is an even function for S/DN/S reflecting on the ESE symmetry. In Fig. 21(b), corresponding $\rho(\omega)$ in the middle of the DF and DN are plotted for S/HM/S and S/DN/S junctions, respectively. The $\rho(\omega)$ in the S/HM/S junction has a large peak at the Fermi energy by contrast to that in S/DN/S junctions. Therefore, the

odd-frequency pairs can be detected experimentally by using the scanning tunneling spectroscopy.^{145,148)}

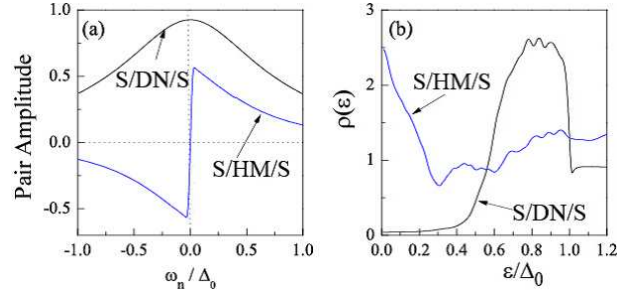


Fig. 21. (Color online) (a) ω_n dependences of pair amplitudes in the middle of HM(half metal) and in a DN (diffusive normal metal). (b) Corresponding local density of state $\rho(\varepsilon)$ [Reproduced from Fig. 4 of Phys. Rev. Lett., **98**,107002,(2007) by Asano *et. al.*]

3. Topology and bulk-edge correspondence

In §2, we discussed various properties of superconductors in terms of symmetry. In this section, we argue topological properties of superconductors.

3.1 Quantum Hall effect and TKNN number

Before going to discuss topological properties of superconductors, we would like to see more details of the integer quantum Hall states, which are a representative example of topological order.

The quantum Hall states are realized in two-dimensional electron systems under uniform magnetic field perpendicular to the plane. In a commensurate periodic potential of the crystal field, each level n is described by the Bloch wave function $\psi_{n,\mathbf{k}}$ with the crystal momentum \mathbf{k} in the magnetic Brillouin zone (BZ). The integer quantum Hall effects occur when the Fermi energy is located in a band gap, and all the levels below it are fully occupied.

To see the topological characterization, consider the first BZ with $-\pi < k_x, k_y < \pi$. Because of the periodicity, we can identify the edges of the 1st BZ, *i.e.*, $k_x = -\pi$ ($k_y = -\pi$) and $k_x = \pi$ ($k_y = \pi$) are equivalent. Therefore, the 1st BZ can be regarded as the torus T^2 , and the occupied Bloch wave functions $\psi_{n,\mathbf{k}}$ defines the mapping from this T^2 to the $U(1)$ phase of the wave functions. The topological index characterizing

	IQH state	superconducting state
bulk	gapped (Landau level)	gapped (Cooper pair)
edge	chiral gapless edge state	gapless ABS

Table VI. Similarity between integer quantum Hall state and superconducting state.

this mapping is so called the Chern number (or the TKNN integer) defined by^{151, 152)}

$$C_1 = \frac{1}{2\pi} \int_{T^2} d^2k \epsilon^{ij} \partial_{k_i} \mathcal{A}_j(\mathbf{k}) = \frac{1}{2\pi} \int_{T^2} d^2k \mathcal{B}_z(\mathbf{k}) \quad (48)$$

Here, $\mathcal{A}_i(\mathbf{k})$ is the “vector potential” of the $U(1)$ phase in the momentum space defined as

$$\mathcal{A}_i(\mathbf{k}) = i \sum_{E_n < E_F} \langle u_{n,\mathbf{k}} | \partial_{k_i} u_{n,\mathbf{k}} \rangle \quad (49)$$

in terms of the periodic part $|u_{n,\mathbf{k}}\rangle$ of the Bloch wave function, and $\mathcal{B}_z = \partial_{k_x} \mathcal{A}_y - \partial_{k_y} \mathcal{A}_x$ is the “magnetic flux density”. It can be seen that C_1 is an integer corresponding to the winding number for the mapping from T^2 to the phase of the Bloch wave function. From the Kubo formula, the Hall conductance σ_H is found to satisfy eq.(1). Thus the quantization of the Hall conductance for IQHE can be naturally explained as the quantization of the Chern number itself.

Recently, the topological characterization has been generalized to superconductors in the name of “topological superconductor”.^{59, 153–159)} The key observation is that there exists a close similarity between the quantum Hall states and superconducting states, summarized in Table VI: Both states are gapped in the bulk, so we need a finite energy to create bulk excitations. On the other hand, we may have gapless states on their boundaries, *i.e.* chiral edge state in quantum Hall states and ABS in superconducting state. The analogy between them enables us to apply the topological idea of the quantum Hall states to superconductors, while they show originally different physical phenomena from each other.

As discussed in §1.2, for quantum Hall states, there is a relation between the chiral gapless edge states and the bulk Chern number C_1 . So one can naturally expect that a similar bulk-edge correspondence also holds for superconductors. In the following sections, we will show that this is the case, and gapless ABSs can be related to bulk topological numbers of superconductors.

3.2 Bulk-edge correspondence

Here we will generalize the idea of the bulk-edge correspondence, or bulk-boundary correspondence.^{160,161)} Except for quantum Hall states, we may not use the Hall conductance to discuss the bulk-edge correspondence, however, we will show in the following that the bulk-edge correspondence can be obtained from a general argument of topology.

First, we discuss how a bulk-topological number can be defined generally. We suppose a band description of theory, and the bulk wave functions of electrons or quasi-particles are given by Bloch wave functions $|u_n(\mathbf{k})\rangle$ in the first BZ. As is illustrated in Fig.22, we assume that the Fermi energy is located in a band gap so the system is a band insulator in the bulk.

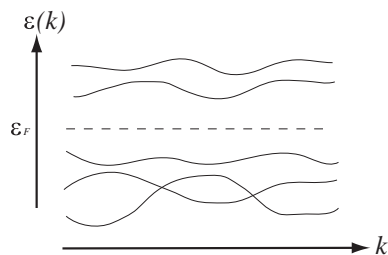


Fig. 22. Schematic picture for the spectrum of a band insulator. The Fermi energy is located in the band gap. All the states below the Fermi energy is fully occupied. [Reproduced from Fig.2 of Bussei Kenkyu **94** 311 (2010) by Sato.]

In this situation, we can introduce a bulk topological number by using occupied Bloch wave functions as follows: Let us first note that a Bloch wave function generally maps a point \mathbf{k} in the momentum space to a point in the Hilbert space. Thus, using the occupied Bloch wave functions, in which all the momentum space is filled with electrons or quasiparticles, we can map the whole of the first BZ to the Hilbert space. Then, depending on a type of wave functions, the image of the BZ may “wind the Hilbert space” in some way so that it can not be deformed into a point smoothly. If this happens, a bulk topological number is defined as a “winding number” of the image of the BZ.

The above definition of topological number is rather abstract, however it is sufficient to derive a general property of bulk topological numbers. The definition infers that the topological number takes only discrete integer values since it counts a “winding number” of the image of the BZ. However, at the same time, the topological number could change

only continuously since it is defined by using the wave functions which can change only continuously. From the consistency, we can conclude that the topological number cannot change actually as long as no singularity arises.

Then a question is when a singularity arises. The answer is when the bulk gap closes. If the bulk gap closes, we have a gap closing point P . (See Fig.23.) Since we cannot distinguish an occupied state from an empty state at P , the concept of occupied states becomes ill-defined, so is the topological number itself. Thus the topological number may change discontinuously in this case.

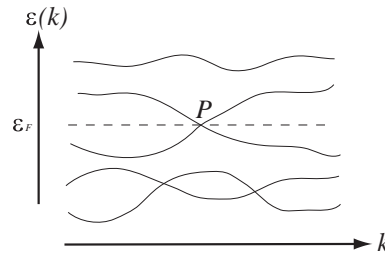


Fig. 23. When the bulk gap closes, a gap closing point P appears. We cannot distinguish an occupied state from an empty state at P . [Reproduced from Fig.4 of *Bussei Kenkyu* **94** 311 (2010) by Sato.]

From the above properties of topological numbers, we can derive a generalized bulk-edge correspondence. Consider an interface between two different band insulators illustrated in Fig.24(a). We suppose that a bulk topological number ν is defined in both sides of insulators, and $\nu \neq 0$ in the left hand side while $\nu = 0$ in the right hand side. Let us see what happens to the topological number when we go from the left to the right. We immediately find that the nonzero value of the topological number changes abruptly to zero near the interface at x_e . Thus, the above discussion of bulk topological numbers implies that the gap of the system must close near the interface. In other words, we have a gapless state near the interface. Regarding the vacuum as the topologically trivial insulator in right hand side, we have a generalized bulk-edge correspondence: *On a boundary (edge or surface) of an insulator with a nonzero bulk topological number, there exist gapless states corresponding to the topological number.*

While the above argument is rather intuitive, we can make it rigorous by introducing the confining potential separating the topological phases.¹⁶¹⁾ The quantitative arguments confirm the robustness of the bulk-edge correspondence.

In the following sections, we will see how the bulk-edge correspondence works for

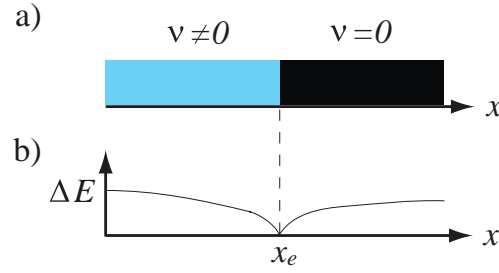


Fig. 24. (Color online) (a) An interface between the insulator with a nonzero topological number $\nu \neq 0$ and that with $\nu = 0$. (b) Gap ΔE of the system. When the topological number ν changes at $x = x_e$, the gap closes. [Reproduced from Fig.5 of Bussei Kenkyu **94** 311 (2010) by Sato.]

superconductors. In the ground state of a fully gapped superconductor, the negative energy states are fully occupied while the positive energy states are empty. So we can regard a superconductor as a kind of “insulator”. This identification enables us to apply the bulk-edge correspondence to superconductors.

3.3 Topology of Andreev bound state with flat dispersion

First, we consider a class of superconductors in which the gap function is a single component real function.^{160–162} It includes conventional s -wave superconductors, p_x -wave (or p_y -wave) superconductors, high T_c cuprates, and so on. When the spin-orbit interaction is negligible, and the Cooper pairs preserve the time-reversal invariance and a spin in a certain direction, say S_z , this class of superconductors is realized.

The Hamiltonian is given by

$$\mathcal{H} = \sum_{\mathbf{k}} \left(c_{\mathbf{k}\uparrow}^\dagger, c_{-\mathbf{k}\downarrow} \right) \mathcal{H}(\mathbf{k}) \begin{pmatrix} c_{\mathbf{k}\uparrow} \\ c_{-\mathbf{k}\downarrow}^\dagger \end{pmatrix} \quad (50)$$

where $\mathcal{H}(\mathbf{k})$ is a 2×2 Bogoliubov de Gennes (BdG) Hamiltonian

$$\mathcal{H}(\mathbf{k}) = \begin{pmatrix} \varepsilon(\mathbf{k}) & \Delta(\mathbf{k}) \\ \Delta(\mathbf{k}) & -\varepsilon(\mathbf{k}) \end{pmatrix}, \quad (51)$$

with

$$\Delta(\mathbf{k}) = \begin{cases} \psi(\mathbf{k}) = \psi(-\mathbf{k}) & \text{for spin-singlet} \\ d_z(\mathbf{k}) = -d_z(-\mathbf{k}) & \text{for spin-triplet} \end{cases}. \quad (52)$$

Here $c_{\mathbf{k}\sigma}$ ($c_{\mathbf{k}\sigma}^\dagger$) is the annihilation (creation) operator of electron with momentum \mathbf{k} and spin σ , and $\varepsilon(\mathbf{k})$ the energy dispersion in the normal state. ($\varepsilon(\mathbf{k}) = \varepsilon(-\mathbf{k})$.) The time-reversal invariance implies that the gap function $\Delta(\mathbf{k})$ can be chosen to be real.

Diagonalizing the 2×2 BdG Hamiltonian $\mathcal{H}(\mathbf{k})$, we find that the quasiparticle spectrum $E(\mathbf{k})$ is given by $E(\mathbf{k}) = \pm \sqrt{\varepsilon(\mathbf{k})^2 + \Delta(\mathbf{k})^2}$. The gap of the system closes when the following condition is satisfied,

$$\varepsilon(\mathbf{k}) = 0, \quad \Delta(\mathbf{k}) = 0. \quad (53)$$

The negative energy state is fully occupied in the ground state.

We will identify the Hilbert space of this model. Since the BdG Hamiltonian is a 2×2 real symmetric matrix, the occupied state $|u(\mathbf{k})\rangle$ is a two component real vector with unit norm, which is given by

$$|u(\mathbf{k})\rangle = \begin{pmatrix} \cos \alpha(\mathbf{k}) \\ \sin \alpha(\mathbf{k}) \end{pmatrix}, \quad (54)$$

with an angle variable $\alpha(\mathbf{k})$. Because of a sign ambiguity in the occupied state, $|u(\mathbf{k})\rangle \rightarrow -|u(\mathbf{k})\rangle$, the angle variable $\alpha(\mathbf{k})$ should be identified with $\alpha(\mathbf{k}) + \pi$,

$$\alpha(\mathbf{k}) \sim \alpha(\mathbf{k}) + \pi. \quad (55)$$

In other words, the state with $\alpha(\mathbf{k})$ is physically the same as that with $\alpha(\mathbf{k}) + \pi$. Thus, instead of the eigenstate (54) itself, the physical state should be rather characterized by the unit vector,

$$\begin{pmatrix} \cos 2\alpha(\mathbf{k}) \\ \sin 2\alpha(\mathbf{k}) \end{pmatrix}. \quad (56)$$

The Hilbert space of the model is a one-dimensional sphere S^1 parameterized by the vector (56).

Now let us see how to define a topological number in this class of superconductors. We first note a subtlety of the system. As was discussed in §3.2, a fully gapped system is needed to obtain a well-defined bulk topological number. However, for superconducting states described by eq.(51), we often have a nodal superconductor such as two-dimensional p_x -wave superconductor or a high T_c cuprate. This is because the gap closing condition (53) is rather easily met in the two- or three-dimensional momentum space. To resolve this problem, we regard the momenta in certain directions as parameters of the system. Fixing them to certain values, we effectively have a “fully gapped one-dimensional system”, in which a bulk topological number can be defined. For concreteness, in the following arguments, we fix the momenta in the y and z -directions, and consider the system as a one-dimensional system extended in the x -direction. (See

Fig.25.)

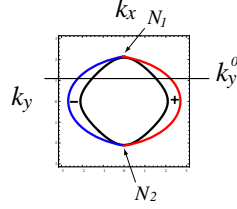


Fig. 25. (Color online) Two-dimensional p_x -wave superconductor. Since nodes exist at N_1 and N_2 , the system is not gapful in the whole of the BZ. However, if we restrict ourself to the momentum space with a fixed $k_y = k_y^0$, we obtain a fully gapped one-dimensional system. [Reproduced from Fig.6 of Bussei Kenkyu **94** 311 (2010) by Sato.]

In the one-dimensional gapped system, the BZ is $-\pi < k_x \leq \pi$. It is essentially a one-dimensional sphere (circle) S^1 since $k_x = \pi$ is identified with $k_x = -\pi$. Thus the occupied state $|u(\mathbf{k})\rangle$ maps S^1 of the Brillouin zone to S^1 of the Hilbert space. Counting how many times the image of the BZ winds around the Hilbert space, we can define a topological number. Every time the image winds around the Hilbert space, $2\alpha(\mathbf{k})$ in eq.(56) changes by 2π . So the winding number w_{1d} is given by

$$w_{1d}(k_y, k_z) = \frac{1}{2\pi} \int_{-\pi}^{\pi} dk_x \partial_{k_x} (2\alpha(\mathbf{k})). \quad (57)$$

Using $\theta(\mathbf{k})$ defined by

$$\begin{aligned} \cos \theta(\mathbf{k}) &= \frac{\varepsilon(\mathbf{k})}{\sqrt{\varepsilon(\mathbf{k})^2 + \Delta(\mathbf{k})^2}}, \\ \sin \theta(\mathbf{k}) &= \frac{\Delta(\mathbf{k})}{\sqrt{\varepsilon(\mathbf{k})^2 + \Delta(\mathbf{k})^2}}, \end{aligned} \quad (58)$$

we can show that the occupied state $|u(\mathbf{k})\rangle$ is given by

$$|u(\mathbf{k})\rangle = \begin{pmatrix} \cos[(\theta(\mathbf{k}) - \pi)/2] \\ \sin[(\theta(\mathbf{k}) - \pi)/2] \end{pmatrix}. \quad (59)$$

Thus, we obtain $\alpha(\mathbf{k}) = \theta(\mathbf{k})/2 - \pi/2$. From this relation, the topological number w_{1d} can be rewritten in terms of the parameters of BdG Hamiltonian,

$$w_{1d} = \frac{1}{2\pi} \int_{-\pi}^{\pi} dk_x \varepsilon^{ab} m_a(\mathbf{k}) \partial_{k_x} m_b(\mathbf{k}), \quad (60)$$

where $m_a(\mathbf{k})$ is given by

$$m_1(\mathbf{k}) = \frac{\varepsilon(\mathbf{k})}{\sqrt{\varepsilon(\mathbf{k})^2 + \Delta(\mathbf{k})^2}},$$

$$m_2(\mathbf{k}) = \frac{\Delta(\mathbf{k})}{\sqrt{\varepsilon(\mathbf{k})^2 + \Delta(\mathbf{k})^2}}. \quad (61)$$

Then, the above integral is evaluated as a simple sum^{160,161,163)}

$$w_{1d} = -\frac{1}{2} \sum_{k_x; \varepsilon(\mathbf{k})=0} \text{sgn}[\Delta(\mathbf{k})] \cdot \text{sgn}[\partial_{k_x} \varepsilon(\mathbf{k})], \quad (62)$$

where the summation is taken for k_x with $\varepsilon(\mathbf{k}) = 0$. From the bulk-edge correspondence, there exist the gapless states on the boundary when w_{1d} is nonzero.

We note here that the resultant ABS has flat dispersion. This is because the topological number $w_{1d}(k_y, k_z)$ is nonzero in a finite region of (k_y, k_z) since it cannot change unless the integration path intersects a gap node. From the bulk-edge correspondence, this implies that the zero energy state also exists in a finite region of (k_y, k_z) . In other words, the ABS corresponding to nonzero w_{1d} has a flat dispersion.

For the flat dispersion ABS, the bulk-edge correspondence is nicely summarized in the form of the index theorem.^{161,164)} Since the BdG Hamiltonian (51) has the so called chiral symmetry

$$\{\mathcal{H}(\mathbf{k}), \sigma_y\} = 0, \quad (63)$$

it can be shown that the ZEABS is an eigenstate of the chirality operator σ_y . Then, denoting the number of the zero energy states with the eigenvalue $\sigma_y = \pm 1$ as $n_0^{(\pm)}$, we can relate the index $n_0^{(+)} - n_0^{(-)}$ to the winding number w_{1d} in the form of the index theorem,

$$w_{1d} = n_0^{(+)} - n_0^{(-)} \quad (64)$$

or

$$w_{1d} = n_0^{(-)} - n_0^{(+)}, \quad (65)$$

where eq.(64) (eq.(65)) holds for the ABS on the surface of the semi-infinite superconductor on $x > 0$ ($x < 0$).¹⁶⁵⁾

Now we will see that the bulk-edge correspondence reproduces the criterion of the ZEABS proposed previously.^{160,161)} In the case where the topology of the Fermi surface is simple as illustrated in Fig.26, it has been known that if the gap function satisfies

$$\Delta(k_x, k_y, k_z) \Delta(-k_x, k_y, k_z) < 0, \quad (66)$$

then a ZEABS exists on the boundary perpendicular to x -direction.^{25,27)} In other words, a sign change of the gap function with respect to $k_x \rightarrow -k_x$ implies the existence of the ZEABS on a surface perpendicular to the x -direction. The bulk-edge correspondence

reproduces this result exactly: Equation (62) leads to

$$w_{1d} = -\frac{1}{2} \left[\text{sgn}[\partial_{k_x} \varepsilon(-k_x^0, k_y, k_z)] \text{sgn}[\Delta(-k_x^0, k_y, k_z)] \right. \\ \left. + \text{sgn}[\partial_{k_x} \varepsilon(k_x^0, k_y, k_z)] \text{sgn}[\Delta(k_x^0, k_y, k_z)] \right], \quad (67)$$

where $(\pm k_x^0, k_y, k_z)$ denotes the intersection points between the integral path of $w_{1d}(k_y)$ and the Fermi surface. See Fig. 26. Noticing that $\text{sgn}[\partial_{k_x} \varepsilon(k_x^0, k_y, k_z)] = -\text{sgn}[\partial_{k_x} \varepsilon(-k_x^0, k_y, k_z)]$, we can rewrite this as

$$w_{1d} = -\frac{1}{2} \text{sgn}[\partial_{k_x} \varepsilon(-k_x^0, k_y, k_z)] \\ \times \left[\text{sgn}[\Delta(-k_x^0, k_y, k_z)] - \text{sgn}[\Delta(k_x^0, k_y, k_z)] \right]. \quad (68)$$

Thus the topological number w_{1d} becomes nonzero only when the gap function satisfies eq.(66), which means that the bulk-edge correspondence reproduces the previous one in this particular simple case.

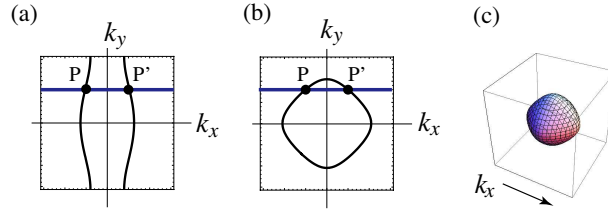


Fig. 26. (Color online) Fermi surfaces with simple topology in (a) quasi-one-dimensional system, (b) quasi-two-dimensional one, and (c) three dimensional one. The thick blue lines denote the integral path of w_{1d} . For simplicity, we illustrate the integral path only in (a) and (b). For each case, the integral path gets across the Fermi surface only twice at $k_x = \pm k_x^0$. In (a) and (b), P and P' denote the intersection point $(-k_x^0, k_y)$ and (k_x^0, k_y) , respectively. [Reproduced from Fig.4 of arXiv:1102.1322 to appear in Phys. Rev B by Sato et al.]

It should be noted here that the bulk-edge correspondence does not merely reproduce the known criterion, but is more informative. It is also applicable to more complicated cases in which the previous criterion does not work. Such examples were presented in refs.¹⁶⁰⁾ and¹⁶¹⁾

As a concrete example, we first consider the two-dimensional d_{xy} -wave superconductor where $\varepsilon(\mathbf{k})$ and $\Delta(\mathbf{k})$ in eq.(51) are given by

$$\varepsilon(\mathbf{k}) = \frac{\mathbf{k}^2}{2m} - \mu, \quad \Delta(\mathbf{k}) = \Delta_0 \frac{k_x k_y}{\mathbf{k}^2}. \quad (69)$$

Here Δ_0 is a positive constant. From eq.(62), the topological number $w_{1d}(k_y)$ is evaluated

as

$$w_{1d}(k_y) = \begin{cases} -1, & \text{for } 0 < k_y < k_F \\ 1, & \text{for } 0 > k_y > -k_F \\ 0, & \text{for } |k_y| > k_F \end{cases}, \quad (70)$$

where $k_F = \sqrt{2m\mu}$ is the Fermi momentum. Thus the index theorems (64) and (65) imply the existence of the corresponding ZEABS.

The ZEABS is obtained by solving the BdG equation directly. For the semi-infinite d_{xy} superconductor on $x > 0$ with the boundary condition $|u(x=0, k_y)\rangle = 0$, the ZEABS on $x=0$ is given by²⁷⁾

$$|u_0(x)\rangle = C \begin{pmatrix} 1 \\ -i\text{sgn}k_y \end{pmatrix} e^{ik_y y} \sin(k_x x) e^{-x/\xi}, \quad (71)$$

where C is a normalization constant, $|k_y| < k_F$, $k_x = \sqrt{k_F^2 - k_y^2}$ and $\xi^{-1} = m\Delta_0 k_y / k_F^2$. Since the ABS is an eigenstate of σ_y with eigenvalue $\sigma_y = -1$ ($\sigma_y = 1$) for $0 < k_y < k_F$ ($0 > k_y > -k_F$), it is found that $n_0^{(+)} = 0$ and $n_0^{(-)} = 1$ for $0 < k_y < k_F$ ($n_0^{(+)} = 1$ and $n_0^{(-)} = 0$ for $0 > k_y > -k_F$). When $|k_y| > k_F$, no ZEABS is found, thus $n_0^{(+)} = n_0^{(-)} = 0$. As summarized in Table VII (a), the index theorem (64) holds.

On the other hand, for the semi-infinite d_{xy} superconductor on $x < 0$, the ZEABS on the surface at $x=0$ is given by

$$|u_0(x)\rangle = C \begin{pmatrix} 1 \\ i\text{sgn}k_y \end{pmatrix} e^{ik_y y} \sin(k_x x) e^{x/\xi}. \quad (72)$$

Thus, the index theorem (65) holds in this case. (See also Table VII (b).)

Now consider the two-dimensional p_x -wave superconductor. The gap function is $\Delta(\mathbf{k}) = \Delta_0 k_x / k$ with $k = \sqrt{\mathbf{k}^2}$ and $\varepsilon(\mathbf{k})$ is the same as that in eq.(69). For the p_x -wave superconductor, we have

$$w_{1d}(k_y) = \begin{cases} -1, & \text{for } |k_y| < k_F \\ 0, & \text{for } |k_y| > k_F \end{cases}, \quad (73)$$

from eq.(62). Correspondingly, if $|k_y| < k_F$, we obtain the following ZEABS on $x=0$

$$|u(x, k_y)\rangle = C \begin{pmatrix} 1 \\ -i \end{pmatrix} e^{ik_y y} \sin(k_x x) e^{-x/\xi_p}, \quad (74)$$

(a) d_{xy} -wave superconductor on $x > 0$				
k_y	$n_0^{(+)}$	$n_0^{(-)}$	$n_0^{(+)} - n_0^{(-)}$	$w_{1d}(k_y)$
$0 < k_y < k_F$	0	1	-1	-1
$0 > k_y > -k_F$	1	0	1	1
$ k_y > k_F$	0	0	0	0

(b) d_{xy} -wave superconductor on $x < 0$				
k_y	$n_0^{(+)}$	$n_0^{(-)}$	$n_0^{(+)} - n_0^{(-)}$	$w_{1d}(k_y)$
$0 < k_y < k_F$	1	0	1	-1
$0 > k_y > -k_F$	0	1	-1	1
$ k_y > k_F$	0	0	0	0

Table VII. The number $n_0^{(\pm)}$ of the zero energy ABSs with the $\sigma_y = \pm 1$ for (a) the semi-infinite d_{xy} -wave superconductor on $x > 0$ and (b) that on $x < 0$. For comparison, we also show the topological number $w_{1d}(k_y)$ given in eq.(70). The index theorem (64) and (65) hold in (a) and (b), respectively.

for the semi-infinite p_x -wave superconductor on $x > 0$, and

$$|u(x, k_y)\rangle = C \begin{pmatrix} 1 \\ i \end{pmatrix} e^{ik_y y} \sin(k_x x) e^{x/\xi_p}, \quad (75)$$

for the semi-infinite p_x -wave superconductor on $x < 0$. Here C is a normalization constant, $k_x = \sqrt{k_F^2 - k_y^2}$ and $\xi_p^{-1} = m\Delta_0/k_F$. It is also found that these solutions are the eigenstates of σ_y with the eigenvalue $\sigma_y = -1$ and $\sigma_y = 1$, respectively. Thus $n_0^{(+)}$ and $n_0^{(-)}$ are summarized as Table VIII (a) and (b). We confirm the relations (64) and (65), respectively again.

Finally, we would like to point out the relevance between the topological structures of the ABS and the odd-frequency pairing. The surface odd-frequency pair amplitude discussed in §2.2.2 is rewritten as

$$\hat{f}_1 = \frac{i \text{sgn}(k_y) \Delta_0 |k_x| |k_y|}{\omega_n \mathbf{k}^2} \quad (76)$$

for spin-singlet d_{xy} -wave superconductor and

$$\hat{f}_1 = \frac{i \Delta_0 |k_x|}{\omega_n \sqrt{\mathbf{k}^2}}, \quad (77)$$

for spin-triplet p -wave superconductor by using $k_x = k_F \cos \theta$ and $k_y = k_F \sin \theta$. As well as the wave function of ABS of spin-singlet d_{xy} and spin-triplet p_x -wave superconductor derived in this section, the factor $\text{sgn}k_y$ exists only for spin-singlet d_{xy} -wave

(a) p_x -wave superconductor on $x > 0$				
k_y	$n_0^{(+)}$	$n_0^{(-)}$	$n_0^{(+)} - n_0^{(-)}$	$w_{1d}(k_y)$
$ k_y < k_F$	0	1	-1	-1
$ k_y > k_F$	0	0	0	0

(b) p_x -wave superconductor on $x < 0$				
k_y	$n_0^{(+)}$	$n_0^{(-)}$	$n_0^{(+)} - n_0^{(-)}$	$w_{1d}(k_y)$
$ k_y < k_F$	1	0	1	-1
$ k_y > k_F$	0	0	0	0

Table VIII. The number $n_0^{(\pm)}$ of the zero energy ABSs with the $\sigma_y = \pm 1$ for (a) the semi-infinite p_x -wave superconductor on $x > 0$ and (b) that on $x < 0$, respectively. For comparison, we also show the topological number $w_{1d}(k_y)$ given in eq.(73). The index theorem (64) and (65) hold in (a) and (b), respectively.

case. This factor decides the difference of the parity of induced Cooper pair. Next, we consider a two-dimensional semi-infinite superconductor in $x < 0$. The corresponding pair amplitude at surface ($x = 0$) is given by

$$\hat{f}_1 = -\frac{i \operatorname{sgn}(k_y) \Delta_0 |k_x| |k_y|}{\omega_n \mathbf{k}^2} \quad (78)$$

for spin-singlet d_{xy} -wave superconductor and

$$\hat{f}_1 = -\frac{i \Delta_0 |k_x|}{\omega_n \sqrt{\mathbf{k}^2}} \quad (79)$$

for spin-triplet p_x -wave one, respectively. Comparing eq. (76) [(77)] with (78) [(79)], it is evident that the difference between them is the presence of $-\operatorname{sgn}$. The present $-\operatorname{sgn}$ exactly corresponds to the different values of $n_0^{(+)}$ and $n_0^{(-)}$ between case (a) and case (b) in Tables VII and VIII.

3.4 Time-reversal breaking superconductors and Majorana fermion

Next, consider time-reversal symmetry breaking superconducting states. The analogy between the quantum Hall states and superconducting states is direct in this case.^{153,154,166,167)} The simplest one is a superconductor with a single complex gap function. As well as the previous subsection, it is realized when the spin-orbit interaction is negligible, and the Cooper pairs preserve S_z , but break the time-reversal invariance in this time. Also, it includes a spinless superconductor where the Cooper pairs are formed by fully spin polarized electrons. We consider the latter case first.

For the spinless superconductor, the Hamiltonian is given by

$$\mathcal{H} = \frac{1}{2} \sum_{\mathbf{k}} \left(c_{\mathbf{k}\uparrow}^\dagger, c_{-\mathbf{k}\uparrow} \right) \mathcal{H}(\mathbf{k}) \begin{pmatrix} c_{\mathbf{k}\uparrow} \\ c_{-\mathbf{k}\uparrow}^\dagger \end{pmatrix}, \quad (80)$$

with

$$\mathcal{H}(\mathbf{k}) = \begin{pmatrix} \varepsilon(\mathbf{k}) & \Delta(\mathbf{k}) \\ \Delta^*(\mathbf{k}) & -\varepsilon(\mathbf{k}) \end{pmatrix}. \quad (81)$$

Here we assume that the electron is fully polarized with up spin. From the Fermi statistics, $\Delta(\mathbf{k})$ is an odd function of \mathbf{k} . Thus the superconducting state is spin-triplet.

The above BdG Hamiltonian $\mathcal{H}(\mathbf{k})$ is a 2×2 hermitian matrix, so the occupied state $|u(\mathbf{k})\rangle$ is a two-dimensional complex vector with unit norm,

$$|u(\mathbf{k})\rangle = \begin{pmatrix} \cos \alpha(\mathbf{k}) e^{-i\beta(\mathbf{k})} \\ \sin \alpha(\mathbf{k}) e^{-i\gamma(\mathbf{k})} \end{pmatrix}, \quad (82)$$

where $\alpha(\mathbf{k})$, $\beta(\mathbf{k})$ and $\gamma(\mathbf{k})$ are angle variables with $0 \leq \alpha(\mathbf{k}) < \pi/2$, $0 \leq \beta(\mathbf{k}) < 2\pi$ and $0 \leq \gamma(\mathbf{k}) < 2\pi$. Using a phase ambiguity of the eigenstate,

$$|u(\mathbf{k})\rangle \rightarrow e^{i\theta(\mathbf{k})} |u(\mathbf{k})\rangle, \quad (83)$$

we can set $\gamma(\mathbf{k}) = 0$ in eq.(82). To identify the Hilbert space, we calculate the expectation value of the Pauli matrices σ_i ,

$$\begin{aligned} & (\langle u(\mathbf{k}) | \sigma_x | u(\mathbf{k}) \rangle, \langle u(\mathbf{k}) | \sigma_y | u(\mathbf{k}) \rangle, \langle u(\mathbf{k}) | \sigma_z | u(\mathbf{k}) \rangle) \\ &= (\sin 2\alpha(\mathbf{k}) \cos \beta(\mathbf{k}), \sin 2\alpha(\mathbf{k}) \sin \beta(\mathbf{k}), \cos 2\alpha(\mathbf{k})). \end{aligned} \quad (84)$$

The vector (84) parameterizes the two-dimensional sphere S^2 . Thus we have a one-to-one correspondence between the occupied state $|u(\mathbf{k})\rangle$ and a point on S^2 . In other words, the Hilbert space in this model is S^2 .

In two dimensions, the BZ is topologically equivalent to the two-dimensional torus T^2 . Thus the occupied state $|u(\mathbf{k})\rangle$ maps T^2 of the BZ into S^2 of the Hilbert space. Since the surface element of S^2 of the Hilbert space is

$$\sin 2\alpha d(2\alpha) d\beta, \quad (85)$$

the winding number of the image of the BZ is evaluated as

$$w_{2d} = \frac{1}{4\pi} \int_{-\pi}^{\pi} \int_{-\pi}^{\pi} dk_x dk_y \sin[2\alpha(\mathbf{k})] \epsilon^{ij} \partial_{k_i} 2\alpha(\mathbf{k}) \partial_{k_j} \beta(\mathbf{k}). \quad (86)$$

Introducing $\theta(\mathbf{k})$ and $\varphi(\mathbf{k})$ as

$$\begin{aligned}\cos \theta(\mathbf{k}) &= \frac{\varepsilon(\mathbf{k})}{\sqrt{\varepsilon(\mathbf{k})^2 + |\Delta(\mathbf{k})|^2}}, \\ \sin \theta(\mathbf{k}) e^{i\varphi(\mathbf{k})} &= \frac{\Delta(\mathbf{k})}{\sqrt{\varepsilon(\mathbf{k})^2 + |\Delta(\mathbf{k})|^2}},\end{aligned}\quad (87)$$

the occupied state is given by

$$|u(\mathbf{k})\rangle = \begin{pmatrix} \cos(\theta(\mathbf{k})/2 - \pi/2) e^{i\varphi(\mathbf{k})} \\ \sin(\theta(\mathbf{k})/2 - \pi/2) \end{pmatrix}, \quad (88)$$

which leads to

$$\alpha(\mathbf{k}) = \theta(\mathbf{k})/2 - \pi/2, \quad \beta(\mathbf{k}) = -\varphi(\mathbf{k}). \quad (89)$$

From this, the winding number is recast into

$$\begin{aligned}w_{2d} &= -\frac{1}{8\pi} \int_{-\pi}^{\pi} \int_{-\pi}^{\pi} dk_x dk_y \epsilon^{ij} \epsilon^{abc} m_a(\mathbf{k}) \partial_{k_i} m_b(\mathbf{k}) \partial_{k_j} m_c(\mathbf{k}),\end{aligned}\quad (90)$$

where $m_a(\mathbf{k})$ is given by

$$\begin{aligned}m_1(\mathbf{k}) &= \frac{\text{Re}\Delta(\mathbf{k})}{\sqrt{\varepsilon(\mathbf{k})^2 + |\Delta(\mathbf{k})|^2}}, \\ m_2(\mathbf{k}) &= \frac{\text{Im}\Delta(\mathbf{k})}{\sqrt{\varepsilon(\mathbf{k})^2 + |\Delta(\mathbf{k})|^2}}, \\ m_3(\mathbf{k}) &= \frac{\varepsilon(\mathbf{k})}{\sqrt{\varepsilon(\mathbf{k})^2 + |\Delta(\mathbf{k})|^2}}.\end{aligned}\quad (91)$$

Finally, this can be evaluated as a simple sum^{160,163)}

$$w_{2d} = -\frac{1}{2} \sum_{\Delta(\mathbf{k})=0} \text{sgn}[\varepsilon(\mathbf{k})] \text{sgn}[\det \partial_{k_i} \Delta_j(\mathbf{k})], \quad (92)$$

with $\Delta_1(\mathbf{k}) = \text{Re}\Delta(\mathbf{k})$ and $\Delta_2(\mathbf{k}) = \text{Im}\Delta(\mathbf{k})$.¹⁶⁸⁾ Here the summation is taken for (k_x, k_y) with $\Delta(\mathbf{k}) = 0$. When w_{2d} is not zero, we have a chiral edge state on the boundary.

In Fig 27, we illustrate the quasiparticle spectra of spinless chiral p -wave superconductors.¹⁶⁰⁾ Here we have used the lattice model with

$$\begin{aligned}\varepsilon(\mathbf{k}) &= -2t_x \cos k_x - 2t_y \cos k_y - \mu, \\ \Delta(\mathbf{k}) &= \Delta_0(\sin k_x + i \sin k_y),\end{aligned}\quad (93)$$

and the quasiparticle spectra are calculated under the open boundary condition at $x = 0$ and $x = L$ in the x -direction. The resultant winding number w_{2d} depends on the topology of the Fermi surface, and correspondingly, the gapless edge modes also depend on the topology of the Fermi surface. For a two-dimensional Fermi surface, we find that $w_{2d} = 1$, so we have a single chiral edge mode on each side of boundary. The relation between the Fermi surface topology and the winding number w_{2d} (and the corresponding edge state) is a general property of spin-triplet superconductors,¹⁶³⁾ as will be explained in §3.7.

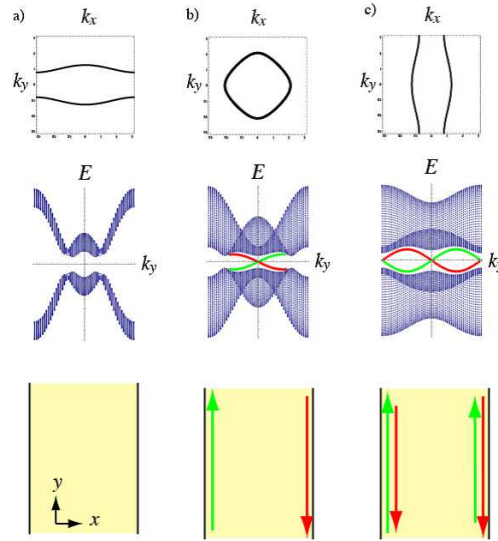


Fig. 27. (Color online) Edge states in spinless chiral $p + ip$ -wave superconductors given by eq.(93). We take (a) $t_x = 0.2$, $t_y = 1$, $\mu = -1$, $\Delta_0 = 0.5$, (b) $t_x = 1$, $t_y = 1$, $\mu = -1$, $\Delta_0 = 0.5$, and (c) $t_x = 1$, $t_y = 0.2$, $\mu = -1$, $\Delta_0 = 0.5$. (Top panels) Fermi surfaces in the normal states. (Middle panels) Quasiparticle spectra of the corresponding superconducting state with edges at $x = 0$ and $x = L$. The gapless modes are localized on the edges. The winding number w_{2d} is (a) $w_{2d} = 0$, (b) $w_{2d} = 1$, and (c) $w_{2d} = 0$, respectively. (bottom panels) Schematic illustration of the corresponding edge state. The arrows indicate the direction of the group velocity of the edge modes.

As well as the edge state, we can apply the bulk-edge correspondence to the vortex in superconductors.^{153,169)} A vortex in a superconductor can be regarded as a hole in the bulk. Then, applying the bulk-edge correspondence to the edge of the hole, we find that there is a zero energy state in the vortex core when $w_{2d} \neq 0$. Some zero modes become non-zero mode when deforming the hole into a real vortex. When w_{2d} is odd, however, at least a single zero mode survives since the zero modes become massive in a pair due to the particle-hole symmetry. In particular, there is a single zero mode in a

vortex when $w_{2d} = \pm 1$.¹⁶⁹⁻¹⁷³⁾

Here we would like to mention that the analogy between the quantum Hall states and superconducting states is direct in this case. The quantum Hall states are topologically characterized by nonzero Chern number. For comparison, let us evaluate the Chern number in this model. By using the occupied state (82), the Chern number is given as

$$C_1 = \frac{1}{2\pi} \int_{-\pi}^{\pi} \int_{-\pi}^{\pi} dk_x dk_y \epsilon^{ij} \partial_{k_i} \mathcal{A}_j(\mathbf{k}). \quad (94)$$

where $\mathcal{A}_i(\mathbf{k}) = i\langle u(\mathbf{k}) | \partial_{k_i} u(\mathbf{k}) \rangle$. From a straightforward calculation, we obtain the relation

$$\epsilon^{ij} \partial_{k_i} \mathcal{A}_j = -\frac{1}{4} \epsilon^{ij} \epsilon^{abc} m_a \partial_{k_i} m_b \partial_{k_j} m_c. \quad (95)$$

This implies that winding number w_{2d} is nothing but the Chern number, $w_{2d} = C_1$.

In spite of the analogy above, there are differences between them. The $U(1)$ electromagnet gauge symmetry is spontaneously broken in the superconductor while it is not in the quantum Hall states. Thus no quantized Hall current is carried by the edge state in the former. Furthermore, the quasiparticle $\Psi_{\mathbf{k}}$ in the superconductor

$$\Psi_{\mathbf{k}} = \begin{pmatrix} c_{\mathbf{k}\uparrow} \\ c_{-\mathbf{k}\uparrow}^\dagger \end{pmatrix}, \quad (96)$$

satisfies the additional condition,

$$\Psi_{-\mathbf{k}}^\dagger = \Gamma \Psi_{\mathbf{k}}, \quad \Gamma = \begin{pmatrix} 0 & 1 \\ 1 & 0 \end{pmatrix}, \quad (97)$$

The condition (97) is called the Majorana condition. It means that the quasiparticle $\Psi_{\mathbf{k}}$ is essentially the same as its antiparticle $\Psi_{-\mathbf{k}}^\dagger$. As a result, the edge state in the superconductor is a $1+1$ dimensional Majorana chiral fermion, not a chiral fermion in the quantum Hall state.

An important consequence of the Majorana condition is that it gives rise to the non-Abelian statistics of the vortices.^{153,174)} As shown in the above, for the spinless chiral p -wave superconductor, there is a single zero mode γ_0 in the vortex core. The zero mode satisfies the anticommutation relation

$$\{\gamma_0^\dagger, \gamma_0\} = 1. \quad (98)$$

At the same time, the Majorana condition reads

$$\gamma_0 = \gamma_0^\dagger. \quad (99)$$

Thus γ_0 is neither the annihilation operator nor the creation operator. To obtain the well-defined creation operator, we need a pair of vortices. Using the zero mode $\gamma_0^{(i)}$ of the vortex i ($i = 1, 2$), we can construct the creation operator γ^\dagger as

$$\gamma^\dagger = \frac{\gamma_0^{(1)} + i\gamma_0^{(2)}}{\sqrt{2}}, \quad (100)$$

which satisfies

$$\gamma \neq \gamma^\dagger, \quad \{\gamma, \gamma^\dagger\} = 1. \quad (101)$$

Since the vortex 1 and 2 are separated from each other, the creation operator is defined non-locally. This non-locality changes the statistics of vortex drastically. Indeed, the vortices obey the non-Abelian statistics.

To see the non-Abelian statistics of the vortices, consider the vortex 1 and 2 illustrated in Fig.28. Then, the vortex 3 encircles the vortex 2 and it goes far away. In classical theory, the final configuration is completely the same as the initial one. In quantum theory, however, the final state can be completely different from the initial one.

Suppose that the initial state $|0\rangle$ is annihilated by γ , $\gamma|0\rangle = 0$. When the vortex 3 encircles the vortex 2, the vortex 2 also encircles the vortex 3 in the rest frame of the vortex 2. Thus the zero mode $\gamma_0^{(2)}$ in the vortex 2 gets the Aharonov-Bohm phase in this process. If an electron (a hole) moves around the vortex 3, the Aharonov-Bohm phase is $e^{ie\Phi_0} = -1$ ($e^{-ie\Phi_0} = -1$), where Φ_0 is the unit magnetic flux of the vortex, $\Phi_0 = \pi/e$. Thus the zero mode $\gamma_0^{(2)}$ gets the same factor,

$$\gamma_0^{(2)} \rightarrow -\gamma_0^{(2)}, \quad (102)$$

since it is a superposition of an electron and a hole. This means that γ changes as

$$\gamma = \frac{\gamma_0^{(1)} + i\gamma_0^{(2)}}{\sqrt{2}} \rightarrow \gamma^\dagger = \frac{\gamma_0^{(1)} - i\gamma_0^{(2)}}{\sqrt{2}}. \quad (103)$$

Therefore, the final state is annihilated by γ^\dagger , $\gamma^\dagger|1\rangle = 0$, not by γ . The final state $|1\rangle$ is completely different from the initial one $|0\rangle$. Indeed, there is no overlap between them, *i.e.* $\langle 0|1\rangle = 0$.

Note that such an exotic phenomenon never occurs if the vortices is boson, fermion, or Abelian anyon. For these cases, the encircling process considered here results in a overall phase at most, so the final state is essentially the same as the initial one. In other words, the above phenomenon is a result of the non-Abelian statistics of vortices. A particle obeying the non-Abelian statistics is called non-Abelian anyon, and a

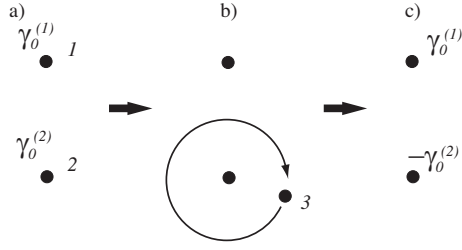


Fig. 28. Movement of the vortex 3 around the vortex 2.

topological phase with non-Abelian anyons is called non-Abelian topological phase.

Up to now, we have focused on the spinless superconductor. Now consider the spinful time-reversal breaking superconductor. An example is a chiral p -wave superconductor in Sr_2RuO_4 or in a ^3He A-phase superfluid thin film. When the spin-orbit interaction is negligible and the Cooper pairs preserve a spin in a certain direction, say S_z , the Hamiltonian is given by

$$\mathcal{H} = \sum_{\mathbf{k}} \left(c_{\mathbf{k}\uparrow}^\dagger, c_{-\mathbf{k}\downarrow} \right) \mathcal{H}(\mathbf{k}) \begin{pmatrix} c_{\mathbf{k}\uparrow} \\ c_{-\mathbf{k}\downarrow}^\dagger \end{pmatrix}, \quad (104)$$

with $\mathcal{H}(\mathbf{k})$ in eq.(81). The gap function $\Delta(\mathbf{k})$ is given by eq.(52). Since $\mathcal{H}(\mathbf{k})$ is the same as that for the spinless superconductor, the Hilbert space is also the same, that is S^2 . Thus the topological number characterizing the state is the same winding number w_{2d} . The difference between the spinless superconductor and the spinful one is the Majorana condition. For the spinful superconductor, the quasiparticle operator $\Psi_{\mathbf{k}}$

$$\Psi_{\mathbf{k}} = \begin{pmatrix} c_{\mathbf{k}\uparrow} \\ c_{-\mathbf{k}\downarrow}^\dagger \end{pmatrix} \quad (105)$$

in eq.(104) does not satisfy the Majorana condition (97). Nevertheless, this does not imply that the Majorana fermion cannot appear in the spinful superconductor. Indeed, in a special kind of vortex called half-quantum vortex, the Majorana fermion appears.

The half-quantum vortex is realized in spinful spin-triplet superconductors, where the spin components of the gap function can rotate around vortex. Using this degrees of freedom, the half-quantum vortex has the following configuration,

$$\mathbf{d}(\mathbf{k}) = \Delta(\mathbf{k}, r) e^{i\theta/2} (\cos \theta/2, \sin \theta/2, 0), \quad (106)$$

where $\mathbf{d}(\mathbf{k})$ is the \mathbf{d} -vector of the spin-triplet gap function, r the distance from the vortex core, and θ the angle around the vortex. Since this configuration does not preserve S_z , its BdG Hamiltonian is not given in the form of eq.(104). Instead, we can treat the

system as two copies of spinless superconductors. Indeed, the matrix representation of the gap function leads to

$$\Delta = \mathbf{d}(\mathbf{k}, r) \boldsymbol{\sigma} \sigma_y = \begin{pmatrix} -\Delta(\mathbf{k}, r) & 0 \\ 0 & \Delta(\mathbf{k}, r) e^{i\theta} \end{pmatrix}, \quad (107)$$

so there is no mixing between the different spin sectors. Then, each spin sector is the spinless superconductor described by eq.(80). (For the down spin sector, $c_{\mathbf{k}\uparrow}$ and $c_{\mathbf{k}\uparrow}^\dagger$ should be replaced by $c_{\mathbf{k}\downarrow}$ and $c_{\mathbf{k}\downarrow}^\dagger$, respectively.) Equation (107) implies that only the down-spin sector has a vortex. Therefore, we can regard as the half quantum vortex as the vortex in spinless superconductor with down spin. This means that if w_{2d} is odd, there is a Majorana zero mode in the half-quantum vortex. Thus the half-quantum vortex can obey the non-Abelian statistics. Recently, an experimental evidence of the half-quantum vortex in Sr_2RuO_4 has been reported.¹⁷⁵⁾ Also, a half-quantum vortex is expected to exist in a thin film of ^3He A phase.^{176,177)}

3.5 Helical edge modes in TI/QSHE

In this subsection, we consider the band insulators without the superconductivity from the viewpoint of the topology. For time-reversal invariant systems, new topological phases arise when the spin-orbit interaction is strong enough. Here we review briefly such states, the quantum spin Hall states^{178–181)} and its three dimensional generalization, topological insulators.^{182–184)}

The quantum spin Hall state is easily understood as a pair of the integer quantum Hall states if S_z is a good quantum number. Consider the following two-dimensional system preserving S_z ,

$$\mathcal{H}(\mathbf{k}) = \begin{pmatrix} \mathcal{H}_+(\mathbf{k}) & 0 \\ 0 & \mathcal{H}_-(\mathbf{k}) \end{pmatrix}, \quad (108)$$

where $\mathcal{H}_+(\mathbf{k})$ ($\mathcal{H}_-(\mathbf{k})$) is the Hamiltonian for up-spin (down-spin) electron. Here we suppose that the spin-orbit interaction works as a kind of magnetic field, and each spin sector realizes an integer quantum Hall state with the Hall conductance $\sigma_H^{(\sigma)} = -C_1^{(\sigma)} e^2/h$ ($\sigma = \pm$). Due to the time-reversal invariance, the Chern numbers of the two spin sectors are opposite from each other, $C_1^{(+)} = -C_1^{(-)}$. Thus, the spin Hall conductance $\sigma_{sH} = \sigma_H^{(+)} - \sigma_H^{(-)}$ is quantized, while the total Hall conductance, $\sigma_H = \sigma_H^{(+)} + \sigma_H^{(-)}$, is zero. Correspondingly, there exist $C_1^{(+)}$ ($C_1^{(-)}$) gapless edge states with up-spin (down-spin) carrying the spin Hall conductance.

Now consider a time-reversal invariant perturbation which does not preserve S_z . The spin indices $\sigma = \pm$ turns into that of pseudo-spin α, β , and the Chern numbers $C_1^{(+)}$ and $C_1^{(-)}$ are replaced by $C_1^{(\alpha)}$ and $C_1^{(\beta)}$. Then, due to the spin mixing, most of the gapless edge states become massive. Nevertheless, if $C_1^{(\alpha)} (= -C_1^{(\beta)})$ is an odd number, at least one pair of gapless edge states survives: Because of the time-reversal invariance, the gapless states form a set of Kramers doublets. Since there is no mixing in the same Kramers doublet, the Kramers doublets become massive in a pair by the mixing with a different Kramers doublet. Thus, if there are an odd number of the Kramers doublets, which is realized when $C_1^{(\alpha)}$ is odd, at least one Kramers doublet of the gapless edge states remains massless without a partner.

As indicated by the above argument, for a generic time-reversal invariant system, where S_z is not a good quantum number, the quantum spin Hall state is characterized by the parity of $C_1^{(\alpha)}$, $(-1)^{\nu_{2d\text{TI}}} \equiv (-1)^{C_1^{(\alpha)}}$, which is called the \mathbf{Z}_2 invariant in the literature. Then the resultant gapless edge state is called the helical edge mode.

The topological insulator is a three dimensional generalization of the quantum spin Hall state.^{182–184} It is characterized by the four \mathbf{Z}_2 invariants $(\nu_0; \nu_1, \nu_2, \nu_3)$, which can take the value 0 or 1. When, $\nu_0 = 1$, the system is called strong topological insulator which supports an odd number of 2D Dirac fermions on the surface. When some of ν_1, ν_2 and ν_3 are 1, while $\nu_0 = 0$, the system is classified into weak topological insulator. In this case, an even number of Dirac fermions are on the surface, which can in principle be paired and gapped due to the disorder scattering etc., and are not stable. However, the weak topological insulator is still distinct from the conventional insulator with all ν 's being zero, as has been evidenced by one-dimensional channels appearing along the dislocation.¹⁸⁵

3.6 Helical superconductors and helical Majorana modes

There exist a topological state of superconductors which is analogous to the quantum spin Hall state. Such a superconductor is called the helical superconductor.^{155, 158} A representative example of the helical superconductor is two-dimensional Rashba non-centrosymmetric superconductors.^{159, 186} Let us see its basic property.

The model Hamiltonian of the Rashba superconductor in two dimensions is

$$\mathcal{H} = \mathcal{H}_{\text{kin}} + \mathcal{H}_{\text{SO}} + \mathcal{H}_{\text{pairing}},$$

$$\mathcal{H}_{\text{kin}} = \sum_{\mathbf{k}, \sigma} \varepsilon_{\mathbf{k}} c_{\mathbf{k}\sigma}^\dagger c_{\mathbf{k}\sigma} - \mu_{\text{B}} H_z \sum_{\mathbf{k}, \sigma} (\sigma_z)_{\sigma\sigma'} c_{\mathbf{k}\sigma}^\dagger c_{\mathbf{k}\sigma'}$$

$$\begin{aligned}\mathcal{H}_{\text{SO}} &= \alpha \sum_{\mathbf{k}, \sigma, \sigma'} \mathcal{L}_{\mathbf{k}} \cdot \boldsymbol{\sigma}_{\sigma\sigma'} c_{\mathbf{k}\sigma}^\dagger c_{\mathbf{k}\sigma'}, \\ \mathcal{H}_{\text{pairing}} &= \frac{1}{2} \sum_{\mathbf{k}\sigma\sigma'} \Delta_{\sigma\sigma'}(\mathbf{k}) c_{\mathbf{k}\sigma}^\dagger c_{-\mathbf{k}\sigma'}^\dagger + \text{h.c.},\end{aligned}\quad (109)$$

where $c_{\mathbf{k}\sigma}^\dagger$ ($c_{\mathbf{k}\sigma}$) is a creation (an annihilation) operator for an electron with momentum $\mathbf{k} = (k_x, k_y)$, spin σ . The energy band dispersion is $\varepsilon_{\mathbf{k}} = -2t(\cos k_x + \cos k_y) - \mu$ with the hopping parameter t and the chemical potential μ , and the Rashba spin-orbit coupling is $\mathcal{L}_{\mathbf{k}} = (\sin k_y, -\sin k_x)$. Because of parity mixing of Cooper pairs, the gap function $\Delta(\mathbf{k})$ has both a spin-triplet component $\mathbf{d}(\mathbf{k})$ and a spin-singlet one $\psi(\mathbf{k})$ at the same time, $\Delta(\mathbf{k}) = i\psi(\mathbf{k})\sigma_y + i\mathbf{d}(\mathbf{k})\boldsymbol{\sigma}\sigma_y$. Due to the strong spin-orbit coupling, the spin-triplet component $\mathbf{d}(\mathbf{k})$ is aligned with the Rashba coupling, $\mathbf{d}(\mathbf{k}) = \Delta_t \mathcal{L}_{\mathbf{k}}$.¹⁸⁷⁾ For the spin-singlet component $\psi(\mathbf{k})$, we assume an s -wave pairing, $\psi(\mathbf{k}) = \Delta_s$. The amplitudes $\Delta_{t,s}$ are chosen as real. The Zeeman coupling $\mu_B H_z \sum_{\mathbf{k}} (c_{\mathbf{k}\uparrow}^\dagger c_{\mathbf{k}\uparrow} - c_{\mathbf{k}\downarrow}^\dagger c_{\mathbf{k}\downarrow})$ with H_z a magnetic field in the z direction has been also introduced for later use.

Before going to study topological properties of the system, we first examine the bulk spectrum of the system. Topological nature of the system changes only when the gap of the bulk spectrum closes. The bulk spectrum $E(\mathbf{k})$ of the system is obtained by diagonalizing the following 4×4 matrix,

$$\begin{aligned}\mathcal{H}(\mathbf{k}) &= \\ &\begin{pmatrix} \varepsilon_{\mathbf{k}} - h\sigma_z + \alpha \mathcal{L}_{\mathbf{k}} \cdot \boldsymbol{\sigma} & i\Delta_s \sigma_y + i\Delta_t \mathcal{L}_{\mathbf{k}} \cdot \boldsymbol{\sigma} \sigma_y \\ -i\Delta_s \sigma_y - i\Delta_t \mathcal{L}_{\mathbf{k}} \sigma_y \cdot \boldsymbol{\sigma} & -\varepsilon_{\mathbf{k}} + h\sigma_z + \alpha \mathcal{L}_{\mathbf{k}} \cdot \boldsymbol{\sigma}^* \end{pmatrix},\end{aligned}\quad (110)$$

with $h = \mu_B H_z$, and we have

$$\begin{aligned}E(\mathbf{k}) &= \pm \left[\varepsilon_{\mathbf{k}}^2 + (\alpha^2 + \Delta_t^2) \mathcal{L}_{\mathbf{k}}^2 + h^2 + \Delta_s^2 \right. \\ &\quad \left. \pm 2\sqrt{(\varepsilon_{\mathbf{k}}\alpha + \Delta_s\Delta_t)^2 \mathcal{L}_{\mathbf{k}}^2 + (\varepsilon_{\mathbf{k}}^2 + \Delta_s^2)h^2} \right]^{1/2}\end{aligned}\quad (111)$$

The gap of the system closes only when

$$\begin{aligned}\varepsilon_{\mathbf{k}}^2 + (\alpha^2 + \Delta_t^2) \mathcal{L}_{\mathbf{k}}^2 + h^2 + \Delta_s^2 \\ = 2\sqrt{(\varepsilon_{\mathbf{k}}\alpha + \Delta_s\Delta_t)^2 \mathcal{L}_{\mathbf{k}}^2 + (\varepsilon_{\mathbf{k}}^2 + \Delta_s^2)h^2},\end{aligned}\quad (112)$$

which is equivalent to

$$\begin{aligned}\varepsilon_{\mathbf{k}}^2 + \Delta_s^2 &= h^2 + (\alpha^2 + \Delta_t^2) \mathcal{L}_{\mathbf{k}}^2, \\ \varepsilon_{\mathbf{k}} \Delta_t \mathcal{L}_{\mathbf{k}} &= \Delta_s \alpha \mathcal{L}_{\mathbf{k}}.\end{aligned}\tag{113}$$

When $\Delta_t \neq 0$, eq.(113) is met either when

$$\varepsilon_{\mathbf{k}} = \frac{\Delta_s}{\Delta_t} \alpha, \quad \left(1 + \frac{\alpha^2}{\Delta_t^2}\right) (\Delta_t^2 \mathcal{L}_{\mathbf{k}}^2 - \Delta_s^2) + h^2 = 0.\tag{114}$$

or

$$\varepsilon_{\mathbf{k}}^2 + \Delta_s^2 = h^2, \quad \mathcal{L}_{\mathbf{k}} = 0.\tag{115}$$

In the absence of the magnetic field, only eqs.(114) can be met and they are rewritten in simpler forms,

$$\varepsilon_{\mathbf{k}}^2 = \alpha^2 \mathcal{L}_{\mathbf{k}}^2, \quad \Delta_t^2 \mathcal{L}_{\mathbf{k}}^2 = \Delta_s^2.\tag{116}$$

Topological nature of the system does not change unless eq.(114) or eq.(115) (or eq.(116) when $H_z = 0$) is satisfied.

When $H_z = 0$, the system is time-reversal invariant, and the topological property is characterized by the \mathbf{Z}_2 invariant like the quantum spin Hall state. Below, we will show that if the spin-triplet pairing is stronger than the spin-singlet one, the \mathbf{Z}_2 number is non-trivial.

To see this, we adiabatically deform the Hamiltonian of the system without gap closing. This process does not change the \mathbf{Z}_2 topological number, since it changes only when the gap closes.^{159,186)} From eq.(116), it is found that if the spin-triplet amplitude $\Delta_t \mathcal{L}_{\mathbf{k}}$ is larger than the spin-singlet one Δ_s on the Fermi surface given by $\varepsilon_{\mathbf{k}} = \alpha \mathcal{L}_0(\mathbf{k})$, we can take $\Delta_s \rightarrow 0$, then $\alpha \rightarrow 0$ without gap closing. (If $\varepsilon_{\mathbf{k}} = 0$ at one of the time-reversal momenta $\mathbf{k} = (0, 0), (\pi, 0), (0, \pi), (\pi, \pi)$, the gap closes when $\Delta_s = 0$. However, this undesirable gap closing can be avoided by changing μ or t slightly.) Thus, its \mathbf{Z}_2 number is the same as that of the pure spin-triplet SC with $\mathbf{d}(\mathbf{k}) = \Delta_t \mathcal{L}_{\mathbf{k}}$. The resultant system preserves S_z , and the BdG Hamiltonian is decomposed into two spinless chiral superconductors in up-spin sector and the down-spin sector, $\mathcal{H}_+(\mathbf{k})$ and $\mathcal{H}_-(\mathbf{k})$, respectively,

$$\mathcal{H}_{\pm}(\mathbf{k}) = \begin{pmatrix} \varepsilon_{\mathbf{k}} & -\Delta_t(\sin k_x \pm i \sin k_y) \\ -\Delta_t(\sin k_x \mp i \sin k_y) & -\varepsilon_{\mathbf{k}} \end{pmatrix}.$$

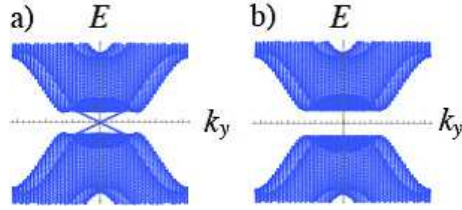


Fig. 29. (Color online) The energy spectra of the 2D noncentrosymmetric superconductor with edges in the absence of magnetic field. We take $t = 1$, $\mu = -3$, $\alpha = 0.6$. (a) noncentrosymmetric superconductor with dominating p -wave paring. $\Delta_t = 0.6$ and $\Delta_s = 0.1$. (b) noncentrosymmetric superconductor with purely s -wave paring. $\Delta_t = 0$ and $\Delta_s = 0.6$.

(117)

If the Fermi surface is two-dimensional and electron-like, their Chern numbers is $C_1^{(\pm)} = \mp 1$ for $\Delta_t > 0$. (see Fig.27). Thus the \mathbf{Z}_2 number is non-trivial.

From the bulk-edge correspondence, there should exist gapless edges if the spin-triplet pairs dominate the superconductivity. In Fig.29 (a), we show the energy spectrum of the 2D noncentrosymmetric superconductor with edges. It is found that there exist gapless edge states in the bulk gap. The gapless edges states form a Kramers pair.

For comparison, we also illustrate the energy spectrum for the 2D noncentrosymmetric superconductor with purely s -wave paring in Fig.29 (b). As is seen clearly, no edge state is obtained. This is also consistent with the trivial \mathbf{Z}_2 number of the purely s -wave paring.

We also notice that the helical Majorana gapless edge states are very sensitive to the direction of the applied magnetic field. As seen in Fig.30, they become unstable under a small magnetic field in the y -direction, while the gapless edge states are stable under a magnetic field in the x - and z -direction. As a result, the magnetic field H_y along the edge causes a tiny gap of the order $O(\mu_B H_y)$ for the edge states. The experimental detection of the edge states have been proposed theoretically.^{159,186,188–194)}

3.6.1 Non-Abelian topological order and Majorana fermion induced by spin-orbit interaction and Zeeman field

The spin-orbit interaction enables us to realize Majorana fermion and non-Abelian topological order in the presence of the Zeeman field.^{159,195,196)} In particular, the Majorana fermion can be realized even if the symmetry of the gap function is spin-singlet dominant.^{195–198)} Here we see this interesting phase of noncentrosymmetric supercon-

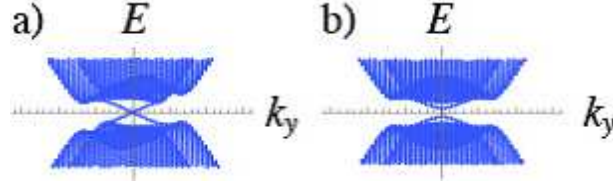


Fig. 30. (Color online) The dependence of gapless edge states on the direction of the magnetic field. We take $t = 1$, $\mu = -3$, $\alpha = 0.6$, $\Delta_t = 0.6$ and $\Delta_s = 0.1$. a) $\mu_B H_x = 0.15$, $\mu_B H_y = 0$ and $\mu_B H_z = 0$. b) $\mu_B H_x = 0$, $\mu_B H_y = 0.15$ and $\mu_B H_z = 0$.

ductors.

An intuitive understanding on this mechanism of non-Abelian topological phase is obtained if we perform the dual transformation of the BdG Hamiltonian.^{195,196)} For the two-dimensional Rashba superconductor (109), the dual Hamiltonian is obtained by the following unitary transformation,

$$\mathcal{H}^D(\mathbf{k}) = D\mathcal{H}(\mathbf{k})D^\dagger, \quad D = \frac{1}{\sqrt{2}} \begin{pmatrix} 1 & i\sigma_y \\ i\sigma_y & 1 \end{pmatrix}, \quad (118)$$

which leads to

$$\mathcal{H}^D(\mathbf{k}) = \begin{pmatrix} \Delta_s + \Delta_t \mathbf{L}_k \cdot \boldsymbol{\sigma} - h\sigma_z & -i\varepsilon_k \sigma_y - i\alpha \mathbf{L}_k \cdot \boldsymbol{\sigma} \sigma_y \\ i\varepsilon_k \sigma_y + i\alpha \mathbf{L}_k \sigma_y \boldsymbol{\sigma} & -\Delta_s + \Delta_t \mathbf{L}_k \cdot \boldsymbol{\sigma}^* + h\sigma_z \end{pmatrix}. \quad (119)$$

From eq. (119), it is found that the Rashba spin-orbit interaction in the original Hamiltonian is formally transformed into a “ p -wave pairing interaction” with the \mathbf{d} vector, $\mathbf{d}(\mathbf{k}) = -\alpha \mathbf{L}_k$, in the dual Hamiltonian $\mathcal{H}^D(\mathbf{k})$. Since $\mathcal{H}^D(\mathbf{k})$ has a nonstandard constant kinetic term, this does not necessarily mean that the topological properties of $\mathcal{H}(\mathbf{k})$ are the same as those of a usual p -wave superconductor. However, we find that that the topological order emerges when h satisfies

$$h^2 > \Delta_s^2 + \varepsilon_{\mathbf{k}=\mathbf{0}}^2, \quad (120)$$

due to the Rashba spin-orbit interaction. Indeed, one can prove that the Chern number $C_1 = -1$ if the condition (120) is met.^{159,195,196)} Also, the same condition (120) is obtained from the analysis of Majorana zero mode in a vortex.¹⁹⁷⁾ In Fig.31, we illustrate the energy bands of our Hamiltonian (109) with edges. This figure clearly shows the existence of a chiral gapless state if the Zeeman field h satisfies eq.(120), even when the spin-triplet superconductor is absent.

From the argument in §3.4, it is evident that a vortex supports a Majorana zero mode in this case. Indeed, we can demonstrate the existence of the Majorana zero mode explicitly by solving the BdG equation for a single vortex.^{159, 195–197, 199)} As explained in §3.4, if there exists a single Majorana fermion zero mode for each vortex, vortices obey the non-Abelian statistics. Following ref.,¹⁹⁵⁾ we use here the dual Hamiltonian $\mathcal{H}^D(\mathbf{k})$ to solve the BdG equation, then construct a solution in the original Hamiltonian $\mathcal{H}(\mathbf{k})$ by using the duality transformation (119). For simplicity, we assume $\varepsilon_{\mathbf{k}=0} = 0$ and $\Delta_t = 0$. Then, if h satisfies $|\Delta_s| < |h| < 2|\Delta_s|$, the low energy properties are governed by quasiparticles on the smaller Fermi surface, which is split from the larger one by the spin-orbit interaction.¹⁹⁶⁾ The larger Fermi surface can be neglected to construct the zero mode. Thus, we concentrate on fermions with $|\mathbf{k}| \sim 0$ for which $\mathcal{H}^D(\mathbf{k})$ is decomposed

$$\mathcal{H}_{\pm}^D(\mathbf{k}) = \begin{pmatrix} \Delta_s \mp h & \alpha(\pm k_y + ik_x) \\ \alpha(\pm k_y - ik_x) & -\Delta_s \pm h \end{pmatrix}. \quad (121)$$

The BdG equations for \mathcal{H}_{\pm}^D with a single vortex can be solved,¹⁵³⁾ then, we find a unique zero energy solution with a quasiparticle field $\gamma^\dagger = \int d\mathbf{r}[u_0\psi_+^\dagger + v_0\psi_+]$, where $u_0 = i(re^{i\theta})^{-1/2}e^{-(h-\Delta_s)r/\alpha}$, $v_0 = -i(re^{-i\theta})^{-1/2}e^{-(h-\Delta_s)r/\alpha}$. The solution is normalizable when eq.(120) is satisfied. This is the Majorana zero energy mode; *i.e.*, $\gamma^\dagger = \gamma$. Using the duality transformation (119), we also found that a vortex in the original Hamiltonian has a single Majorana zero mode, which implies that the vortex is a non-Abelian anyon.

Here note that the condition (120) implies the Zeeman energy larger than the s -wave BCS gap Δ_s . Thus the orbital depairing effect could destroy the superconductivity while the Pauli depairing effect is suppressed in the presence of the Rashba spin-orbit interaction.^{200, 201)} If the spin-triplet amplitude is dominant and the s -wave pair amplitude is small enough, the condition (120) can be met for a weak magnetic field without destroying the superconducting gap.¹⁵⁹⁾ On the other hand, if the s -wave pair amplitude is dominant, one always needs a strong magnetic field larger than the superconducting gap. Several schemes to realize the non-Abelian topological phase in this case has been proposed, (i) s -wave superfluids in neutral ultracold fermionic atoms with laser generated spin-orbit interaction,^{195, 196)} (ii) heterostructure semiconductor device,^{197, 202)} and (iii) heavy fermion systems.¹⁹⁶⁾

If we consider $d_{x^2-y^2}$ -wave or d_{xy} -wave pairing instead of the s -wave pairing, the

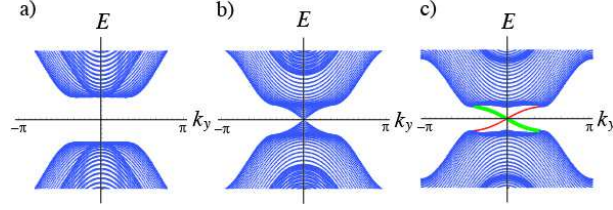


Fig. 31. (Color online) Majorana edge modes in an s -wave superconducting state with Rashba spin-orbit interaction under the Zeeman magnetic field h in the z -direction. Energy spectra of the system with open boundary in the x -direction and the periodic boundary condition in the y -direction. (a) $h = 0$ (b) $h = h_c \equiv \sqrt{\varepsilon_{\mathbf{k}=0}^2 + \Delta_s^2}$ (c) $h > h_c$. When the Zeeman field h is larger than the critical value h_c , the Majorana zero mode appears. [Reproduced from Fig.1 of Phys. Rev. Lett.**103**, 020401 (2009) by Sato *et al.*]

condition (120) changes as¹⁹⁸⁾

$$h^2 > \varepsilon_{\mathbf{k}=\mathbf{0}}^2, \quad (122)$$

since these pair amplitudes vanish at $\mathbf{k} = \mathbf{0}$. Thus now the condition (122) is independent of the superconducting gap. This means that the Majorana fermion and the non-Abelian topological phase could be realized in a weak magnetic field without destroying superconductivity for systems with small $\varepsilon_{\mathbf{k} = \mathbf{0}}$. In Fig.32, we illustrate the Majorana edge modes in this case. The Majorana fermion state is topologically protected in spite of the presence of bulk gapless nodal excitations. Due to the existence of bulk nodes, one cannot obtain a well-defined Chern number, but the particle-hole symmetry makes the parity of the Chern number well-defined.¹⁹⁸⁾ The non-Abelian nodal superconductor is realizable in an interface between a centrosymmetric nodal superconductor such as high- T_c cuprates and a semiconductor. In such a system, because of the considerably large superconducting gap, the experimental detection of Majorana modes may be easier.

3.6.2 Dispersionless Majorana fermion

For a certain type of noncentrosymmetric superconductors, novel Majorana fermion is possible.^{161,203,204)} It preserves the time-reversal symmetry, however, unlike the helical Majorana fermions, it consists of a single branch of flat dispersion.

The time-reversal invariant Majorana fermion is realized for the $d_{xy} + p$ -wave Rashba noncentrosymmetric superconductor. Such a pairing symmetry has been suggested for heterointerface LaAlO₃/SrTiO₃.²⁰⁵⁾ Figure 33 illustrates the quasiparticle spectrum for the semi-infinite $d_{xy} + p$ -wave Rashba noncentrosymmetric superconductor on $x > 0$.

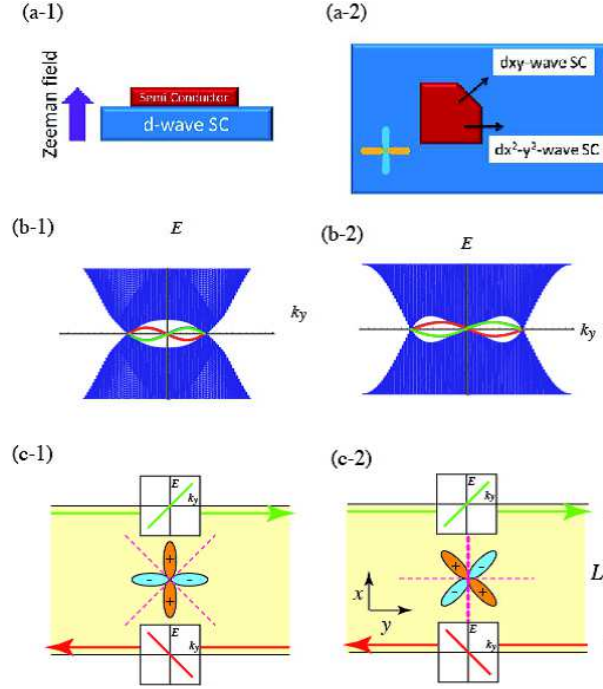


Fig. 32. (Color online) Majorana fermions in nodal superconductors. (a) Possible realization scheme to realize nodal superconductor with Majorana fermion. Due to the proximity effect and the potential gradient at the interface, d -wave superconducting state with the Rashba spin-orbit coupling is realized in the interface between the high T_c cuprate and the semiconductor. (a-1) Side view (a-2) Top view. (b) Energy spectra of the systems with open boundaries at $x = 0$ and $x = L$ in the x -direction and the periodic boundary condition in the y -direction for (b-1) $d_{x^2-y^2}$ -wave pairing, and (b-2) d_{xy} -wave pairing. Majorana gapless edge modes at $x = 0$ and $x = L$ are depicted, respectively, in green and red curves. (c) Schematic illustration of Majorana edge modes counterpropagating on two opposite edges for (c-1) $d_{x^2-y^2}$ -wave pairing and (c-2) d_{xy} -wave pairing. [(b) and (c): Reproduced from Fig.1 of Phys. Rev. Lett. **105**, 217001 (2010) by Sato and Fujimoto]

Due to the Rashba spin-orbit interaction, the Fermi surface is split into two with the Fermi momenta k_1 and k_2 ($k_1 < k_2$). See Fig.33. There exists a single branch of zero energy edge state in the momentum region $k_1 < |k_y| < k_2$ between the Fermi surfaces. The wave function for the zero energy edge state $\Psi_m(k_y)$ can be written as $T\Psi_m(k_y) = (u_1(k_y), u_2(k_y), v_1(k_y), v_2(k_y))$ with $u_1(k_y) = v_1^*(-k_y)$, $u_2(k_y) = v_2^*(-k_y)$. The Bogoliubov quasiparticle creation operator for this state is constructed in the usual way as $\gamma^\dagger(k_y) = u_1(k_y)c_\uparrow^\dagger(k_y) + u_2(k_y)c_\downarrow^\dagger(k_y) + v_1(k_y)c_\uparrow(-k_y) + v_2(k_y)c_\downarrow(-k_y)$, and satisfies the Majorana condition $\gamma^\dagger(k_y) = \gamma(-k_y)$.

Unlike Majorana fermions discussed in previous sections, the present single Majorana bound state at k_y is realized with time-reversal symmetry. The time-reversal invariant Majorana bound state has the following three characteristics. (a) It has a

unique flat dispersion: To be consistent with the time-reversal invariance, the single branch of zero mode should be symmetric under $k_y \rightarrow -k_y$. Therefore, by taking into account the particle-hole symmetry as well, the flat dispersion is required. On the other hand, the conventional time-reversal breaking Majorana bound state has a linear dispersion. (b) The spin-orbit coupling is necessary to obtain the time-reversal invariant Majorana bound state. Without spin-orbit coupling, the time-reversal invariant Majorana bound state vanishes. (c) The time-reversal invariant Majorana bound state is topologically stable under small deformations of the Hamiltonian preserving k_y . The topological stability is ensured by the topological invariant W ^{161,204)}

$$W(k_y) = \frac{1}{2\pi} \text{Im} \left[\int dk_x \partial_{k_x} \ln \det \hat{q}(\mathbf{k}) \right], \quad (123)$$

with $\hat{q}(\mathbf{k}) = [\varepsilon_{\mathbf{k}} - i\psi(\mathbf{k})]\sigma_y + [\alpha\mathcal{L}_{\mathbf{k}} - i\mathbf{d}(\mathbf{k})] \cdot \boldsymbol{\sigma}\sigma_y$. The flat dispersion of the Majorana fermion is terminated in a gap node. The last property is closely related to the topological stability of line nodes of noncentrosymmetric superconductors.^{206,207)}

It is noted that the appearance of surface flat bands in three-dimensional non-centrosymmetric superconductors or topological media have been also discussed recently.^{208–211)}

3.7 Topological phase in odd-parity superconductors

In §3.4, we have seen that the topological properties of the spinless superconductor changes as the topology of the Fermi surface changes. This is a general property of spin-triplet odd-parity superconductors.^{163,212)}

To see this, consider a general Hamiltonian H for odd-parity superconductors,

$$H = \frac{1}{2} \sum_{\mathbf{k}\alpha\alpha'} (c_{\mathbf{k}\alpha}^\dagger, c_{-\mathbf{k}\alpha}) H(\mathbf{k}) \begin{pmatrix} c_{\mathbf{k}\alpha'} \\ c_{-\mathbf{k}\alpha'}^\dagger \end{pmatrix},$$

$$H(\mathbf{k}) = \begin{pmatrix} \mathcal{E}(\mathbf{k})_{\alpha\alpha'} & \Delta(\mathbf{k})_{\alpha\alpha'} \\ \Delta^\dagger(\mathbf{k})_{\alpha\alpha'} & -\mathcal{E}^T(-\mathbf{k})_{\alpha\alpha'} \end{pmatrix}, \quad (124)$$

where $c_{\mathbf{k}\alpha}^\dagger$ ($c_{\mathbf{k}\alpha}$) denotes the creation (annihilation) operator of electron with momentum \mathbf{k} . The suffix α labels other degrees of freedom for electron such as spin, orbital degrees of freedom, sub-lattice indices, and so on. $\mathcal{E}(\mathbf{k})$ is the Hamiltonian of the electron in the normal state. The system in the normal state is supposed to be invariant under the inversion $c_{\mathbf{k}\alpha} \rightarrow \sum_{\alpha'} P_{\alpha\alpha'} c_{-\mathbf{k}\alpha'}$ with $P^2 = 1$, $P^\dagger \mathcal{E}(\mathbf{k}) P = \mathcal{E}(-\mathbf{k})$. We also assume that the parity of the gap function $\Delta(\mathbf{k})$ is odd, $P^\dagger \Delta(\mathbf{k}) P^* = -\Delta(-\mathbf{k})$.

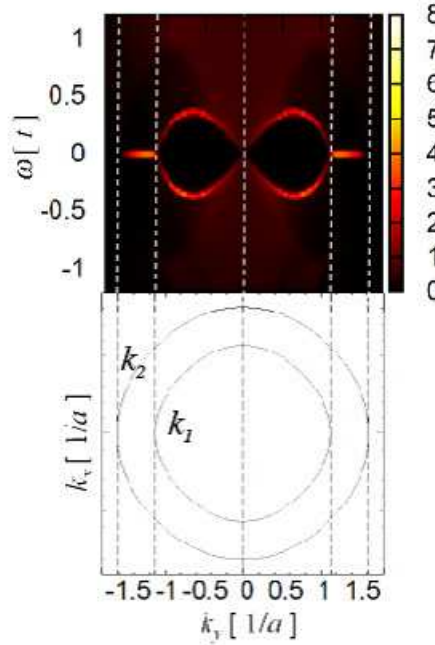


Fig. 33. (Color online) (Top) Angle-resolved LDOS for $d_{xy} + p$ -wave pairing as a function of k_y . $\Delta_t \neq 0$ and $\Delta_s = 0$. (Bottom) The corresponding Fermi surfaces of the system. The Fermi surfaces are split into two by the Rashba spin-orbit interaction. Single branch of zero energy ABS exist in the region of $k_1 < |k_y| < k_2$.

First, consider the case with the time-reversal symmetry breaking. The BdG Hamiltonian (124) has the following particle-hole symmetry,

$$CH(\mathbf{k})C^\dagger = -H^*(-\mathbf{k}), \quad C = \begin{pmatrix} 0 & 1 \\ 1 & 0 \end{pmatrix}. \quad (125)$$

From this, we can say that if $|u_n(\mathbf{k})\rangle$ is a quasiparticle state with positive energy $E_n(\mathbf{k}) > 0$ satisfying $H(\mathbf{k})|u_n(\mathbf{k})\rangle = E_n(\mathbf{k})|u_n(\mathbf{k})\rangle$, then $C|u_n^*(-\mathbf{k})\rangle$ is a quasiparticle state with negative energy $-E_n(-\mathbf{k}) < 0$. We use a positive (negative) n for $|u_n(\mathbf{k})\rangle$ to represent a positive (negative) energy quasiparticle state, and set

$$|u_{-n}(\mathbf{k})\rangle = C|u_n^*(-\mathbf{k})\rangle. \quad (126)$$

Let us define the gauge fields

$$A_i^{(+)}(\mathbf{k}) = i \sum_{n>0} \langle u_n(\mathbf{k}) | \partial_{k_i} | u_n(\mathbf{k}) \rangle, \quad A_i^{(-)}(\mathbf{k}) = i \sum_{n<0} \langle u_n(\mathbf{k}) | \partial_{k_i} | u_n(\mathbf{k}) \rangle, \quad (127)$$

where the relation

$$A_i^{(+)}(\mathbf{k}) = A_i^{(-)}(-\mathbf{k}) \quad (128)$$

holds from (126). In addition, we have

$$A_i^{(-)}(\mathbf{k}) + A_i^{(+)}(\mathbf{k}) = i \text{tr} [U^\dagger(\mathbf{k}) \partial_{k_i} U(\mathbf{k})] = i \partial_{k_i} \ln \det U(\mathbf{k}), \quad (129)$$

with the unitary matrix $U(\mathbf{k})$ given by

$$U_{nm}(\mathbf{k}) = u_n^m(\mathbf{k}) \quad (130)$$

where $u_n^m(\mathbf{k})$ is the m -th component of $|u_n(\mathbf{k})\rangle = (\dots, u_n^1(\mathbf{k}), u_n^2(\mathbf{k}), \dots)^T$.

Now consider the time-reversal invariant path C_{ij} in the BZ, which passes through the time-reversal invariant momenta Γ_i and Γ_j . See Fig.34. Note that C_{ij} is a closed path because of the periodicity of the BZ. The periodicity of the BZ implies that the integration of $A_i^{(-)}(\mathbf{k})$ along C_{ij} is quantized as,

$$\begin{aligned} \oint_{C_{ij}} dk_i A_i^{(-)}(\mathbf{k}) &= \frac{1}{2} \oint_{C_{ij}} dk_i [A_i^{(-)}(\mathbf{k}) + A_i^{(+)}(\mathbf{k})] \\ &= \frac{1}{2} \oint_{C_{ij}} dk_i i \partial_{k_i} \ln \det U(\mathbf{k}) \\ &= N\pi, \quad (N: \text{integer}). \end{aligned} \quad (131)$$

Thus the Berry phases $e^{i \oint_{C_{ij}} A_i^{(-)}(\mathbf{k})}$ takes only two possible values, and we use it as the topological index,

$$(-1)^{\nu[C_{ij}]} = e^{i \oint_{C_{ij}} A_i^{(-)}(\mathbf{k})} = \pm 1. \quad (132)$$

Like the one-dimensional winding number w_{1d} in §3.3, the topological index $(-1)^{\nu[C_{ij}]}$ characterizes the ‘‘one-dimensional gapped superconductor’’ along the path C_{ij} . When $(-1)^{\nu[C_{ij}]} = -1$, the bulk-edge correspondence yields that there exists a zero energy edge state at the corresponding momentum in the surface BZ. On the other hand, when $(-1)^{\nu[C_{ij}]} = 1$, no ZEABS is required at the corresponding momentum in the surface BZ.

Up to now, we have not used the specific property of odd-parity superconductors. For odd-parity superconductors, the combination of the inversion and the electromagnetic $U(1)$ gauge symmetry, $c_{\mathbf{k}\alpha} \rightarrow iP_{\alpha\alpha'} c_{\mathbf{k}\alpha'}$, is manifestly preserved. Thus, $H(\mathbf{k})$ has the following symmetry

$$\Pi^\dagger H(\mathbf{k}) \Pi = H(-\mathbf{k}), \quad \Pi = \begin{pmatrix} P & 0 \\ 0 & -P^* \end{pmatrix}. \quad (133)$$

From this, we have $[H(\Gamma_i), \Pi] = 0$ for the time-reversal invariant momentum Γ_i . Thus,

the quasiparticle state $|u_n(\Gamma_i)\rangle$ at Γ_i is simultaneously an eigenstate of Π ,

$$\Pi|u_n(\Gamma_i)\rangle = \pi_n(\Gamma_i)|u_n(\Gamma_i)\rangle. \quad (134)$$

Then, the product of $\pi_n(\Gamma_i)$ for occupied states, $\prod_{n<0} \pi_n(\Gamma_i)$, has the following interesting properties: (a) it takes only discrete values $\prod_{n<0} \pi_n(\Gamma_i) = \pm 1$, and (b) its value can change only when the gap of the system closes at Γ_i . These properties are what we expect for the topological index, and suggest that $\prod_{n<0} \pi_n(\Gamma_i)$ is a kind of topological index. Indeed, we can relate $\prod_{n<0} \pi_n(\Gamma_i)$ to the topological index $(-1)^{\nu[C_{ij}]}$ as,²¹²⁾

$$(-1)^{\nu[C_{ij}]} = \prod_{n<0} \pi_n(\Gamma_i)\pi_n(\Gamma_j). \quad (135)$$

For ordinary superconductors, the superconducting gap is much smaller than the Fermi energy. Therefore, we reasonably assume that the typical energy scale of the gap function $\Delta(\Gamma_i)$ at the time-reversal invariant momentum is much smaller than that of $\mathcal{E}(\Gamma_i)$. Under this assumption, we can deform the gap function $\Delta(\mathbf{k})$ adiabatically so as $\Delta(\Gamma_i) \rightarrow 0$ without closing the bulk energy gap. Because of the topological nature of $(-1)^{\nu[C_{ij}]}$, this adiabatic process does not change the value of $(-1)^{\nu[C_{ij}]}$. In the process $\Delta(\Gamma_i) \rightarrow 0$, the BdG Hamiltonian at Γ_i reduces to $H(\Gamma_i) \rightarrow \text{diag}(\mathcal{E}(\Gamma_i), -\mathcal{E}^T(\Gamma_i))$. For this simple Hamiltonian, we can evaluate $\pi_n(\Gamma_i)$ rather easily, and we obtain the final expression,²¹²⁾

$$(-1)^{\nu[C_{ij}]} = \prod_{\alpha} \text{sgn}\varepsilon_{\alpha}(\Gamma_i)\text{sgn}\varepsilon_{\alpha}(\Gamma_j), \quad (136)$$

where $\varepsilon_{\alpha}(\Gamma_i)$ is an eigenvalue of $\mathcal{E}(\Gamma_i)$ and the product of α is taken for all eigenstates of $\mathcal{E}(\Gamma_i)$. This formula implies that for odd-parity superconductors the gapless boundary state can be predicted by the Fermi surface structure.

When the odd-parity superconductors are fully-gapped in two dimensions, the Chern number C_1 also characterizes the topological phases. By using eqs. (48) and (128), it can be linked to the topological index $\nu[C_{ij}]$ as

$$\begin{aligned} C_1 &= \frac{1}{2\pi} \int_{T^2} d^2k \mathcal{B}_z(\mathbf{k}) = \frac{1}{\pi} \int_{T_+^2} d^2k \mathcal{B}_z(\mathbf{k}) \\ &= \frac{1}{\pi} \oint_{\partial T_+^2} dk_i A_i^{(-)}(\mathbf{k}) = \nu[C_{12}] - \nu[C_{34}], \end{aligned} \quad (137)$$

where T_+^2 is the upper half of T^2 , and C_{ij} is the time-reversal invariant path illustrated in Fig.34(b). Therefore, eq.(136) yields

$$(-1)^{C_1} = \prod_{\alpha, i=1,2,3,4} \text{sgn}\varepsilon_{\alpha}(\Gamma_i). \quad (138)$$

One can confirm the validity of the formulas (136) and (138) by applying them to the spinless superconductors in Fig.27. For example, from the Fermi surface structures illustrated in the top row, we find that only the case of Fig.27 (b) has an odd Chern number. Correspondingly, a single edge mode appears on each edge in Fig.27 (b). Furthermore, it is found that the difference between Fig.27 (a) and (c) can be understood as the difference in $(-1)^{\nu[C_{ij}]}$ for each case: One find that $(-1)^{\nu[C_{12}]} = (-1)^{\nu[C_{34}]} = -1$ for Fig. 27 (c), while $(-1)^{\nu[C_{12}]} = (-1)^{\nu[C_{34}]} = 1$ for (a). The zero energy edge states in (c) are originated from the non-trivial values of these topological indices.

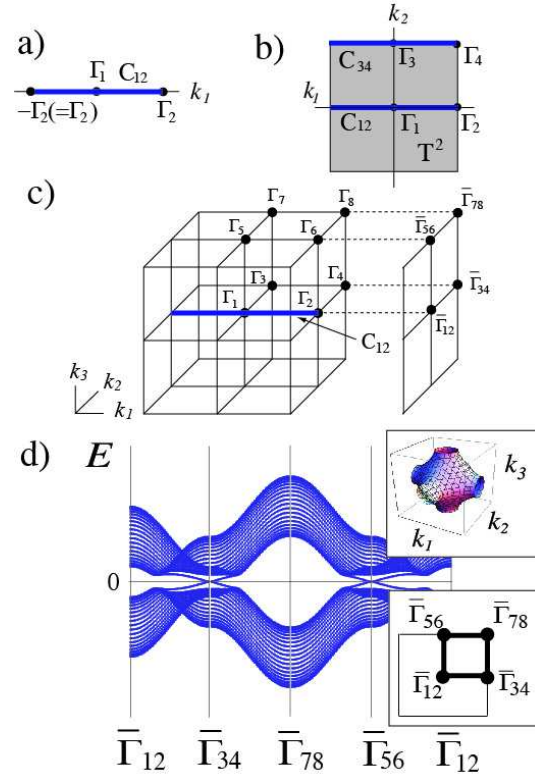


Fig. 34. (Color online) The time-reversal invariant momenta Γ_i , and the time-reversal invariant closed path C_{ij} passing through Γ_i and Γ_j in the BZ. a) 1D BZ. The solid line denotes C_{12} . b) 2D BZ T^2 . c) 3D BZ and the surface BZ of a (100) face. d) 2D band structure for a slab with a (100) face for the 3D time-reversal invariant odd parity superconductor that has the Fermi surface with $(-1)^{\tilde{\nu}[C_{34}]} = (-1)^{\tilde{\nu}[C_{56}]} = -1$ and the gap function $\Delta(\mathbf{k}) = i\mathbf{d}(\mathbf{k}) \cdot \boldsymbol{\sigma} \sigma_y$ with $d_i(\mathbf{k}) = \Delta \sin k_i$. The insets show the Fermi surface (top) and the 2D surface BZ (bottom). [Reproduced from Fig.1 of Phys. Rev. B **81**, 220504(R) (2010) by Sato]

Now consider the time-reversal invariant case. The time-reversal invariance implies that $(-1)^{\nu[C_{ij}]}$ is always trivial, *i.e.* $(-1)^{\nu[C_{ij}]} = 1$. However, use of the time-reversal

invariance as well as the particle-hole symmetry makes it possible to define another topological index.

Because of the time-reversal invariance, the quasiparticle states form Kramers pairs, $|u_n^s(\mathbf{k})\rangle$ ($s = \text{I, II}$), $|u_n^{\text{I}}(\mathbf{k})\rangle = T|u_n^{\text{II}}(-\mathbf{k})\rangle$, with the time-reversal operator T . The new topological index is defined by the gauge field for the ‘‘half’’ of the Kramers doublets, say, $A_i^{\text{I}(-)}(\mathbf{k}) = i \sum_{n<0} \langle u_n^{\text{I}}(\mathbf{k}) | \partial_{k_i} | u_n^{\text{I}}(\mathbf{k}) \rangle$. Then the topological index $(-1)^{\tilde{\nu}[\text{C}_{ij}]}$ is defined as

$$(-1)^{\tilde{\nu}[\text{C}_{ij}]} = e^{i \oint_{\text{C}_{ij}} A_i^{\text{I}(-)}(\mathbf{k})}. \quad (139)$$

In a manner similar to the above, for odd-parity superconductors, $(-1)^{\tilde{\nu}[\text{C}_{ij}]}$ are determined by the Fermi surface structure,²¹²⁾

$$(-1)^{\tilde{\nu}[\text{C}_{ij}]} = \prod_{\alpha} \text{sgn} \varepsilon_{2\alpha}(\Gamma_i) \text{sgn} \varepsilon_{2\alpha}(\Gamma_j), \quad (140)$$

where $\varepsilon_{\alpha}(\Gamma_i)$ is an eigenvalue of $\mathcal{E}(\Gamma_i)$, and we have set $\varepsilon_{2\alpha}(\Gamma_i) = \varepsilon_{2\alpha+1}(\Gamma_i)$ by using the Kramers degeneracy.

Furthermore, other topological indices characterizing time-reversal invariant superconductors can be linked to the Fermi surface topology. For the full-gapped two-dimensional case, their topological nature is characterized by the \mathbf{Z}_2 number $(-1)^{\nu_{2\text{dTI}}}$ introduced in §3.5 and §3.6. For odd-parity superconductors, it satisfies^{163, 212)}

$$(-1)^{\nu_{2\text{dTI}}} = \prod_{\alpha, i=1,2,3,4} \text{sgn} \varepsilon_{2\alpha}(\Gamma_i), \quad (141)$$

where Γ_i is the time-reversal invariant momenta in Fig.34(b). Thus, we can predict the helical Majorana edge mode from the knowledge of the Fermi surface. In addition, for the full-gapped three-dimensional case, we have another topological index known as the three-dimensional winding number $w_{3\text{d}}$.^{154, 156, 157, 213)} (When $w_{3\text{d}}$ takes a nonzero integer n , there exist n Majorana cones on the surface.) We can also connect this to the Fermi surface structure as^{163, 212, 214)}

$$(-1)^{w_{3\text{d}}} = \prod_{\alpha, i=1, \dots, 8} \text{sgn} \varepsilon_{2\alpha}(\Gamma_i), \quad (142)$$

with Γ_i in Fig.34 (c). The last formula determines the parity of the three-dimensional winding number, thus it gives a sufficient condition for nonzero $w_{3\text{d}}$. In Fig.34 (d), we illustrate surface states of a three-dimensional time-reversal invariant topological superconductor. The Fermi surface of this model leads to $(-1)^{w_{3\text{d}}} = 1$, but $(-1)^{\tilde{\nu}[\text{C}_{34}]} = -1$ and $(-1)^{\tilde{\nu}[\text{C}_{56}]} = -1$. Consistently, we have two Majorana cones on the surface at the time-

reversal invariant points $\bar{\Gamma}_{34}$ and $\bar{\Gamma}_{56}$ in the surface Brillouin zone. (For the definition of $\bar{\Gamma}_{ij}$, see Fig 34(c).)

We would like to emphasize here that the correspondence between the Fermi surface and the gapless surface state discussed in the above are inherent to spin-triplet/odd-parity superconductors. Thus we may identify the spin-triplet/odd-parity superconductivity through the direct measurement of the surface state, irrespective of the details of the gap function.^{163,212)} For instance, the formula (142) has been applied to $\text{Cu}_x\text{Bi}_2\text{Se}_3$ in order to identify its possible odd-parity superconductivity.²¹⁴⁾ Detailed information on ABS for such a material can be predicted by using the formulas (140) and (141) as well.

3.8 Majorana fermion on the surface of topological insulator

As discussed in §3.5, the topological insulator is a new state of matter with time-reversal (T -symmetry).^{178–181,215)} Especially, on the surface of the 3D strong topological insulator (STI), there appears odd number of 2D Dirac fermions. Even with a disorder scattering etc., at least one Dirac fermion is protected by the gap and topology of the bulk states and is stable as long as the perturbation is T -symmetric and does not destroy the bulk gap. In the case of Bi_2Se_3 and Bi_2Te_3 ,²¹⁶⁾ there appears only one surface Dirac fermion, which can be regarded as the "half" of the 2D electrons because the spin direction is determined by the momentum. This "fractionalization" of the electrons is one of the key concepts in the topologically ordered states. This situation is similar to the case of spinless fermion, and when the Cooper pairing occurs, there is a possibility that Majorana fermions will appear.²¹⁷⁾ Fu and Kane were the first to study the superconductivity of the surface Dirac fermions of the STI induced by the proximity effect by the superconductors attached to it.²¹⁸⁾ Also they considered the ferromagnetic insulator (FI) put on the STI, and its interface with the conventional superconductor (S). They predicted the emergence of the one-dimensional chiral Majorana mode as an Andreev bound state.²¹⁸⁾ This situation is similar to that discussed in §3.4. Also by applying the magnetic field, the vortices penetrate the sample. At the core of each vortex, the Majorana bound state is realized at zero energy.^{218,219)}

Majorana interferometry has been proposed to detect the Majorana fermions.^{220–223)} The schematic configuration is shown in Fig.35. Everything is on top of the STI, and there appears the chiral fermion channel at the interface of two magnetic domains with \uparrow and \downarrow magnetization, while the chiral Majorana fermions appear at the interface

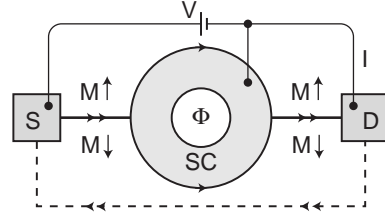


Fig. 35. Majorana interferometer on top of a strong topological insulator. [Reproduced from Fig. 1 of Phys. Rev. Lett. **102** 216403 (2009) by Fu and Kane.]

between FI and S. Let c^\dagger and c being the creation and annihilation operators of this chiral fermion. At the branching points, this chiral fermion is connected to the two Majorana edge channels for upper and lower semicircles. Let γ_1 (γ_2) be the operator of the Majorana fermion in the upper (lower) semicircle. Let us consider the process that an electron is entering from the left to the branching point described by

$$c \rightarrow \gamma_1 + i\gamma_2. \quad (143)$$

At the right branching point, these two Majorana fermions merge into an electron as

$$\gamma_1, \gamma_2 \rightarrow c = \gamma_1 + i\gamma_2 \quad (144)$$

or

$$\gamma_1, \gamma_2 \rightarrow c^\dagger = \gamma_1 - i\gamma_2 \quad (145)$$

depending on the even or odd number of vortices Φ/ϕ_0 ($\phi_0 = hc/2e$) trapped by the superconducting donut according to the Aharonov-Bohm effect. This leads to strong Φ -dependence of the conductance G between the left and right leads. Namely, $G = 2e^2/h$ when $\Phi = 2n \times \phi_0$ while $G = 0$ when $\Phi = (2n + 1) \times \phi_0$ with n being an integer. This prediction is based on the fact that the Majorana fermion contains the particle and hole components with equal weight, or an electron is composed of two Majorana fermions.

The other direction of the research is to study the possible manipulation of the Majorana fermion and its relevance to the transport properties in the transverse direction to the interface,^{224–226}) For that purpose we consider the Hamiltonian for the surface state on STI influenced by the superconductor and ferromagnet (Fig. 36) as given by

$$\check{H}_S = \begin{pmatrix} \hat{H}(\mathbf{k}) + \hat{M} & \hat{\Delta} \\ -\hat{\Delta}^* & -\hat{H}^*(-\mathbf{k}) - \hat{M}^* \end{pmatrix} \quad (146)$$

where $\hat{H}(\mathbf{k}) = v_F(\hat{\sigma}_x k_x + \hat{\sigma}_y k_y) - \mu[\Theta(-x) + \Theta(x - d)]$ describes the 2D Dirac fermion,

and $\hat{M} = \mathbf{m} \cdot \hat{\boldsymbol{\sigma}} \Theta(d-x) \Theta(x)$ is the magnetic exchange interaction with $\mathbf{m} \cdot \hat{\boldsymbol{\sigma}} = m_x \hat{\sigma}_x + m_y \hat{\sigma}_y + m_z \hat{\sigma}_z$. Here, μ , $\hat{\boldsymbol{\sigma}}$, v_F , \mathbf{m} denote chemical potential, Pauli matrices, velocity, and magnetization (times the exchange coupling constant which we assume to be 1), respectively.²¹⁸⁾ Interestingly, \mathbf{m} couples to the Dirac fermion as an effective vector potential \mathbf{A} of the electromagnetic field. For the moment, we assume that the pairing symmetry of superconductor is spin-singlet s -wave and $\hat{\Delta}$ is given as $\hat{\Delta} = i\hat{\sigma}_y \Delta \Theta(x-d)$ and $\hat{\Delta} = i\hat{\sigma}_y [\Delta \Theta(x-d) + \Delta \Theta(-x) \exp(i\varphi)]$ for N/FI/S (Fig. 36 (a)) and S/FI/S (Fig. 36 (b)) junctions formed on the surface of STI, respectively, where φ denotes the macroscopic phase difference between left and right superconductor. (N represents the normal metal which is the 2D Dirac fermion in the present case.) We also assume that the magnitude of Δ is smaller than that of the bulk energy gap of superconductor deposited on STI because the S/TI interface is not ideal.²²⁷⁾

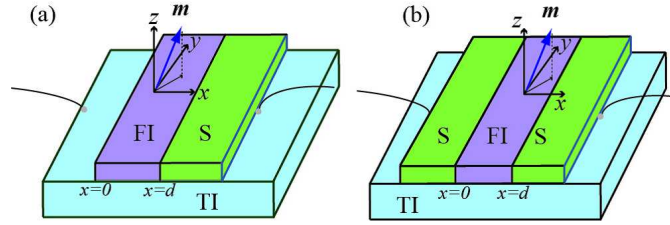


Fig. 36. (Color online) Schematic illustration of the junction. (a) Normal metal (N) / Ferromagnetic insulator (FI) / Superconductor (S) junction and (b) S/FI/S junction formed on the surface of 3D topological insulator (STI). The current is flowing on the surface of STI. [Reproduced from Fig. 1 of Phys. Rev. Lett. **103** 107002 (2009) by Tanaka *et. al.*]

First, we solved the Andreev bound state (ABS) at the interface of FI/S. As an example, we show in Fig. 37 the energy dispersion as a function of the angle θ (corresponding to the momentum along the interface) in the right panel, and the corresponding conductance σ of the N/FI/S junction in the left panel for several values of μ/m_z . Note that the slope of the energy dispersion affects the conductance σ sensitively. Therefore, it is concluded that the 1D Majorana channel can be controlled by the magnetization of the FI and the chemical potential μ .

Next, we consider the Josephson effect in S/FI/S junction (Fig. 36(b)). This is mainly due to the tunneling process between the two Majorana edge channels at the two interfaces between S and FI. One interesting prediction is that the current-phase relation can be shifted by the m_x . Figure 38 shows the Josephson current as a function

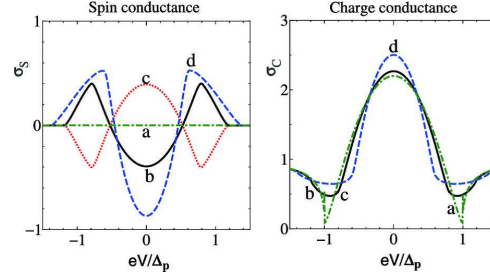


Fig. 37. (Color online) Left Panel: Chiral Majorana mode energy dispersion E_b as a function of the incident angle θ . Right Panel: Normalized tunneling conductance σ in N/FI/S junctions. $m_z d/v_F = 1$ and $m_y/m_z = 0$. a: $\mu/m_z = 1$, b: $\mu/m_z = 2$ and c: $\mu/m_z = 0.5$. [Reproduced from Fig. 2 of Phys. Rev. Lett. **103** 107002 (2009) by Tanaka *et. al.*]

of the phase different φ between the two superconductors for different values of m_x , where the parallel shift of the curves is seen.

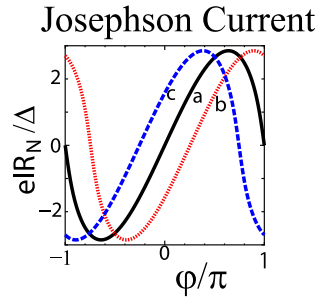


Fig. 38. (Color online) Josephson current in S/FI/S junctions is plotted with a: $m_x/m_z = 0$, b: $m_x/m_z = 0.4$ and c: $m_x/m_z = -0.4$. We choose $m_z d/v_F = 1$, $\mu/m_z = 1$ and $m_y/m_z = 0$. $T = 0.05T_C$ with transition temperature T_C . [Reproduced from Fig. 4 from Phys. Rev. Lett. **103** 107002 (2009) by Tanaka *et. al.*]

The generalization to the anisotropic pairing superconductors on STI has been discussed in ref.^{225,226} . It is found that the proximity effect to the superconductivity is strongly dependent on the pairing symmetry. For spin-triplet p -wave superconductor, there occurs no proximity effect because the spin direction of the 2D Dirac electrons is not consistent with that of the p -wave pairing. In the cases of spin-singlet s -wave and d -wave pairings, there occurs the proximity effect, and the Majorana fermions appear at the interface of FI and S. For spin-singlet d_{xy} -pairing, the zero energy states appear along the edge of the sample even without the magnetization of FI, *i.e.*, without T -symmetry breaking, which has been well-known. However, the new aspect here is that the zero energy dispersionless bound states are Majorana fermions due to the

	ZEABS	dispersion	top. index	odd- ω pairing	Majorana	section
s	No	-	-	No	-	2.2, 3.3
d_{xy}	Yes	No	w_{1d}	OSO	double	2.2, 3.3
p_x	Yes	No	w_{1d}	OTE	double	2.2, 3.3
chiral p (spinless)	Yes	Yes	w_{2d}	OTE	chiral	3.4
chiral p (spinful)	Yes	Yes	w_{2d}	OTE	double	3.4
$s + p$ ($p > s$)	Yes	Yes	Z_2	OTE+OSO	helical	3.6
$s + p$ ($p < s$)	No	-	-	No	-	3.6
$d_{xy} + p$	Yes	No	W	OSO+OTE	flat	3.6

Table IX. Edge states of various superconductors. Each column describes the type of bulk superconductor, zero energy Andreev bound state (ZEABS), the presence or absence of the energy dispersion, topological index characterizing the ZEABS, symmetry of the induced odd-frequency pairing, the type of Majorana fermion, and the corresponding sections in the text, respectively.

proximity to STI. With the z -component of the magnetization, the Majorana fermion obtains the dispersion, which results in the very different behavior of the conductance compared with the case of spin-singlet s -wave superconductors.

4. Discussion

4.1 Interplay between symmetry and topology

Up to now, we have studied induced odd-frequency pairings in §2 and topological bulk-edge correspondence in §3. In this section, we discuss the relation between these two.

First, all the known zero energy edge states at the surface of superconductors can be characterized by the topological indices, and are topologically protected. These zero energy states are always associated with the pure odd-frequency pairing at the surface. (When the ABS has the energy dispersion, this statement applies only to the sector of $k_y = 0$.) In Table IX, we summarize the results for various situations studied thus far.

For s -wave superconductor, which belongs to ESE, there is no ZEABS because it is topologically trivial. At the same time, odd-frequency pairing is absent at the surface. However, d_{xy} -wave superconductor, which also belongs to ESE, has ZEABS characterized by the topological index w_{1d} . w_{1d} is the winding number defined for the one-dimensional systems when k_y is fixed as discussed in §3.3. The formation of the ZEABS stems from the sign change of the pair potential felt by injected and reflected quasiparticles. The similar situation occurs for p_x -wave superconductor which belongs

to ETO pairing. In these cases, pure odd-frequency pair amplitudes (OSO for d_{xy} , OTE for p_x) exist at the surface. The ZEABSs can be regarded as double Majorana modes satisfying

$$\gamma_\sigma(k_y) = \gamma_{-\sigma}(-k_y), \quad (\sigma = \uparrow, \downarrow). \quad (147)$$

Next, we discuss the spinless chiral p -wave superconductor where the time-reversal symmetry is broken in the bulk. There exists ABS, however, in contrast to the cases above, it has a dispersion linear in k_y . Because of the broken time-reversal symmetry, it is characterized by the Chern number w_{2d} in a manner similar to the quantum Hall states. The induced odd-frequency pair amplitude at the surface belongs to OTE symmetry. The present ABS is a chiral Majorana mode, which is a genuine Majorana fermion. The case of the spinful chiral p -wave superconductor can be regarded as the two copies of the spinless case discussed above. Lastly, the noncentrosymmetric superconductors (NCSs) are discussed. In these superconductors, the parity of the pair amplitudes are mixed. For the case of s -wave and p -wave mixture, there are two topologically distinct states depending on the relative magnitudes of the corresponding pair potentials. When p -wave component is dominant, the ABS is generated as a helical Majorana edge mode. The pair amplitude induced at the surface has OTE+OSO symmetry. The topological index characterizing the ABS is the \mathbf{Z}_2 invariant. On the other hand, when s -wave component is dominant, no ABS is generated because it is smoothly connected to the topologically trivial s -wave superconductor case without closing the bulk gap. For $(d_{xy} + p)$ -wave pair potential case, a single branch of dispersionless ABS appears if k_y satisfies some condition. This ZEABS is a single Majorana fermion. The topological index W defined by eq.(123) ensures its topological stability.¹⁶¹⁾ The symmetry of induced odd-frequency pair amplitude is OSO+OTE.

4.2 Related topics

There are several important issues which are not addressed in this review article due to the limited space. We will briefly mention each of them by indicating relevant references.

In this review article, we mainly focus on the interface and surface of superconductors. There are several works on the bulk superconductors from the viewpoint of topology and/or odd-frequency pairings. Non-interacting topological insulators and topological superconductors have been classified based on the universal class of the

Anderson localization.^{156,157)} The similar results have been reached independently by Kitaev²²⁸⁾ in the framework of K-theory. The classification scheme also has been applied for solitons in topological insulators and topological superconductors.²²⁹⁾ Possible bulk odd-frequency superconductors have been an important issue in many-body physics. Recently, there are several proposals of odd-frequency gap functions in quasi one-dimensional systems,^{14,15)} magnetic superconductors,²³⁰⁾ heavy fermion systems,^{12,13)} and strongly coupled electron-phonon systems.¹⁷⁾ However, it is noted that the thermodynamic stability and physical properties of the bulk odd-frequency pairing superconductors are still controversial issues.^{16,231,232)}

Since superfluid ^3He is a well established spin-triplet p -wave superfluid, it is natural to expect ABS.^{23,24)} ABSs in superfluid ^3He have been predicted in the 1980's.^{23,24)} However, the detection of them is not easy since Cooper pairs of superfluid ^3He do not have electric charge. Surface ABS of ^3He B phase has been observed experimentally by the transverse acoustic impedance²³³⁾ in 2005 and specific heat measurements²³⁴⁾ in 2006. In the actual surface of ^3He B phase, diffusive scattering by surface roughness plays an important role.^{235,236)} When a surface is specular, SABS has a Dirac like linear dispersion which have been recently interpreted as Majorana fermion.^{155,237)} There are several theoretical discussions about SABS from the viewpoint of topological superconductivity and Majorana fermions.^{155–157,238–242)} It is noted that surface Majorana cone has been experimentally observed for highly specular wall of ^3He B phase.^{243,244)} Surface Majorana ABS (SMABS) has been also discussed in slab geometry of ^3He A and B phases.^{241,242)} An analogous system of diffusive normal metal/spin-triplet superconductor can be realized in superfluid aerogel/ ^3He hybrid system. Anomalous proximity effects discussed in §2.4 are also expected in the aerogel, since it can be regarded as a diffusive Fermi liquid.²⁴⁵⁾

Recently, promising candidate of topological superconductor has been discovered in doped topological insulator $\text{Cu}_x\text{Bi}_2\text{Se}_3$.²⁴⁶⁾ Several experimental^{247,248)} and theoretical^{214,249)} researches have started. MSABS are also expected in the present new superconductors.

Majorana fermion can be a platform of topological quantum computation. Various systems have been proposed to produce Majorana fermion; spin-triplet p -wave superconductors / superfluids,^{174,176,177,241,250–254)} $\nu = 5/2$ fractional quantum Hall system,²⁵⁵⁾ spin singlet s -wave superconductor on topological insulator surface with vortex or the interface with ferromagnet,^{221,256,257)} noncentrosymmetric superconductors

with Zeeman field,^{196,198,258} s -wave superfluid of cold atoms with laser generated spin-orbit interaction,^{195,196} semiconductor/SC systems including Rashba spin-orbit coupling with FM¹⁹⁷ or Zeeman field,²⁰² one-dimensional system made of 2D QSHS²²⁰ or nanowire,^{259–265} quantum anomalous Hall/ SC hybrid system,^{266,267} and Half metal /SC system.^{268,269}

The detection of Majorana fermion is not a trivial issue since it is a neutral particle. Majorana fermions in condensed matter physics are emergent particles resulting from the many-body interactions of electrons which are charged. Thus, they can be detected through the conversion processes to electron influenced by the phases of the superconducting order parameters. In addition to the Majorana interferometry on topological insulator discussed in §3.8,^{220–223} there are many other proposals for this purpose: (i) Josephson effect,^{220,224,259,270–272} (ii) charge transport thorough Majorana fermion,^{222,273–277} (iii) transport noise,^{278,279} and (iv) spin anisotropy.^{159,204,237,238,280}

4.3 Perspectives

The two major fields opened up in 80's are the quantum Hall effect and the high- T_c superconductors. The former introduced the concept of topology and the latter the electron correlation in condensed matter physics. The idea of the topology extended to the time-reversal symmetric systems and the topological insulators have been discovered. On the other hand, the electron correlation naturally leads to the anisotropic Cooper pairings with various symmetries. These two streams are now merging into one producing many interesting new directions in the current condensed matter physics.

It is now recognized that there are 3 distinct classes of currents in solids; (i) One is the conventional Ohmic currents with dissipation. (ii) The second is the superconducting currents and/or the superfluid flow with broken gauge symmetry and macroscopic quantum coherence. (iii) The third one is the “topological currents” induced by the nontrivial topology of wavefunctions, and does not require the broken gauge symmetry. The last two have the common feature of dissipationless currents. The last one has not been paid attention thus far, but will be very unique because it can operate at room temperature when the gap protecting the topology is larger than its energy scale.

These three classes have been considered to be rather clearly separated. However, as we have described in this review article, class (ii) and class (iii) are overlapping each other. Namely, there is a class of topological supercurrent at the edge/surface of the superconductors/superfluid. Therefore, the interplay of the broken gauge symmetry and

topology offers an intriguing new arena for the future condensed matter physics.

These fundamental understandings of the currents in solids will be essential to develop the electronics in the next generation. The dissipationless operations of devices are the key ingredient for the future applications to electronics, and hopefully the topological supercurrent will serve this goal. The other important issue is the quantum computing. Majorana fermion is regarded as the promising candidate for fault-tolerant qubit. In general, the topological orders bring about the electron fractionalization, which gives the robustness of the quantum states. The three degrees of freedom of electrons, *i.e.*, spin, chirality, particle-antiparticle, can be fractionalized at the edge/surface of topologically ordered bulk states, and chiral Majorana fermions can be regarded as the ultimate fractionalized quantum state. On the other hand, the other direction is to recombine these fractionalized particles into new types of particles.²⁸¹⁾ The more the degrees of freedom, the more the system is susceptible to the external stimuli, and hence we can adjust the robustness and sensitivity of the system at will by manipulating the fractionalization/recombination.

To verify these theoretical proposals, experimental progresses are indispensable. There are several relevant experimental techniques such as μ SR, NMR, neutron scattering, X-ray diffraction, and magneto transport. In particular, the direct observation of edge/surface states by the tunneling spectroscopy and ARPES is highly desired. For more details, the readers are referred to other contributions in this special volume.

Finally, we would like to stress that physics of interface/surface superconductivity includes unexplored quantum phenomena and will be a central topic in condensed matter physics in the decades to come.

Acknowledgements

The authors thank T. Akazaki, Y. Ando, Y. Asano, A.V. Balatsky, Y. Fominov, S. Fujimoto, A. Furusaki, Y. Fuseya, A.A. Golubov, N. Hayashi, S. Higashitani, M. Ichioka, J. Inoue, S. Kashiwaya, M. Kohmoto, H. Kusunose, J. Linder, Y. Maeno, K. Miyake, T. Mizushima, K. Nagai, S. Onari, M. Oshikawa, X.L. Qi, A. P. Schnyder, R. Shindou, A. Sudbo, Y. Takahashi, Y. Tanuma, M. Ueda, K. Yada, T. Yokoyama, S.C. Zhang for valuable discussions. This work is supported by Grant-in-Aid for Scientific Research (Grants No. 17071007, No. 17071005, No.19048008, No. 19048015, No. 20654030, No. 22103005(Innovative Areas "Topological Quantum Phenomena"), No. 22340096, No. 21244053 and No.22540383) from the Ministry of Education, Culture, Sports, Science

and Technology of Japan, Strategic International Cooperative Program (Joint Research Type) from Japan Science and Technology Agency, and Funding Program for World-Leading Innovative RD on Science and Technology (FIRST Program).

References

- 1) D. Thouless: in *The Quantum Hall Effect*, ed. R. E. Prange and S. M. Girvin (Springer-Verlag New York Inc., 1987), p. 101.
- 2) M. Sigrist and K. Ueda: *Rev. Mod. Phys.* **63** (1991) 239.
- 3) E. Bauer, G. Hilscher, H. Michor, C. Paul, E. Scheidt, A. Griбанov, Y. Seropegin, H. Noël, M. Sigrist, and P. Rogl: *Phys. Rev. Lett.* **92** (2004) 027003.
- 4) M. Sigrist, D. F. Agterberg, P. A. Frigeri, N. Hayashi, R. P. Kaur, A. Koga, I. Milat, K. Wakabayashi, and Y. Yanase: *J. Magn. Magn. Matter.* **310** (2007) 536.
- 5) It is noted that the exchange of the two time variables does not mean the time reversal. Therefore the odd-frequency pairing does not mean necessarily the time reversal symmetry breaking.
- 6) V. L. Berezinskii: *JETP Lett.* **20** (1974) 287.
- 7) A. Balatsky and E. Abrahams: *Phys. Rev. B* **45** (1992) 13125.
- 8) E. Abrahams, A. Balatsky, D. J. Scalapino, and J. R. Schrieffer: *Phys. Rev. B* **52** (1995) 1271.
- 9) P. Coleman, A. Georges, and A. M. Tsvelik: *J. Phys. Condens. Matter* **9** (1997) 345.
- 10) P. Coleman, E. Miranda, and A. Tsvelik: *Phys. Rev. B* **49** (1994) 8955.
- 11) M. Vojta and E. Dagotto: *Phys. Rev. B* **59** (1999) R713.
- 12) Y. Fuseya, H. Kohno, and K. Miyake: *J. Phys. Soc. Jpn.* **72** (2003) 2914.
- 13) T. Hotta: *J. Phys. Soc. Jpn.* **78** (2009) 123710.
- 14) K. Shigeta, S. Onari, K. Yada, and Y. Tanaka: *Phys. Rev. B* **79** (2009) 174507.
- 15) K. Shigeta, Y. Tanaka, K. Kuroki, S. Onari, and H. Aizawa: *Phys. Rev. B* **83** (2011) 140509(R).
- 16) H. Kusunose, Y. Fuseya, and K. Miyake: *J. Phys. Soc. Jpn.* **80** (2011) 054702.
- 17) H. Kusunose, Y. Fuseya, and K. Miyake: *J. Phys. Soc. Jpn.* **80** (2011) 044711.
- 18) F. S. Bergeret, A. F. Volkov, and K. B. Efetov: *Phys. Rev. Lett.* **86** (2001) 4096.
- 19) Y. Tanaka and A. A. Golubov: *Phys. Rev. Lett.* **98** (2007) 037003.
- 20) Y. Tanaka, A. A. Golubov, S. Kashiwaya, and M. Ueda: *Phys. Rev. Lett.* **99** (2007) 037005.

- 21) Y. Tanaka, Y. Tanuma, and A. A. Golubov: Phys. Rev. B **76** (2007) 054522.
- 22) M. Eschrig, T. Löfwander, T. Champel, J. Cuevas, and G. Schön: J. Low Temp. Phys. **147** (2007) 457.
- 23) L. J. Buchholtz and G. Zwicknagl: Phys. Rev. B **23** (1981) 5788.
- 24) J. Hara and K. Nagai: Prog. Theor. Phys. **76** (1986) 1237.
- 25) S. Kashiwaya and Y. Tanaka: Rep. Prog. Phys. **63** (2000) 1641.
- 26) T. Löfwander, V. S. Shumeiko, and G. Wendin: Supercond. Sci. Technol. **14** (2001) R53.
- 27) C. R. Hu: Phys. Rev. Lett. **72** (1994) 1526.
- 28) Y. Tanaka and S. Kashiwaya: Phys. Rev. Lett. **74** (1995) 3451.
- 29) M. Matsumoto and H. Shiba: J. Phys. Soc. Jpn **64** (1995) 1703.
- 30) Y. Tanaka and S. Kashiwaya: Phys. Rev. B **53** (1996) 9371.
- 31) Y. Asano, Y. Tanaka, and S. Kashiwaya: Phys. Rev. B **69** (2004) 134501.
- 32) A. F. Andreev: Sov. Phys. JETP **19** (1964) 1228.
- 33) G. E. Blonder, M. Tinkham, and T. Klapwijk: Phys. Rev. B **25** (1982) 4515.
- 34) C. Bruder: Phys. Rev. B **41** (1990) 4017.
- 35) S. Kashiwaya, Y. Tanaka, M. Koyanagi, and K. Kajimura: Phys. Rev. B **53** (1996) 2667.
- 36) S. Kashiwaya, Y. Tanaka, M. Koyanagi, H. Takashima, and K. Kajimura: Phys. Rev. B **51** (1995) 1350.
- 37) S. Kashiwaya, Y. Tanaka, N. Terada, M. Koyanagi, S. Ueno, L. Alff, H. Takashima, Y. Tanuma, and K. Kajimura: J. Phys. Chem. Solid **59** (1998) 2034.
- 38) M. Covington, M. Aprili, E. Paraoanu, L. H. Greene, F. Xu, J. Zhu, and C. A. Mirkin: Phys. Rev. Lett. **79** (1997) 277.
- 39) L. Alff, H. Takashima, S. Kashiwaya, N. Terada, H. Ihara, Y. Tanaka, M. Koyanagi, and K. Kajimura: Phys. Rev. B **55** (1997) R14757.
- 40) J. Y. T. Wei, N.-C. Yeh, D. F. Garrigus, and M. Strasik: Phys. Rev. Lett. **81** (1998) 2542.
- 41) I. Iguchi, W. Wang, M. Yamazaki, Y. Tanaka, and S. Kashiwaya: Phys. Rev. B **62** (2000) R6131.

- 42) A. Biswas, P. Fournier, M. M. Qazilbash, V. N. Smolyaninova, H. Balci, and R. L. Greene: Phys. Rev. Lett. **88** (2002) 207004.
- 43) B. Chesca, H. J. H. Smilde, and H. Hilgenkamp: Phys. Rev. B **77** (2008) 184510.
- 44) Y. Tanaka and S. Kashiwaya: Phys. Rev. B **53** (1996) R11957.
- 45) Y. Tanaka and S. Kashiwaya: Phys. Rev. B **56** (1997) 892.
- 46) Y. S. Barash, H. Burkhardt, and D. Rainer: Phys. Rev. Lett. **77** (1996) 4070.
- 47) S. Kashiwaya, Y. Tanaka, N. Yoshida, and M. R. Beasley: Phys. Rev. B **60** (1999) 3572.
- 48) S. Higashitani: J. Phys. Soc. Jpn. **66** (1997) 2556.
- 49) H. Walter, W. Prusseit, R. Semerad, H. Kinder, W. Assmann, H. Huber, H. Burkhardt, D. Rainer, and J. Sauls: Phys. Rev. Lett. **80** (1998) 3598.
- 50) Y. Tanaka, Y. Asano, A. Golubov, and S. Kashiwaya: Phys. Rev. B **72** (2005) 140503(R).
- 51) M. Yamashiro, Y. Tanaka, and S. Kashiwaya: Phys. Rev. B **56** (1997) 7847.
- 52) M. Yamashiro, Y. Tanaka, Y. Tanuma, and S. Kashiwaya: J. Phys. Soc. Jpn. **67** (1998) 3224.
- 53) X. G. Wen: *Quantum Field Theory of Many-Body Systems* (Oxford University Press, Oxford, 2004).
- 54) Note that the plateau observed experimentally is explained by the disorder and consequent Anderson localization effect. See for example Chap. 3 of ref.1.
- 55) B. I. Halperin: Phys. Rev. B **25** (1982) 2185.
- 56) Y. Hatsugai: Phys. Rev. Lett. **71** (1993) 3697.
- 57) Y. Hatsugai: J. Phys.: Condens. Matter **9** (1997) 2507.
- 58) M. Z. Hasan and C. L. Kane: Rev. Mod. Phys. **82** (2010) 3045.
- 59) X.-L. Qi and S.-C. Zhang: arXiv:1008.2026 .
- 60) P. W. Anderson: J. Phys. Chem. Solids **26** (1959) 26.
- 61) T. Yokoyama, Y. Tanaka, and A. Golubov: Phys. Rev. B **75** (2007) 134510.
- 62) T. Yokoyama, Y. Tanaka, and A. A. Golubov: Phys. Rev. B **72** (2005) 052512.
- 63) Y. Tanaka, A. A. Golubov, S. Kashiwaya, and M. Ueda: Phys. Rev. Lett. **99** (2007) 037005.

- 64) N. Kopnin: *Theory of Nonequilibrium Superconductivity* (Oxford University Press, 2001).
- 65) M. Ashida, S. Aoyama, J. Hara, and K. Nagai: Phys. Rev. B **40** (1989) 8673.
- 66) M. Matsumoto and H. Shiba: J. Phys. Soc. Jpn. **64** (1995) 4867.
- 67) J. W. Serene and D. Rainer: Phys. Rep. **101** (1983) 221.
- 68) G. Eilenberger: Z. Phys. **214** (1968) 195.
- 69) M. Eschrig: Phys. Rev. B **61** (2000) 9061.
- 70) W. L. McMillan: Phys. Rev. **175** (1968) 537.
- 71) J. M. Rowell and W. L. McMillan: Phys. Rev. Lett. **16** (1966) 453.
- 72) K. Ichimura and K. Nomura: J. Phys. Soc. Jpn. **75** (2006) 051012.
- 73) F. Laube, G. Goll, H. v. Löhneysen, M. Fogelström, and F. Lichtenberg: Phys. Rev. Lett. **84** (2000) 1595.
- 74) Z. Mao, K. Nelson, R. Jin, Y. Liu, and Y. Maeno: Phys. Rev. Lett. **87** (2001) 037003.
- 75) S. Kashiwaya, H. Kashiwaya, H. Kambara, T. Furuta, H. Yaguchi, Y. Tanaka, and Y. Maeno: Phys. Rev. Lett. **107** (2011) 077003.
- 76) C. Wälti, H. R. Ott, Z. Fisk, and J. L. Smith: Phys. Rev. Lett. **84** (2000) 5616.
- 77) C. S. Turel, J. Y. T. Wei, W. M. Yuhasz, and M. B. Maple: Physica C **463-465** (2007) 32.
- 78) P. M. C. Rourke, M. A. Tanatar, C. S. Turel, J. Berdeklis, C. Petrovic, and J. Y. T. Wei: Phys. Rev. Lett. **94** (2005) 107005.
- 79) Y. Tanaka and A. A. Golubov: Phys. Rev. Lett. **98** (2007) 037003.
- 80) Y. Tanaka, Y. Nazarov, and S. Kashiwaya: Phys. Rev. Lett. **90** (2003) 167003.
- 81) Y. Tanaka, Y. Nazarov, A. Golubov, and S. Kashiwaya: Phys. Rev. B **69** (2004) 144519.
- 82) Y. Tanaka and S. Kashiwaya: Phys. Rev. B **70** (2004) 012507.
- 83) Y. Tanaka, S. Kashiwaya, and T. Yokoyama: Phys. Rev. B **71** (2005) 094513.
- 84) Y. Asano, Y. Tanaka, and S. Kashiwaya: Phys. Rev. Lett. **96** (2006) 097007.
- 85) Y. Asano, Y. Tanaka, A. A. Golubov, and S. Kashiwaya: Phys. Rev. Lett. **99** (2007) 067005.

- 86) T. Yokoyama, Y. Tanaka, and A. A. Golubov: Phys. Rev. B **78** (2008) 012508.
- 87) A. Abrikosov: *Superconductivity* (Marcel Dekker, New York, 1969).
- 88) G. Blatter, M. V. Feigel'man, V. B. Geshkenbein, A. I. Larkin, and V. M. Vinokur: Rev. Mod. Phys. **66** (1994) 1125.
- 89) C. Caroli, P. G. de Gennes, and J. Matricon: Phys. Lett. **9** (1964) 307.
- 90) H. F. Hess, R. B. Robinson, R. C. Dynes, J. M. Valles, , and J. V. Waszczak: Phys. Rev. Lett. **62** (1989) 214.
- 91) Y. G. Makhlin and G. E. Volovik: JETP Lett. **62** (1995) 737.
- 92) A. I. Larkin and Y. N. Ovchinnikov: Phys. Rev. B **57** (1998) 5457.
- 93) N. B. Kopnin and G. E. Volovik: Phys. Rev. Lett. **62** (1997) 1377.
- 94) G. E. Volovik: JETP Lett. **70** (1999) 609.
- 95) F. Gygi and M. Schlüter: Phys. Rev. B **43** (1991) 7609.
- 96) N. Hayashi, T. Isoshima, M. Ichioka, and K. Machida: Phys. Rev. Lett. **80** (1998) 2921.
- 97) O. Fischer, M. Kugler, I. Maggio-Aprile, C. Berthod, and C. Renner: Rev. Mod. Phys. **79** (2007) 353.
- 98) N. Schopohl and K. Maki: Phys. Rev. B **52** (1995) 490.
- 99) N. Schopohl: arXiv:cond-mat/9804064 .
- 100) Y. Tanaka, H. Takayanagi, and A. Hasegawa: Solid. State Commun. **85** (1993) 321.
- 101) A. S. Mel'nikov and V. M. Vinokur: Nature **415** (2002) 415.
- 102) Y. Tanuma, N. Hayashi, Y. Tanaka, and A. A. Golubov: Phys. Rev. Lett. **102** (2009) 117003.
- 103) Y. Kato: J. Phys. Soc. Jpn. **69** (2000) 3378.
- 104) Y. Kato and N. Hayashi: J. Phys. Soc. Jpn. **71** (2002) 1721.
- 105) N. Hayashi and Y. Kato: J. Low Temp. Phys. **131** (2003) 893.
- 106) Y. Kato and N. Hayashi: Physica C **388-389** (2003) 519.
- 107) T. Yokoyama, M. Ichioka, and Y. Tanaka: J. Phys. Soc. Jpn. **79** (2010) 034702.
- 108) K. D. Usadel: Phys. Rev. Lett. **25** (1970) 507.
- 109) A. Volkov, A. Zaitsev, and T. Klapwijk: Physica C **210** (1993) 21.

- 110) A. Golubov and M. Kupriyanov: J. Low Temp. Phys. **70** (1988) 83.
- 111) W. Belzig, C. Bruder, and G. Schön: Phys. Rev. B **54** (1996) 9443.
- 112) Y. Tanaka, A. A. Golubov, and S. Kashiwaya: Phys. Rev. B **68** (2003) 054513.
- 113) C. Honerkamp and M. Sigrist: J. Low Temp. Phys. **111** (1998) 895.
- 114) W. Belzig, C. Bruder, and G. Schön: Phys. Rev. B **53** (1996) 5727.
- 115) O. Narikiyo and H. Fukuyama: J. Phys. Soc. of Jpn. **58** (1989) 4557.
- 116) S. Higashitani: J. Phys. Soc. Jpn. **66** (1997) 2556.
- 117) Y. S. Barash, M. S. Kalenkov, and J. Kurkijärvi: Phys. Rev. B **62** (2000) 6665.
- 118) H. Walter, W. Prusseit, R. Semerad, H. Kinder, W. Assmann, H. Huber, H. Burkhardt, D. Rainer, and J. Sauls: Phys. Rev. Lett. **80** (1998) 3598.
- 119) Y. Asano, A. A. Golubov, Y. Fominov, and Y. Tanaka: arXiv:1010.1574 .
- 120) F. S. Bergeret, A. F. Volkov, and K. B. Efetov: Rev. Mod. Phys. **77** (2005) 1321.
- 121) F. S. Bergeret, A. F. Volkov, and K. B. Efetov: Phys. Rev. B **68** (2003) 064513.
- 122) A. F. Volkov, Y. V. Fominov, and K. B. Efetov: Phys. Rev. B **72** (2005) 184505.
- 123) A. Kadigrobov, R. I. Shekter, and M. Jonson: Euro Phys. Lett. **90** (2001) 394.
- 124) A. A. Golubov, M. Y. Kupriyanov, and Y. V. Fominov: JETP Lett. **75** (2002) 190.
- 125) A. I. Buzdin: Rev. Mod. Phys. **77** (2005) 935.
- 126) J. Linder, T. Yokoyama, and A. Sudbo: Phys. Rev. B **77** (2008) 174507.
- 127) J. Linder, A. M. Black-Schaffer, and A. Sudbo: Phys. Rev. B **82** (2010) 041409.
- 128) T. Löfwander, T. Champel, J. Durst, and G. Schön: Phys. Rev. Lett. **95** (2005) 187003.
- 129) R. S. Keizer, S. T. B. Goennenwein, T. M. Klapwijk, G. Miao, G. Xiao, and A. Gupta: Nature **439** (2006) 825.
- 130) I. Sosnin, H. Cho, V. T. Petrashov, and A. F. Volkov: Phys. Rev. Lett. **96** (2006) 157002.
- 131) T. S. Khaire, M. A. Khasawneh, J. W. P. Pratt, and N. O. Birge: Phys. Rev. Lett. **104** (2010) 137002.
- 132) W. A. Robinson, J. D. S. Witt, and M. G. Blamire: Science **329** (2010) 59.
- 133) Y. Kalcheim, T. Kirzhner, G. Koren, and O. Millo: Phys. Rev. B **83** (2011) 064510.
- 134) A. Buzdin: Phys. Rev. B **62** (2000) 11377.

- 135) M. Zareyan, W. Belzig, and Y. V. Nazarov: Phys. Rev. Lett **86** (2001) 308.
- 136) I. Baladie and A. Buzdin: Phys. Rev. B **64** (2001) 224514.
- 137) F. S. Bergeret, A. F. Volkov, and K. B. Efetov: Phys. Rev. B **65** (2002) 134505.
- 138) T. Yokoyama, Y. Tanaka, and A. A. Golubov: Phys. Rev. B **72** (2005) 052512.
- 139) T. Yokoyama, Y. Tanaka, and A. A. Golubov: Phys. Rev. B **73** (2006) 094501.
- 140) J. Linder, T. Yokoyama, A. Sudbo, and M. Eschrig: Phys. Rev. Lett. **102** (2009) 107008.
- 141) J. Linder, A. Sudbo, T. Yokoyama, R. Grein, and M. Eschrig: Phys. Rev. B **81** (2010) 214504.
- 142) T. Yokoyama and Y. Tserkovnyak: Phys. Rev. B **80** (2009) 104416.
- 143) T. Yokoyama, Y. Tanaka, and N. Nagaosa: Phys. Rev. Lett. **106** (2011) 246601.
- 144) M. Eschrig, J. Kopu, J. C. Cuevas, and G. Schön: Phys. Rev. Lett. **90** (2003) 137003.
- 145) Y. Asano, Y. Tanaka, and A. A. Golubov: Phys. Rev. Lett. **98** (2007) 107002.
- 146) V. Braude and Y. V. Nazarov: Phys. Rev. Lett. **98** (2007) 077003.
- 147) M. Eschrig and T. Löfwander: Nature Physics **4** (2008) 138.
- 148) Y. Asano, Y. Sawa, Y. Tanaka, and A. A. Golubov: Phys. Rev. B **76** (2007) 224525.
- 149) S. Takahashi, S. Hikino, M. Mori, J. Martinek, and S. Maekawa: Phys. Rev. Lett. **99** (2007) 057003.
- 150) M. S. Anwar, F. Czeschka, M. Hesselberth, M. Porcu, and J. Aarts: Phys. Rev. B **82** (2010) 100501(R).
- 151) D. J. Thouless, M. Kohmoto, M. P. Nightingale, and M. den Nijs: Phys. Rev. Lett. **49** (1982) 405.
- 152) M. Kohmoto: Ann. Phys. **160** (1985) 343.
- 153) N. Read and D. Green: Phys. Rev. B **61** (2000) 10267.
- 154) G.R. Volovik: *The Universe in a Helium Droplet* (Oxford Science Publications, 2003).
- 155) X. L. Qi, T. L. Hughes, S. Raghu, and S. C. Zhang: Phys. Rev. Lett. **102** (2009) 187001.
- 156) A. P. Schnyder, S. Ryu, A. Furusaki, and A. W. W. Ludwig: Phys. Rev. B **78** (2008) 195125.

- 157) S. Ryu, A. P.Schnyder, A. Furusaki, and A. Ludwig: New J. Phys. **12** (2010) 065010.
- 158) R. Roy: arXiv:0803.2881 .
- 159) M. Sato and S. Fujimoto: Phys. Rev. B **79** (2009) 094504.
- 160) M. Sato: Bussei Kenkyu **94** (2010) 311.
- 161) M. Sato, Y. Tanaka, K. Yada, and T. Yokoyama: Phys. Rev. B **83** (2011) 224511.
- 162) S. Ryu and Y. Hatsugai: Phys. Rev. Lett. **89** (2002) 077002.
- 163) M. Sato: Phys. Rev. B **79** (2009) 214526.
- 164) For the index theorem, see for example ref..²⁸²⁾
- 165) Note that w_{1d} is different from w in ref.¹⁶¹⁾ by a factor -1 while they are essentially the same topological index.
- 166) J. Goryo and K. Ishikawa: Phys. Lett. A **260** (1999) 294.
- 167) A. Furusaki, M. Matsumoto, and M. Sigrist: Phys. Rev. B **64** (2001) 054514.
- 168) Here we implicitly assume that $\text{sgn}[\det \partial_{k_j} \Delta_j(\mathbf{k})] \neq 0$ at \mathbf{k} with $\Delta(\mathbf{k}) = 0$. If this is not the case, one needs to deform the gap function slightly to satisfy the assumption. After this regularization, one can apply the formula. This prescription does not change the value of the topological index.
- 169) R. Roy: Phys. Rev. Lett. **105** (2010) 186401.
- 170) N. B. Kopnin and M. M. Salomaa: Phys. Rev. B **44** (1991) 9667.
- 171) T. Fukui and T. Fujiwara: J. Phys. Soc. Jpn. **79** (2010) 033701.
- 172) T. Fukui and T. Fujiwara: Phys. Rev. B **82** (2010) 184536.
- 173) L. Santos, Y. Nishida, C. Chamon, and C. Mudry: Phys. Rev. B **83** (2011) 104522.
- 174) D. A. Ivanov: Phys. Rev. Lett. **86** (2001) 268.
- 175) J. Jang, D. G. Ferguson, V. Vakaryuk, R. Budakian, S. B. Chung, P. M. Goldbart, and Y. Maeno: Science **331** (2011) 186.
- 176) T. Kawakami, Y. Tsutsumi, and K. Machida: Phys. Rev. B **79** (2009) 092506.
- 177) T. Kawakami, T. Mizushima, and K. Machida: J. Phys. Soc. Jpn. **80** (2011) 044603.
- 178) C. L. Kane and E. J. Mele: Phys. Rev. Lett. **95** (2005) 146802.
- 179) C. L. Kane and E. J. Mele: Phys. Rev. Lett. **95** (2005) 226801.
- 180) B. A. Bernevig and S. C. Zhang: Phys. Rev. Lett. **96** (2006) 106802.

- 181) B. A. Bernevig, T. L. Hughes, and S. C. Zhang: Science **314** (2006) 1757.
- 182) L. Fu, K. C. L, and E. J. Mele: Phys. Rev. Lett. **98** (2007) 106803.
- 183) J. E. Moore and L. Balents: Phys. Rev. B **75** (2007) 121306(R).
- 184) R. Roy: Phys. Rev. B **79** (2009) 195322.
- 185) Y. Ran, Y. Zhang, and A. Vishwanath: Nature Physics **5** (2009) 298.
- 186) Y. Tanaka, T. Yokoyama, A. V. Balatsky, and N. Nagaosa: Phys. Rev. B **79** (2009) 060505.
- 187) P. A. Frigeri, D. F. Agterberg, A. Koga, and M. Sigrist: Phys. Rev. Lett. **92** (2004) 097001.
- 188) T. Yokoyama, Y. Tanaka, and J. Inoue: Phys. Rev. B **72** (2005) 220504(R).
- 189) C. Iniotakis, N. Hayashi, Y. Sawa, T. Yokoyama, U. May, Y. Tanaka, and M. Sigrist: Phys. Rev. B **76** (2007) 012501.
- 190) M. Eschrig, C. Iniotakis, and Y. Tanaka: arXiv:1001.2486 .
- 191) A. Vorontsov, I. Vekhter, and M. Eschrig: Phys. Rev. Lett. **101** (2008) 127003.
- 192) C. Lu and S. Yip: Phys. Rev. B **80** (2009) 024504.
- 193) A. P. Schnyder, P. M. R. Brydon, D. Manske, and C. Timm: Phys. Rev. B **82** (2010) 184508.
- 194) A. P. Schnyder, S. Ryu, and A. W. W. Ludwig: Phys. Rev. Lett. **102** (2009) 196804.
- 195) M. Sato, Y. Takahashi, and S. Fujimoto: Phys. Rev. Lett. **103** (2009) 020401.
- 196) M. Sato, Y. Takahashi, and S. Fujimoto: Phys. Rev. B **82** (2010) 134521.
- 197) J. D. Sau, R. M. Lutchyn, S. Tewari, and S. D. Sarma: Phys. Rev. Lett. **104** (2010) 040502.
- 198) M. Sato and S. Fujimoto: Phys. Rev. Lett. **105** (2010) 217001.
- 199) J. D. Sau, S. Tewari, R. Lutchyn, T. Stanescu, and S. D. Sarma: Phys. Rev. B **82** (2010) 214509.
- 200) P. A. Frigeri, D. F. Agterberg, A. Koga, and M. Sigrist: Phys. Rev. Lett. **92** (2004) 097001.
- 201) S. Fujimoto: J. Phys. Soc. Jpn. **76** (2007) 051008.
- 202) J. Alicea: Phys. Rev. B **81** (2010) 125318.

- 203) Y. Tanaka, Y. Mizuno, T. Yokoyama, K. Yada, and M. Sato: Phys. Rev. Lett. **105** (2010) 097002.
- 204) K. Yada, M. Sato, Y. Tanaka, and T. Yokoyama: Phys. Rev. B. **83** (2011) 064505.
- 205) K. Yada, S. Onari, Y. Tanaka, and J. Inoue: Phys. Rev. B **80** (2009) 140509.
- 206) M. Sato: Phys. Rev. B **73** (2006) 214502.
- 207) B. Béri: Phys. Rev. B **81** (2010) 134515.
- 208) A. P. Schnyder and S. Ryu: arXiv:1011.1438 .
- 209) P. M. R. Brydon, A. P. Schnyder, and C. Timm: arXiv:1104.2257 .
- 210) T. T. Heikkilä and G. E. Volovik: JETP Lett. **93** (2011) 59.
- 211) T. T. Heikkilä, N. B. Kopnin, and G. E. Volovik: arXiv:1012.0905 .
- 212) M. Sato: Phys. Rev. B **81** (2010) 220504(R).
- 213) P. Grinevich and G. E. Volovik: J. Low Temp. Phys. **72** (1988) 371.
- 214) L. Fu and E. Berg: Phys. Rev. Lett. **105** (2010) 097001.
- 215) L. Fu and C. L. Kane: Phys. Rev. B **74** (2006) 195312.
- 216) For review, see refs.⁵⁸⁾ and.⁵⁹⁾
- 217) A. Kitaev: Ann. Phys. **321** (2006) 2.
- 218) L. Fu and C. L. Kane: Phys. Rev. Lett. **100** (2008) 096407.
- 219) A similar Majorana bound state in a vortex and its non-Abelian statistics for an *s*-wave superconducting state have been discussed for the first time in ref.²⁸³⁾ in a different context. For the relation to Fu-Kane model, see also appendix E in ref..¹⁹⁶⁾
- 220) L. Fu and C. L. Kane: Phys. Rev. Lett. **102** (2009) 216403.
- 221) A. R. Akhmerov, J. Nilsson, and C. W. J. Beenakker: Phys. Rev. Lett. **102** (2009) 216404.
- 222) K. T. Law, P. A. Lee, and T. K. Ng: Phys. Rev. Lett. **103** (2009) 237001.
- 223) C. Benjamin and J. K. Pachos: Phys. Rev. B **81** (2010) 085101.
- 224) Y. Tanaka, T. Yokoyama, and N. Nagaosa: Phys. Rev. Lett. **103** (2009) 107002.
- 225) J. Linder, Y. Tanaka, T. Yokoyama, A. Sudbo, and N. Nagaosa: Phys. Rev. Lett. **104** (2010) 067001.

- 226) J. Linder, Y. Tanaka, T. Yokoyama, A. Sudbo, and N. Nagaosa: Phys. Rev. B **81** (2010) 184525.
- 227) G. Fagas, G. Tkachov, A. Pfund, and K. Richter: Phys. Rev. B **71** (2005) 224510.
- 228) A. Kitaev: AIP Conf. Proc. **1134** (2009) 22.
- 229) J. C. Y. Teo and C. L. Kane: Phys. Rev. B **82** (2010) 11512.
- 230) K. Shigeta, S. Onari, and Y. Tanaka: arXiv:1104.4693 .
- 231) D. Solenov, I. Martin, and D. Mozyrsky: Phys. Rev. B **79** (2009) 132502.
- 232) Y. Fuseya and K. Miyake: J. Phys. Soc. Jpn. **80** (2011) 054705.
- 233) Y. Aoki, Y. Wada, M. Saitoh, R. Nomura, Y. Okuda, Y. Nagato, M. Yamamoto, S. Higashitani, and K. Nagai: Phys. Rev. Lett. **95** (2005) 075301.
- 234) H. Choi, J. P. Davis, J. Pollanen, and W. P. Halperin: Phys. Rev. Lett. **96** (2006) 125301.
- 235) Y. Nagato, M. Yamamoto, and K. Nagai: J. Low Temp. Phys **110** (1998) 1135.
- 236) K. Nagai, Y. Nagato, M. Yamamoto, and S. Higashitani: J. Phys. Soc. Jpn. **77** (2008) 111003.
- 237) B. Chung and S. C. Zhang: Phys. Rev. Lett. **103** (2009) 235301.
- 238) Y. Nagato, S. Higashitani, and K. Nagai: J. Phys. Soc. Jpn. **78** (2009) 123603.
- 239) G. Volovik: JETP Lett. **90** (2009) 587.
- 240) G. Volovik: JETP Lett. **90** (2009) 398.
- 241) Y. Tsutsumi, T. Mizushima, M. Ichioka, and K. Machida: J. Phys. Soc. Jpn. **79** (2010) 113601.
- 242) Y. Tsutsumi, M. Ichioka, and K. Machida: Phys. Rev. B **83** (2011) 094510.
- 243) S. Murakawa, Y. Tamura, Y. Wada, M. Wasai, M. Saitoh, Y. Aoki, R. Nomura, Y. Okuda, Y. Nagato, M. Yamamoto, S. Higashitani, and K. Nagai: Phys. Rev. Lett. **103** (2009) 155301.
- 244) S. Murakawa, Y. Wada, Y. Tamura, M. Wasai, M. Saitoh, Y. Aoki, R. Nomura, Y. Okuda, Y. Nagato, M. Yamamoto, S. Higashitani, and K. Nagai: J. Phys. Soc. Jpn. **80** (2011) 013602.
- 245) S. Higashitani, Y. Nagato, and K. Nagai: J. Low Temp. Phys. **155** (2009) 83.
- 246) Y. Hor, A. Williams, J. Checkelsky, P. Roushan, J. Seo, Q. Xu, H. Zandbergen, A. Yazdani, N. Ong, and R. Cava: Phys. Rev. Lett **104** (2010) 057001.

- 247) L. A. Wray, S. Y. Xu, Y. Xia, Y. S. Hor, D. Qian, A. V. Fedorov, H. Lin, A. Bansil, R. J. Cava, and M. Z. Hasan: *Nature Phys.* **6** (2010) 855.
- 248) M. Kriener, K. Segawa, Z. Ren, S. Sasaki, and Y. Ando: *Phys.Rev. Lett.* **106** (2011) 127004.
- 249) L. Hao and T. K. Lee: *Phys.Rev. Lett.* **83** (2011) 134516.
- 250) S. Tewari, S. D. Sarma, C. Nayak, C. Zhang, and P. Zoller: *Phys. Rev. Lett.* **98** (2007) 010506.
- 251) T. Mizushima, M. Ichioka, and K. Machida: *Phys. Rev. Lett.* **101** (2008) 150409.
- 252) C. Zhang, S. Tewari, R. M. Lutchyn, and S. D. Sarma: *Phys. Rev. Lett.* **101** (2008) 160401.
- 253) N. R. Cooper and G. V. Shlyapnikov: *Phys. Rev. Lett.* **103** (2009) 155302.
- 254) T. Mizushima and K. Machida: *Phys. Rev. A* **81** (2010) 053605.
- 255) G. Moore and N. Read: *Nucl. Phys. B* **360** (1991) 362.
- 256) L.Fu and C. L. Kane: *Phys. Rev. Lett.* **100** (2008) 096407.
- 257) T. Neupert, S. Onoda, and A. Furusaki: *Phys. Rev. Lett.* **105** (2010) 206404.
- 258) S. Fujimoto: *Phys. Rev. B* **77** (2008) 220501(R).
- 259) A. Y. Kitaev: *Usp. Fiz. Nauk (Suppl.)* **171** (2001) 131.
- 260) R. M. Lutchyn, T. Stanescu, and S. D. Sarma: *Phys. Rev. Lett.* **106** (2011) 127001.
- 261) Y. Oreg, G. Refael, and F. von Oppen: arXiv:1003.1145 .
- 262) J. Alicea, Y. Oreg, G. Refael, F. von Oppen, and M. P. A. Fisher: arXiv:1006.4395 .
- 263) P. W. Brouwer, M. Duckheim, A. Romito, and F. von Oppen: arXiv:1103.2746 .
- 264) P. W. Brouwer, M. Duckheim, A. Romito, and F. von Oppen: arXiv:1104.1531 .
- 265) J. D. Sau, C. H. Lin, H.-Y. Hui, and S. D. Sarma: arXiv:1103.2770 .
- 266) X. L. Qi, T. L. Hughes, and S. C. Zhang: *Phys. Rev. B* **82** (2010) 184516.
- 267) A. Ii, K. Yada, M. Sato, and Y. Tanaka: *Phys. Rev. B* **83** (2011) 224524.
- 268) S. B. Chung, H.-J. Zhang, X.-L. Qi, and S.-C. Zhang: arXiv:1011.6422 .
- 269) P. A. Lee: arXiv:0907.2681v2 .
- 270) R. M. Lutchyn, T. Stanescu, and S. D. Sarma: *Phys. Rev. Lett.* **105** (2010) 077001.
- 271) Y. Asano, Y. Tanaka, and N. Nagaosa: *Phys. Rev. Lett.* **105** (2010) 056402.

- 272) D. I. Pikulin and Y. V. Nazarov: arXiv:1103.0780 .
- 273) K. Flensberg: Phys. Rev. B **82** (2010) 180516(R).
- 274) V. Shivamoggi, G. Refael, and J. E. Moore: Phys. Rev. B **82** (2010) 041405(R).
- 275) L. Fu: Phys. Rev. Lett. **104** (2010) 056402.
- 276) I. Serban, B. Beri, A. R. Akhmerov, and C. W. J. Beenakker: Phys. Rev. Lett. **104** (2010) 147001.
- 277) B. Beri: arXiv:1102.4541 .
- 278) S. B. Chung, X.-L. Qi, J. Maciejko, and S.-C. Zhang: Phys. Rev. B **83** (2011) 100512.
- 279) A. Golub and B. Horovitz: arXiv:1101.3025 .
- 280) R. Shindou, A. Furusaki, and N. Nagaosa: Phys. Rev. B **82** (2010) 180505.
- 281) Y. Tanaka and N. Nagaosa: Phys. Rev. Lett. **103** (2009) 166403.
- 282) M. Nakahara: *Geometry, Topology and Physics* (Institute of Physics Publishing, Bristol and Philadelphia, 2003).
- 283) M.Sato: Phys. Lett. B **575** (2003) 126.